

# **Therapeutic Targeting of MYC in T-cell acute lymphoblastic leukemia of Childhood**

## **Inaugural-Dissertation**

zur Erlangung des Doktorgrades (Dr. rer. nat.)  
der Mathematisch-Naturwissenschaftlichen Fakultät  
der Heinrich-Heine-Universität Düsseldorf

vorgelegt von

**Heinz Ahlert**

aus Krefeld

Düsseldorf, Mai 2021

**aus dem Institut für Kinder-Onkologie,- Hämatologie und Klinische  
Immunologie der Heinrich-Heine-Universität Düsseldorf**

Angefertigt mit der Genehmigung der Mathematisch-  
Naturwissenschaftlichen Fakultät der Heinrich-Heine-Universität  
Düsseldorf

Referentin: Prof. Dr. Julia Hauer

Korreferent: Prof. Dr. Thomas Kurz

Tag der mündlichen Prüfung:

15.09.2021

## **Affirmation**

I hereby declare on oath that I have written this dissertation independently. I have used only the sources and aids indicated in this thesis. With the exception of such citations, the work presented in this thesis is my own. I have identified all sources that have helped me as such. This dissertation has never been submitted or presented in a similar form to any other institution or examination board. I have not yet passed any doctoral examination without success.

---

Heinz Ahlert, May 20th, 2021

## Curriculum Vitae

### *Personal Data*

*Name* | Heinz Ahlert  
*Date of Birth* | 21.09.1991  
*City of Birth* | Krefeld

### *Education*

*08/2017-Present* | **PhD student**  
Clinic for Pediatric Oncology, Hematology, and Clinical Immunology,  
University Hospital Düsseldorf, Scholarship by the German Cancer  
Research Center (DKFZ)  
Title: "Therapeutic Targeting of MYC in T-cell acute lymphoblastic  
leukemia of Childhood".  
Field of research: Oncology, Immunology

*04/2015-07/2017* | **Master thesis**  
Clinic for General Pediatrics, Neonatology and Pediatric Cardiology,  
University Hospital Düsseldorf  
Title: "The role of the interleukin-2 receptor on T cells in the  
development of autoimmunity using type 1 diabetes as an example".  
Field of research: Immunology, Infectiology  
grade: 2.4

*10/2011-03/2015* | **Bachelor thesis**  
Chair of Functional Genome Research of Microorganisms, Heinrich-  
Heine-University, Düsseldorf  
Title: "Mutation analysis of the protein LIPP from Chlamydia  
pneumoniae"  
Research area: Microbiology, Infectiology  
grade: 1.7

*06/2011* | **Abitur**  
Robert-Jungk Gesamtschule  
Krefeld-Hüls



## Publications, Posters, and Presentations

### Publication included in this thesis

2020

Partial results of the present work were submitted for publication to the Journal of Medicinal Chemistry as following:

#### **4-Acyl pyrrole capped HDAC inhibitors: a new scaffold for hybrid inhibitors of BET proteins and histone deacetylases as anti-leukemia drug leads**

Linda Schäker-Hübner #, Robin Warstat #, Heinz **Ahlert** #, Pankaj Mishra, Fabian B. Kraft, Julian Schliehe-Diecks, Andrea Schöler, Arndt Borkhardt, Bernhard Breit, Sanil Bhatia, Martin Hügler, Stefan Günther, Finn K. Hansen

#shared first authorship

The part of this work that was done by myself relates to the biological *in vitro* validation of the dual inhibitors on different cell line models of leukemia.

### Other publications

2020

#### **An autochthonous mouse model of Myd88- and BCL2-driven diffuse large B cell lymphoma reveals actionable molecular vulnerabilities**

Reinhardt H, Flümann R, Rehkämper T, Nieper P, Pfeiffer P, Holzem A, Klein S, Bhatia S, Kochanek M, Kisis I, Pelzer B, **Ahlert H**, Hauer J, da Palma-Guerreiro A, Ryan J, Reimann M, Riabinska A, Wiederstein J, Krüger M, Deckert M, Altmüller J, Klatt A, Frenzel L, Pasqualucci L, Beguelin W, Melnick A, Sander S, Montesinos-Rongen M, Brunn A, Lohneis P, Büttner R, Kashkar H, Borkhardt A, Letai A, Persigehl T, Peifer M, Schmitt C, Knittel G  
Blood Cancer Discovery (2020)

2018

#### **Discovery of the First-in-Class Dual Histone Deacetylase-Proteasome Inhibitor**

Bhatia S, Krieger V, Groll M, Osko JD, Reßing N, **Ahlert H**, Borkhardt A, Kurz T, Christianson DW, Hauer J, Hansen FK.  
J Med Chem. (2018)

#### **Targeting HSP90 dimerization via the C-terminus is effective in imatinib resistant CML and lacks heat shock response**

Bhatia S, Diedrich D, Frieg B, **Ahlert H**, Stein S, Bopp B, Lang F, Zang T, Kröger T, Ernst T, Kögler G, Krieg A, Lüdeke S, Kunkel H, Rodrigues Moita AJ, Kassack MU, Marquardt V, Opitz FV, Oldenburg M, Remke M, Babor F, Grez M, Hochhaus A, Borkhardt A, Groth G, Nagel-Steger L, Jose J, Kurz T, Gohlke H, Hansen FK, Hauer J  
Blood (2018)

#### **CISH promoter polymorphism effects on T cell cytokine receptor signaling and type 1 diabetes susceptibility**

Seyfarth J, **Ahlert H**, Rosenbauer J, Baechle C, Roden M, Holl RW, Mayatepek E, Meissner T, Jacobsen M  
Mol Cell Pediatr. (2018)

#### **Interleukin-7 receptor $\alpha$ -chain haplotypes differentially affect soluble IL-7 receptor and IL-7 serum concentrations in children with type 1 diabetes.**

Seyfarth J, Lundtoft C, Förtsch K, **Ahlert H**, Rosenbauer J, Baechle C, Roden M, Holl RW, Mayatepek E, Kummer S, Meissner T, Jacobsen M. Pediatric Diabetes (2018)

- 2017 | **Dominant TNF $\alpha$  and impaired IL-2 cytokine profiles of CD4 + T cells from children with type-1 diabetes**  
Seyfarth J, Förtsch K, **Ahlert H**, Laws HJ, Karges B, Deenen R, Köhrer K, Mayatepek E, Meissner T, Jacobsen M  
Immunol. Cell Biol. (2017)

### Poster

- 2019 | **Therapeutic Stratification of PTEN-MYC Axis as a Therapy Option in Refractory and Relapsed T-ALL**  
61<sup>st</sup> American Society of Hematology Annual Meeting 2019 (ASH), Orlando, FL, USA
- The clinical relevance of indirect MYC inhibitors for personalized T-ALL treatment**  
2<sup>nd</sup> Translational Oncology Symposium (ETOS), Essen, Germany

### Presentations

- 2019 | **The clinical relevance of indirect MYC inhibitors for personalized T-ALL treatment**  
14<sup>th</sup> BMFZ RETREAT Kardinal-Schulte-Haus, Bergisch Gladbach, Germany
- 2018 | **The clinical relevance of indirect MYC inhibitors for personalized T-ALL treatment**  
13<sup>th</sup> BMFZ RETREAT Schloss Mickeln, Düsseldorf, Germany

## Acknowledgements

I would like to express my sincere thanks to:

**Dr. Sanil Bhatia** for the excellent supervision throughout my thesis and the many suggestions and conversations we had. I would especially like to thank him for the fact that I could ask for advice at any time (even during vacations) and that he always managed to motivate me.

**Prof. Dr. Julia Hauer** for the opportunity to work on the interesting topic and your kind support, especially during my early days in the pediatric clinic. I would also like to thank her for her continued support even after her move to the University Hospital Dresden.

**Prof. Dr. Thomas Kurz** for taking on the role of second reviewer and for showing interest in my work and providing the HSP90 inhibitory agents. Our meetings together were always enriching and gave me many interesting insights into pharmaceutical development processes.

**Prof. Dr. Arnd Borkhardt** for giving me the opportunity to work in the excellent Institute for Hematology, Immunology and Oncology at the Children's Hospital Düsseldorf.

To the entire members of our international working group “**Team Target**” for the constructive discussions and the excellent support in the laboratory. I would also like to thank you for the great time we have had visiting restaurants on a regular schedule. I would like to make special mention of my fellow **Melf**, who accompanied me through most of my PhD and gave me a lot of support in difficult times and made a significant contribution to the good times.

The “**Kinder Office**” for the warm welcome in our office and the fun times we had together, especially when I think of Carnival and Christmas, where we had great moments together. Also, a big thanks goes out to the “**Kiosk Troop**” for the great conversations we had. Many thanks also to **Daniel Pickard**, who organized numerous board game evenings, which were always very entertaining and fun. Btw. the Halloween parties were legendary.

To my best friends, **Gino** and **Viktor** for your patience and tolerance, because I rarely showed up at your place, especially during the time I was writing this thesis. Nevertheless, I would like to thank you for the great time when I was back in Krefeld.

**My family**, who have supported me wherever possible. I would especially like to thank my brother **Johann**, with whom I could live for a short time together, where we had a really nice time.

Last but not least, I would like to thank my fiancée **Friederike** for the great support. The many uplifting discussions have given me the necessary motivation to persevere and successfully complete the work. I am looking forward to our wedding and the time ahead of us.

## Table of content

Affirmation .....	I
Curriculum Vitae.....	II
Publications, Posters, and Presentations.....	III
Acknowledgements .....	V
Table of content.....	VI
List of Figures.....	X
List of tables .....	XI
Abbreviations .....	XII
Summary.....	XV
Zusammenfassung.....	XVI
1. Introduction .....	1
1.1. Leukemia .....	1
1.2. Etiology of Pediatric ALL .....	2
1.3. Clinical Presentation of ALL .....	3
1.4. T-cell acute lymphoblastic leukemia .....	4
1.5. T cell development .....	4
1.6. T-ALL classification .....	6
1.7. T-ALL treatment .....	8
1.8. Genetic landscapes of T-ALL .....	9
1.8.1. Translocations .....	9
1.8.2. Mutations .....	10
1.9. MYC.....	10
1.9.1. The role of MYC in T-ALL .....	11
1.9.2. Indirect Targeting of MYC .....	12
1.9.2.1. Upstream pathways.....	12
1.9.2.2. Regulatory pathways.....	14
1.9.2.3. Downstream pathways .....	14
1.9.3. Novel approaches to target MYC .....	15
1.9.3.1. HDACs and MYC .....	15
1.9.3.2. HSP90, a MYC chaperone .....	17
1.10. Aim of the thesis .....	18
2. Materials and methods .....	19
2.1. Used machines and devices.....	19
2.2. Consumables for cell culture .....	20

## Table of content

---

2.2.1.	Cell lines .....	20
2.2.2.	Media and supplements for cell culture .....	20
2.3.	Chemicals .....	21
2.4.	Buffers and solutions .....	22
2.5.	Consumables for transfection .....	23
2.5.1.	Plasmids and lentiviral packaging system .....	23
2.6.	Consumables for RNA isolation and RT-qPCR .....	23
2.6.1.	Primer Mix .....	24
2.7.	Consumables for drug screening .....	24
2.7.1.	Compound library for high throughput drug screening .....	24
2.8.	Consumables for protein analysis .....	29
2.8.1.	Antibodies and chemicals for flow cytometry .....	29
2.8.2.	Antibodies for Western Blot .....	30
2.9.	<i>In vivo</i> experiments .....	31
2.9.1.	Mouse strain .....	31
2.9.2.	consumables for <i>in vivo</i> experiments .....	31
2.10.	Software .....	32
2.11.	Cell culture methods .....	32
2.11.1.	Thawing cells .....	32
2.11.2.	Culturing leukemic cell lines .....	32
2.11.3.	Culturing HEK293T (Human Embryonic Kidney 293T) .....	33
2.11.4.	Culturing primary patient cells .....	33
2.11.5.	Culturing doxycycline inducible target knock down cells .....	33
2.11.6.	Determination of cell count .....	34
2.11.6.1.	Automated cell count .....	34
2.11.6.2.	Manual cell count .....	34
2.11.7.	Flow cytometry .....	34
2.12.	RNA analysis .....	35
2.12.1.	RNA isolation .....	35
2.12.2.	RNA concentration determination using a spectrophotometer .....	35
2.12.3.	cDNA synthesis .....	36
2.12.4.	qPCR .....	36
2.13.	Protein analysis .....	37
2.13.1.	Protein isolation .....	37
2.13.2.	Western Blotting (WB) .....	37
2.13.2.1.	Preparation of the SDS polyacrylamide gel .....	37

## Table of content

---

2.13.2.2.	SDS-polyacrylamide gel electrophoresis (SDS-PAGE).....	38
2.13.3.	WB analysis .....	39
2.13.3.1.	Set-up of the blot apparatus: .....	39
2.13.3.2.	Antibody staining on PVDF- or nitrocellulose membrane.....	39
2.13.4.	Digital quantitative WB .....	39
2.13.5.	MYC Activity Assay .....	40
2.14.	Lentiviral transduction .....	40
2.14.1.	Virus production in HEK293T .....	41
2.14.2.	Transduction of cells .....	41
2.14.3.	Selection of positively transduced cells .....	41
2.15.	Gene expression analysis.....	42
2.16.	Drug screening .....	42
2.16.1.	Compound screening for IC <sub>50</sub> determination.....	42
2.16.2.	Compound library.....	43
2.16.3.	High throughput drug screening .....	43
2.16.4.	Synergy drug screening .....	43
2.17.	Molecular biological techniques .....	44
2.17.1.	Apoptosis assays .....	44
2.17.1.1.	Annexin V.....	44
2.17.1.2.	Caspase 3/7 .....	44
2.17.2.	Cell cycle assay .....	45
2.18.	<i>In vivo</i> methods.....	46
2.18.1.	Laboratory Animal Facility .....	46
2.18.2.	PDX cell enrichment.....	46
2.18.3.	<i>In vivo</i> optical imaging .....	46
2.18.4.	<i>In vivo</i> testing of copanlisib and JQ1 .....	47
2.18.5.	<i>In vivo</i> testing afuresertib and birabresib .....	47
3.	Results.....	49
3.1.	Characterization of MYC in T-ALL cell line models.....	49
3.1.1.	Identification of MYC expression on mRNA and protein level in T-ALL cell line models .....	49
3.1.2.	Characterization of post-transcriptional MYC regulatory pathways .....	50
3.1.3.	Characterization of T-ALL Patient derived xenograft cells.....	53
3.1.4.	Establishment of an inducible PTEN knock down cell line model .....	54
3.1.5.	Investigation of glucocorticoid therapy resistance .....	55
3.2.	High-Throughput drug screening of T-ALL cell lines .....	59

## Table of content

---

3.2.1.	Investigation of PI3K/AKT inhibitors .....	61
3.3.	<i>In vitro</i> validation of inhibitors .....	64
3.3.1.	<i>In vitro</i> validation of copanlisib and JQ1 .....	64
3.3.2.	<i>In vitro</i> validation of afuresertib and birabresib .....	67
3.3.3.	<i>In vitro</i> validation of AURKA inhibitors in MYC dependent cell lines .....	71
3.3.4.	<i>In vitro</i> validation of MEK inhibitors in high MEK phosphorylated T-ALL cell lines .. .....	74
3.4.	<i>In vivo</i> validation of compound combinations.....	78
3.4.1.	<i>In vivo</i> validation of PI3K inhibitor copanlisib and BRD4 inhibitor JQ1.....	78
3.4.2.	<i>In vivo</i> experiments with AKT inhibitor afuresertib and BRD4 inhibitor birabresib	80
3.5.	Identification of novel MYC targeting drugs .....	81
3.5.1.	Investigation of novel dual HDAC/BRD4 inhibitors .....	82
3.5.2.	Investigation of novel C-terminal HSP90 inhibitors.....	89
4.	Discussion.....	97
4.1.	PTEN Mutations are associated with increased MYC stability .....	97
4.2.	PTEN mutations increase susceptibility for GC resistance .....	98
4.3.	PI3K and AKT inhibitors are well suited for PTEN <sup>mut</sup> cells .....	99
4.3.1.	PI3K and AKT inhibitors in combination with other, MYC related inhibitors demonstrated promising effectivity <i>in vitro</i> .....	100
4.4.	<i>In vivo</i> validation of Copanlisib and JQ1 demonstrated a partially successful therapeutic approach in PTEN <sup>mut</sup> T-ALL.....	103
4.5.	<i>In vivo</i> validation of afuresertib and birabresib.....	104
4.6.	Biological validation of novel dual HDAC/BRD4 inhibitors demonstrated high activity in MYC dependent cell lines.....	104
4.7.	Development of novel CTD-HSP90 inhibitors .....	106
5.	Outlook.....	108
6.	Literature .....	110

## List of Figures

Figure 1: Simplified representation of hematopoiesis of the major blood cells. ....	2
Figure 2: Schematic figure of T cell development adopted from [30]. ....	5
Figure 3: Simplified representation of cell marker for T-ALL classification modeled on [36]. ..	7
Figure 4: Overview of MYC-regulated genes and the respective cellular function adopted from [86]. ....	11
Figure 5: MYC regulatory pathways in T-ALL. ....	13
Figure 6: Example for Nicoletti Assay analysis ....	45
Figure 7: Analysis of MYC expression on mRNA and protein level ....	50
Figure 8: Characterization of MYC related signaling pathways ....	51
Figure 9: Correlation of MYC protein level between PTEN <sup>wt</sup> and PTEN <sup>mut</sup> ....	52
Figure 10. Correlation of MYC activity between PTEN <sup>wt</sup> and PTEN <sup>mut</sup> ....	52
Figure 11: The role of PI3K/AKT pathway in MYC stability regulation ....	53
Figure 12: PTEN protein detection of T-ALL patient cells ....	54
Figure 13: Investigation of an inducible PTEN knockdown cell model DND4 ....	55
Figure 14: Correlation between PTEN mutation and glucocorticoid resistance using the example of Dexamethasone ....	56
Figure 15: Molecular validation of MYC overexpression cell model T-ALL1 ....	57
Figure 16: Genetic hallmarks of PTEN mutant cell lines ....	58
Figure 17: Validation of increased ABCA5 expression in T-ALL cell lines ....	59
Figure 18: High throughput drugscreening pipeline for leukemia ....	60
Figure 19: Focused heatmap of PI3K and AKT inhibitors ....	61
Figure 20: Drug response curves of PBMCs from three different healthy donors ....	62
Figure 21: Focused drug screening of PI3K and AKT inhibitors ....	62
Figure 22: Validation of AKT inhibition efficacy in T-ALL PDX samples. ....	63
Figure 23: Drug response curves of selected inhibitors of the inducible PTEN knockdown cell model DND41 ....	64
Figure 24: Synergy matrices of copanlisib with JQ1 ....	65
Figure 25: Biological validation of compound effectivity in MOLT4 ....	66
Figure 26: Synergy matrices of afuresertib with birabresib ....	67
Figure 27: Apoptosis measurement of three different PTEN <sup>mut</sup> cell lines treated with afuresertib, birabresib and the combination of both ....	69
Figure 29: Biological validation of afuresertib and birabresib with regard to cell cycle and caspase ....	70
Figure 30: Targeting strategy on molecular level ....	71
Figure 31: Biological validation of AURKAi with PI3Ki in PTEN <sup>mut</sup> cell line HPBALL ....	73
Figure 32: Introducing the SUPB15 cell line model and its imatinib resistant lineage model SUPB15 ImR. ....	74
Figure 33: The role of MEKi in an inducible PTEN knock down model DND41 ....	75
Figure 34: Synergy analysis of cobimetinib in combination with copanlisib in dependency of different stratification markers. ....	76
Figure 35: Biological validation of MEK and PI3K inhibitors ....	77
Figure 36: <i>In vivo</i> validation of copanlisib and JQ1 in MOLT4 xenotransplated mice ....	79
Figure 37: <i>In vivo</i> validation of afuresertib and birabresib ....	81
Figure 38: Strategy for the production of new dual inhibitors based on the combination of pharmacophore regions of the respective reference inhibitors. ....	82



Figure 39: Biological validation of 61 in comparison to 62 or 63 and their combination.....	85
Figure 40: Biological evaluation of dual HDAC/BRD4 targeting inhibitors .....	87
Figure 41: Cytotoxic activity of dual HDAC/BRD4 targeting inhibitors 20, 49 and 61 in comparison to the reference HDACi ricolinostat and reference BET inhibitor birabresib .....	88
Figure 42: Preliminary drug screening with two concentrations in three different cell lines ...	90
Figure 43: <i>In vitro</i> validation of first generation of small molecule HSP90-CTD inhibitors .....	91
Figure 44: <i>In vitro</i> validation of second-generation small molecule HSP90-CTD inhibitors ...	93
Figure 45: <i>In vitro</i> validation of third-generation small molecule HSP90-CTD inhibitors .....	96

## List of tables

Table 1: List of used machines and devices .....	19
Table 2: List of used cell lines.....	20
Table 3: List of consumables used for cell culture .....	20
Table 4: List of consumables used for transfection .....	23
Table 5: List of plasmids used for transfection .....	23
Table 6: List of doxycycline inducible shRNA plasmids used for transfection.....	23
Table 7: List of consumables used for RNA analysis .....	23
Table 8: List of primer mixes purchased from Qiagen (Hilden, Germany).....	24
Table 9: List of consumables used for drug screening .....	24
Table 10: Selection of compounds for leukemia-specific high throughput drug screening.....	24
Table 11: List of consumables used for protein analysis.....	29
Table 12: List of fluorochrome-conjugated antibodies and chemicals used for flow cytometry .....	29
Table 13: List of primary- and HSR-conjugated secondary antibodies used for Western .....	30
Table 14: List of secondary, HRP-linked antibodies.....	31
Table 15: List of consumables used for <i>in vivo</i> experiments .....	31
Table 16: List of software used in this thesis .....	32
Table 17: Absorbance spectrum of used antibodies and chemicals for flow cytometry .....	35
Table 18: qPCR Mix for one well of 96-well plates.....	37
Table 19: Machine settings for RT-qPCR .....	37
Table 20: Recipe for stacking gel .....	38
Table 21: Recipe for separation gel .....	38
Table 22: Vehicle for iv. injection (5 mg/kg) .....	47
Table 23: Vehicle for iv. injection (5 mg/kg) .....	47
Table 24: Vehicle for oral gavage (50 mg/kg) .....	48
Table 25: Vehicle for oral gavage (50 mg/kg) .....	48
Table 26: IC <sub>50</sub> values of copanlisib and auresertib in T-ALL cell lines .....	63
Table 27: Target activity of the first generation dual HDAC/BRD4 targeting inhibitors .....	83
Table 28: Target activity of the second generation dual HDAC/BRD4 targeting inhibitors.....	84
Table 29: IC <sub>50</sub> values of dual HDAC/BET compounds for different leukemia entities .....	86
Table 30: Results of extended drug screening of 2 <sup>nd</sup> and 3 <sup>rd</sup> generation HSP90 inhibitors.....	95

## Abbreviations

<b>µg</b>	Microgram
<b>µl</b>	Microliter
<b>AF 700</b>	Alexa Flour 700 (Fluorescence dye)
<b>ALL</b>	Acute lymphoblastic leukemia
<b>APC</b>	Allophycocyanin
<b>APS</b>	Ammoniumperoxidsulfate
<b>ATP</b>	Adenosine triphosphate
<b>AX</b>	Aminoxyrone
<b>B-cell</b>	B-lymphocyte: Bone marrow lymphocyte
<b>BET</b>	Bromodomain and extra terminal domain
<b>BMT</b>	Bone marrow transplantation
<b>BSA</b>	Bovine serum albumin
<b>CD</b>	Cluster of differentiation
<b>cDNA</b>	Complementary DNA
<b>CNS</b>	Central nervous system
<b>Ct</b>	Cycle of threshold
<b>dH<sub>2</sub>O</b>	Distilled H <sub>2</sub> O
<b>ddH<sub>2</sub>O</b>	Double distilled H <sub>2</sub> O
<b>DMEM</b>	Dulbecco's Modified Eagle Medium
<b>DMSO</b>	Dimethyl sulfoxide
<b>DNA</b>	Deoxyribonucleic acid
<b>dNTP</b>	Deoxynucleotide
<b>EDTA</b>	Ethylendiamintetraacetat
<b>ELISA</b>	Enzyme-Linked Immunosorbent Assay
<b>et. al</b>	<i>Lat: et alii</i> (and others)
<b>EtOH</b>	Ethanol
<b>ETP</b>	Early T cell precursor
<b>FACS</b>	Fluorescence Activated Cell Sorting
<b>FCS</b>	Forward scatter
<b>FDA</b>	Food and Drug Administration
<b>FITC</b>	Fluorescein isothiocyanate
<b>FSC</b>	Forward Scatter
<b>GAPDH</b>	Glycerinaldehyd-3-Phosphate-Dehydrogenase
<b>GFP</b>	Green fluorescent protein
<b>h</b>	Hours

## Abbreviations

---

<b>HAT</b>	Histone acetyltransferase
<b>HDAC</b>	Histone deacetylase
<b>HRP</b>	Horse Radish Peroxidase
<b>HSC</b>	Hematopoietic stem cell
<b>HTDS</b>	High-throughput drug screening
<b>i.p.</b>	Intraperitoneal
<b>i.v.</b>	Intravenous
<b>IC<sub>50</sub></b>	Half maximal inhibitory concentration
<b>ImR</b>	Imatinib resistant
<b>kDa</b>	Kilodalton
<b>mA</b>	Milliampere
<b>min</b>	Minutes
<b>ml</b>	Milliliters
<b>mM</b>	Millimole
<b>MRD</b>	Minimal residual disease
<b>mRNA</b>	Messenger RNA
<b>mut</b>	Mutated
<b>nm</b>	nanometer
<b>MTT</b>	Molecular targeted therapies
<b>MYC (c-Myc)</b>	Avian Myelocytomatosis Viral Oncogene Homolog
<b>NAD<sup>+</sup></b>	Nicotinamide adenine dinucleotide
<b>NK-cell</b>	Natural killer cell
<b>OS</b>	Overall survival
<b>PBMC</b>	Peripheral blood mononuclear cells
<b>PBS</b>	Phosphate buffered saline
<b>PCR</b>	Polymerase chain reaction
<b>PDX</b>	Patient derived xenograft
<b>PI</b>	Propidium iodide
<b>PI3K</b>	Phosphatidylinositol 3-kinase
<b>PPIA</b>	Peptidylprolyl isomerase A
<b>PTEN</b>	Phosphatase and Tensin homolog
<b>PS</b>	Phosphatidyl serine
<b>PVDF</b>	Polyvinylidene fluoride
<b>qPCR</b>	Quantitative PCR
<b>RNA</b>	Ribonucleic acid
<b>RNAi</b>	RNA interference
<b>ROI</b>	Region of interest

## Abbreviations

---

<b>rpm</b>	Rounds per minute
<b>RT</b>	Room temperature
<b>SD</b>	Standard deviation
<b>SDS</b>	Sodium dodecyl sulfate
<b>SDS PAGE</b>	SDS-Polyacrylamidgelelectrophoresis
<b>sec.</b>	Seconds
<b>SEM</b>	Standard error of the mean
<b>shRNA</b>	Small hairpin RNA
<b>SSC</b>	Side Scatter
<b>SCT</b>	Stam cell transplantation
<b>STR</b>	Short tandem repeat
<b>T cell</b>	T-lymphocyte: Thymus dependenT-lymphocyte
<b>Taq</b>	<i>Thermophilus aquaticus</i>
<b>TBS</b>	Tris-buffered saline
<b>TBS-T</b>	Tris-buffered saline Tween20
<b>TCR</b>	T cell receptor
<b>TEMED</b>	Tetramethylethylendiamin
<b>TR</b>	Therapy refractory (leukemia)
<b>Tris</b>	Tris-(hydroxymethyl)-aminomethan
<b>TKI</b>	Tyrosine kinase inhibitor
<b>V</b>	Volts
<b>vs.</b>	versus
<b>Western Blot</b>	WB
<b>WBC</b>	White blood count

## Summary

T-cell acute lymphoblastic leukemia (T-ALL) is a highly proliferative hematological disease, which is driven by genetic aberrations in hematopoietic progenitor cells. This malignancy occurs with a frequency of 10 to 15% of all acute lymphoblastic leukemia (ALL). With the great success of leukemia treatment in the past decades, the overall survival at five years from diagnosis has improved to nearly 80%. However, induction failure (IF) or relapse leads to a worse prognosis, ranging from 20% to 30% in children. Overall survival and event-free survival are dramatically reduced in these cases. Promising treatments for these cases do not yet exist. Therefore, finding novel therapy options is urgently needed. Up to date, one promising approach represents molecular targeted therapy (MTT). The aim of this work was to identify and validate novel and known drugs, which are suitable for therapy refractory and relapsed T-ALL patients. Therefore, T-ALL cell line models, and patient samples were characterized at the molecular level for known T-ALL driver mutations and subsequently tested for response to inhibitors using drug screening. One of the currently most discussed oncogenes is the transcription factor MYC, which plays a major role in T cell development. Attempts to inhibit MYC using agents in a direct pathway failed, so far. This led to a change in strategy to inhibit signaling pathways responsible for the maintenance and stability of the MYC protein such as the BRD4 protein. Post-transcriptional modifications of MYC are controlled by the Raf/MEK/ERK and PI3K/AKT signaling pathways, which protect MYC from proteasome-mediated degradation. The most promising inhibitors that restart MYC degradation were extensively tested in *in vitro* analyses and subsequently evaluated in a preclinical mouse model. The results show that the MTT method may have an important impact on future cancer therapies. The increased heterogeneity of tumors can thus be used to identify signaling pathways that are individually critical for tumor survival and therefore represent a weak point. A unique vulnerability could be identified in PTEN mutant T-ALL cell lines. These cells are particularly dependent on the PI3K/AKT signaling pathway. Inhibition of this pathway leads to effective apoptosis and cell death of tumor cells *in vitro*, both in cell lines and in patient-derived leukemia cells. In summary, this work provides a novel strategy for stratifying relapsed or treatment-resistant T-ALL with the biomarker PTEN, which represents a promising approach for a future treatment strategy by inhibiting the PI3K/AKT pathway.

## Zusammenfassung

Die akute T-lymphoblastische Leukämie (T-ALL) ist eine hoch proliferative hämatologische Erkrankung, die durch genetische Aberrationen in hämatopoetischen Vorläuferzellen angetrieben wird und 10 bis 15 % aller akuten lymphoblastischen Leukämien (ALL) darstellt. Mit den großen Erfolgen der Leukämiebehandlung in den letzten Jahrzehnten hat sich das Gesamtüberleben bis fünf Jahre nach der Diagnose auf fast 80 % verbessert. Patienten, die therapieresistent sind oder einen Rückfall erleiden haben eine deutlich schlechtere Prognose. Gesamtüberleben und ereignisfreies Überleben sind in diesen Fällen erheblich reduziert. Erfolgversprechende Therapiemöglichkeiten gibt es für diese Patienten kaum. Daher ist die Suche nach neuen therapeutischen Optionen dringend notwendig. Bislang stellt die zielgerichtete Therapie einen aussichtsreichen Ansatz dar. Das Ziel dieser Arbeit war es, neue und bekannte Medikamente zu identifizieren und zu validieren, die für refraktäre und rezidierte T-ALL-Patienten geeignet sind. Zu diesem Zweck wurden T-ALL-Zelllinienmodelle und Patientenproben auf molekularer Ebene für bekannte T-ALL-Treibermutationen charakterisiert und anschließend einem Wirkstoffscreening unterzogen. Das Onkogen MYC stand im Mittelpunkt der Charakterisierung, da es sich um einen Transkriptionsfaktor handelt, der ein tumortypisches Expressionsmuster hervorruft und als nicht inhibierbar gilt, da die Proteinstruktur kein individualisiertes Angriffsziel bietet. Dies führte zu einem Strategiewechsel hin zur Hemmung von Signalwegen, die für die Expression des MYC-Proteins verantwortlich sind, oder verschiedener Signalwege, die MYC vor dem Proteasom-vermittelten Abbau schützen. Die vielversprechendsten Inhibitoren wurden in *in-vitro*-Analysen ausgiebig getestet und anschließend in präklinischen Mausmodellen evaluiert. Die Ergebnisse deuten darauf hin, dass die zielgerichtete Therapie einen wichtigen Einfluss auf zukünftige Krebstherapien haben könnte. So eine vermeintliche Schwachstelle wurde in PTEN-mutierten T-ALL-Zelllinien identifiziert. Diese Zellen schienen besonders abhängig von dem PI3K/AKT-Signalweg zu sein. Die Inhibition dieses Weges führte zu einer effektiven Apoptose und einem anschließenden Zelltod der Tumorzellen. Zusammenfassend beschreibt diese Arbeit eine aussichtsreiche Strategie zur Stratifizierung von rezidivierter oder behandlungsresistenter T-ALL mit dem Biomarker PTEN, der einen vielversprechenden Ansatz für eine zukünftige Behandlungsstrategie durch Inhibition des PI3K/AKT-Signalwegs darstellt.

# 1. Introduction

## 1.1. Leukemia

Leukemia describes a non-solid tumor of white blood cells and the most common cancer in children between 0 to 14 years representing up to 25% among all cancer types [1]. Historically, the occurrence of a leukemia case was first correctly interpreted by Alfred François Donné in 1844, who described the pathological condition of an unusually high number of white blood cells, observed in a peripheral blood sample, regardless of an inflammation. The name for the disease was given two years later by the German pathologist Rudolph Virchow after the Greek term for “white blood”. Typical for leukemia is the high proliferation activity of the neoplasia followed by the complete loss of their physiological functions. Progenitor cells emerge from the hematopoiesis, which plays an important role for leukemia development. During hematopoiesis, the hematopoietic stem cells undergo several developmental steps that determine cell fate [2]. A schematic overview of the different cell types that differentiate from a hematopoietic stem cell is shown in Figure 1. Particularly early on, there is a decision where the cell takes on the developmental direction of either a myeloid cell or a lymphoid cell. Myeloid cells finally develop into red blood cells, platelets, or granulocytes. Lymphoid stem cells, on the other hand, may develop into B cells and subsequently into plasma cells, T cells, or NK cells. During the course of hematopoiesis, the stem or precursor cells may degenerate and cause either a leukemia of myeloid or lymphoid origin [3]. Usually, defective cells are highly controlled by the immune system, but genetic predispositions, mutations and environmental factors can promote errors in the immunoregulation [4]. The fact that these cells are impaired in differentiation and apoptosis mechanisms enables the cells to proliferate rapidly, accompanied by the displacement of other cells of hematopoietic origin in the bone marrow and the blood stream, which cause anemia, thrombocytopenia, and neutropenia [5, 6]. Referring to a short or long clinical history of symptoms, the type of leukemia is either termed “acute” or “chronic” leukemia, respectively. Therefore, leukemia can be divided into four major groups based on these categorizations: acute lymphoblastic leukemia (ALL), acute myeloid leukemia (AML), chronic lymphoblastic leukemia (CLL) and chronic myeloid leukemia (CML), with ALL being the most common disease among them in children. Moreover, ALL is responsible for around 30% of all malignancies in children and adolescents, making it the most common cancer type.

ALL arises from lymphoblastic progenitors such as cells from B-lineage, T-lineage and very rarely from NK-lineage.

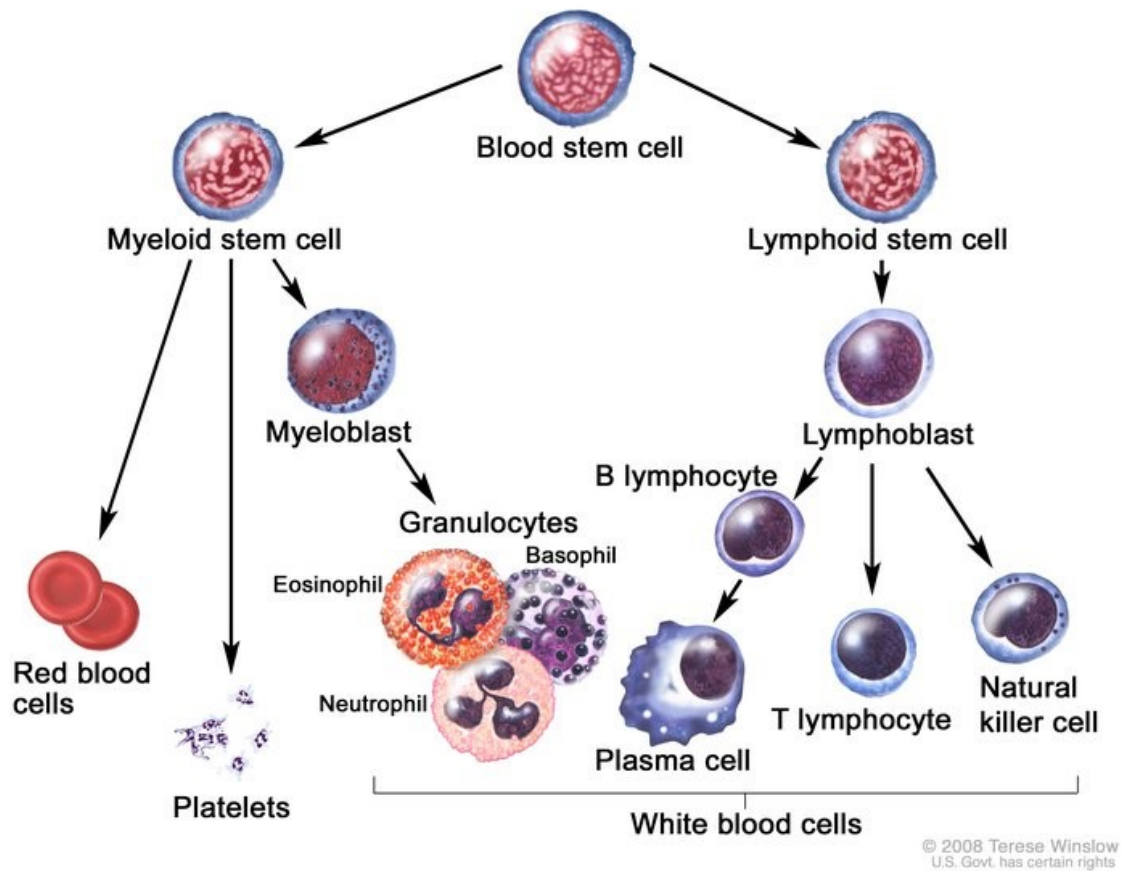


**Figure 1: Simplified representation of hematopoiesis of the major blood cells.**

Permission granted. Schematic representation of hematopoiesis of major immunological cell types.

## 1.2. Etiology of Pediatric ALL

In Europe, ALL is responsible for approximately 80% of all leukemia subtypes in children aged between 0 to 14 years [7]. ALL has an annual incidence of up to 40 cases per million children in industrialized western European countries and up to 30 to 35 cases per million in eastern European countries, but less than 20 per million in sub-Saharan Africa [8]. In addition, ALL is more common in boys than girls, but male sex is not suitable as a prognostic marker, even with higher incidences and poorer prognoses in boys [9]. From all ALL subtypes, B-cell acute lymphoblastic leukemia (B-ALL) occurs most frequently with 85% followed by T-cell lymphoblastic leukemia (T-ALL) with 10 to 15% and the very rare aggressive NK cell leukemia (ANKL) with less than 1%. The etiology of B-ALL is relatively advanced compared to T-ALL due to the



high frequency of this disease. The identification of disease-causing reasons and efforts in improving chemotherapy in B-ALL has increased the 5-year overall survival (OS) rate enormous in the past decades from around 20% in the 60s to over 95% in the 2010s. This is different in T-ALL cases. Although survival has also steadily increased in T-ALL, the 5-year OS rate is close to 80% [10]. The increased prognosis for T-ALL is also due to the similarities with B-ALL, so it is not surprising that T-ALL patients are treated commonly in the same way as B-ALL patients. Nevertheless, the optimization of chemotherapy is now reaching its limits. Although T-ALL treatment results in a relatively high chance of recovery, patients who are refractory to therapy usually have a poor prognosis and more importantly it is thus still one of the most common causes for cancer-related deaths in children [11, 12]. Altogether, the 10-year OS of relapsed patients remains relatively low with 21% +/- 8%, according to the Austrian Berlin-Frankfurt-Münster study group [13]. A better understanding of the etiology and the use of novel therapy options are the key for increased prognosis.

### **1.3. Clinical Presentation of ALL**

The most common symptoms associated with hematological malignancies are related to their impact on bone marrow infiltration. Typical symptoms and clinical findings are anemia, thrombocytopenia, and neutropenia, which reflects in the failure of normal hematopoiesis and thus, patients often suffer from pallor, fatigue, bone pain, petechiae, purpura, bleeding, and fever [14]. Lymphadenopathy, hepatomegaly, and splenomegaly are symptoms frequently accompanied with the diagnosis of ALL. In most cases lymphadenopathy and hepatomegaly are asymptomatic, whereas patients with splenomegaly suffer usually from stomach pain and back pain [15]. Extramedullary site involvement in the orbit, breast, urinal bladder or pancreas are less frequent [16]. Especially in younger patients, bone pain with a limp or refusal to walk can occur [17]. The involvement of the central nervous system (CNS) is generally rare with an incidence of 6% but it has a severe impact on prognosis and treatment [18]. The risk of CNS involvement also increases during a relapse and is partly responsible for poorer chances of survival [19, 20]. Importantly, T-ALL patients are associated with a higher incidence of CNS involvement than patients with other leukemia entities [18, 21]. Only a few molecules are known to drive CNS involvement with CCR7 as the most prominent one in T-ALL patients [22].

## **1.4. T-cell acute lymphoblastic leukemia**

T-ALL is an aggressive malignancy of T cells characterized by clonal proliferation and displacement of other lymphocytes in the bone marrow. Compared to B-ALL, T-ALL affects more older patients and is accompanied with an enlarged thymus, which cause breathing problems. Other than B-ALL, T-ALL may also spread to the cerebrospinal fluid in the early course of the disease and can trigger some severe problems. In addition to T-ALL, T cell derived neoplasms can also be termed as T-cell lymphoblastic lymphomas (T-LBL), which are characterized by mediastinal mass or an invasion of the lymph organs like thymus, lymph nodes or extranodal sites without exceeding 20% of the bone marrow content [23]. Cases with 20% or more bone marrow involvement are considered to be T-ALL. Since 2016, T-ALL and T-LBL were united by the World Health Organization (WHO) because of the similarities of the diseases and the treatment response. In the following, this work mainly relates to the T-ALL entity. To better understand the pathogenesis of T-ALL, it is necessary to consider the development of T cells.

## **1.5. T cell development**

As with all blood progenitor cells, the formation of T-lymphocytes begins in the bone marrow and then the precursor cell journeys to the thymus, where it passes through several zones of the thymus (Figure 2). The T cell fate begins as a hematopoietic stem cell (HSC) that first differentiates as a long-term repopulating stem cell into a short-term repopulating stem cell and then subsequently differentiates into a lymphoid primed multipotent progenitor (LMPP) that is able to migrate through the blood via chemotaxis processes to reach the thymus [24]. Once the LMPPs entered the thymus the cells are further called early T cell progenitors (ETP). ETPs are phenotypically double negative (DN) T cells, since they express neither cluster of differentiation (CD) marker CD4, nor CD8, which are two important T cell specific immune receptors. Development of DN cells is divided into 4 different stages and can be classified by the expression of specific receptors like c-KIT (negative in DN2), CD25 (negative in DN3) and CD44 (negative in DN4) [24]. During this process, ETPs are localized near epithelial stromal cells, which supply these cells with important growth factors like IL-7 and express Notch1 ligands [25]. Further, Notch1 seems to promote the cell survival through activation of the PI3K/AKT signaling pathway [26]. After the development of

the DN stages are completed the DN4 cells lose their dependence on Notch1 and IL-7 and start with the simultaneous expression of CD4 and CD8. Hence, the cells are now recognized as double positives (DP). At this stage, the unique specificity of the T-cell receptor (TCR) was carried out by DNA processing with recombinase activating genes (RAG), resulting in the so-called V(D)J translocation [27]. Subsequently, DP cells undergo a negative selection, if the TCR recognize self-antigens [28]. If this is not the case, the stronger binding affinity of CD4 or CD8 decides the cell fate of the cortical T cell. CD4<sup>+</sup> cells will develop finally into regulatory T cells and CD8<sup>+</sup> into effector T cells. However, even at this stage T cells are not in a physiologically active state. This happens once the TCR recognizes an antigen that turns a naïve T cell into an active T cell, leading to their proliferation and inducing the respective immune response. After activation, T cells remain long-term as memory T cells even after elimination of an infection to mount a more rapid immune response by rapidly converting to effector T cells upon re-exposure to the same antigen [29]. The onset of T-ALL can occur throughout all stages of T cell development. Depending on the developmental stage at which T-ALL occurs, T-ALL can be differentiated into multiple subtypes, which will have a particular impact on treatment options. Therefore, T-ALL classification is an important consideration.

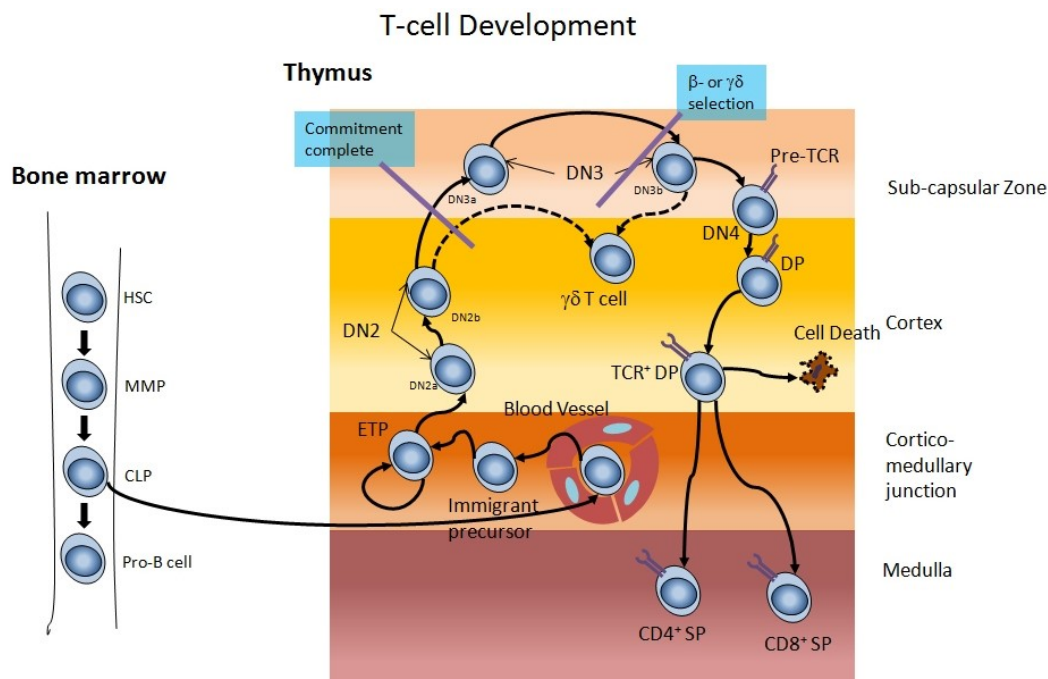


**Figure 2: Schematic figure of T cell development adopted from [30].**

The developmental steps of a T cell from its origin in the bone marrow to its final maturation in the thymus. The developmental steps are dependent upon the exact localization in the thymus.

## 1.6. T-ALL classification

To identify the T-ALL phenotype and differentiate it from B-ALL phenotype or other leukemic diseases, immunophenotyping via flow cytometry is required. In the diagnostic, fluorescence-conjugated antibodies are used for peripheral blood (PB) samples that bind on specific CD molecules, which are present on the surface of blood cells. T-ALL can be classified with the presence of typical T cell associated surface molecules like TCR CD3, co-receptors CD4 and CD8, T cell surface glycoprotein CD5, T cell antigen CD7, T cell surface antigen CD2 and the T cell surface glycoprotein CD1a. Besides that, cells of the T lineage are exclusively positive for cytoplasmic CD3 (CyCD3) and Terminal deoxynucleotidyl transferase (TdT), which belongs to the group of DNA polymerases and are important for the V(D)J diversification [27]. Depending on the appearance of T cell specific differentiation markers and their combinations, subtypes of T-ALL can be identified. Following the 1995 EGIL classification of leukemias, T-ALL can be divided into 5 groups, including ETP-ALL as well as pro-T, pre-T, cortical, and mature T-ALL [31]. The differentially expressed CD molecules on the surface and in the cytosol are schematically shown in figure 3. The most rudimentary subset belonging to T-ALL is ETP-ALL and due to the early hematopoietic stage expresses a relatively high number of stem cell markers consisting of CD34, CD33, CD117, CD65, HLA-DR, in addition to the T-cell specific surface molecules CD5 and CD7 and the cytosolic cyCD3. Pro- and pre-T-ALL are subsets that express the fewest receptors on their surface. At the stage in which a T cell's cell fate is ultimately initiated, they lose the stem cell markers on their surface that are characteristic of stem cells. Pro-T-ALL express CD7 in combination with CyCD3 and TdT. Pre-T-ALL additionally express CD2 and CD5.

Pro- and pre-T-ALL cases are often recognized as early-T-ALL and make up about 23% of all T-ALL, referring to a patient cohort of 744 adult T-ALL cases [32]. The most common subtype of T-ALL is the cortical T-ALL (coT-ALL) or also known as thymic-T-ALL, with an incidence of around 56% [32]. As the name suggests, coT-ALL arises in the thymus and show an arrest of the differentiation during the cortical stage [33-35].

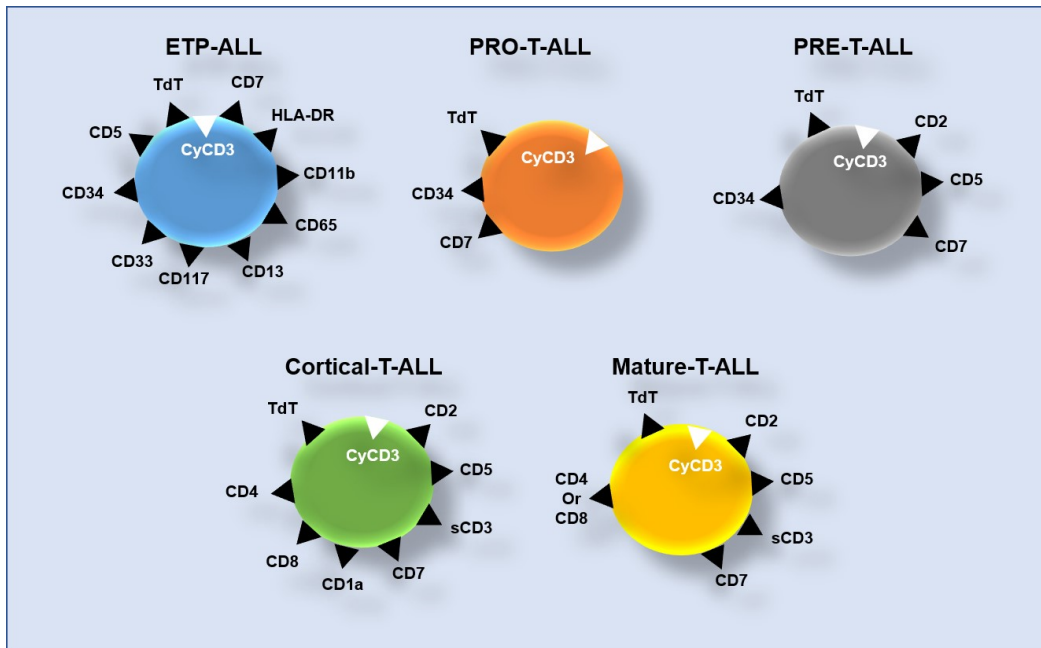


**Figure 3: Simplified representation of cell marker for T-ALL classification modeled on [36].**

The corresponding cell markers on the surface or in the cytosol are shown to distinguish the individual T-ALL subtypes. Each subset of T-ALL harbors a characteristic set of biomarkers.

The expression of CD1a and the co-expression of the co-receptors CD4 and CD8 are typical for this subtype. Neoplasms that originate from T cells, which have already completed their development are called mature or medullary T-ALL. They are characterized by the expression of CD3 on the surface (sCD3) and one of the co-receptors, either CD4 or CD8. Additionally, mature-T-ALL cells do not express CD1a anymore and since the V(D)J recombination has been completed at this stage, TdT is also no longer expressed [27]. Mature-T-ALL were the rarest group in the study cohort of 744 adult T-ALL, with an incidence of around 21% [32]. Despite the lack of significant conclusions about disease severity, the two major types of pro- and pre-T-ALL among the 5 groups represent an unfavorable prognosis for patients [37]. These patients often undergo more intensive therapy from diagnosis. Nevertheless, the frequent ambiguities in surface molecules provide much room for better stratification, which is often a challenge for choosing the optimal therapy. In this context, WHO published guidelines in 2016 for the uniform identification of T-ALL subtypes, based on the 2008 work of Borowitz et al. [38]. One of the results of the evaluation of leukemia cases in recent years showed that the recently introduced sup-group of ETP-ALL has a significantly worse prognosis and should be urgently considered in the selection of therapeutic approaches [39]. ETP-ALL exhibit similarities to hematopoietic stem cells and thus can be classified by the presence of hematopoietic stem cell markers such

as CD13, CD33, CD34, CD117, CD11b, CD65, and HLA-DR, as well as T cell specific markers such as CD5, CD7, CyCD3, and TdT [40]. Furthermore, ETP-ALL show similarities to hematopoietic stem cells and myeloid progenitor cells through their gene expression profile [41, 42]. The classification of ETP-ALL is recognized as a provisional entity, since previous studies has shown that the overall survival of ETP-ALL vary fundamentally from the other T-ALL subgroups with a poorer prognosis, as it was demonstrated in a cohort of 91 Japanese children, where 5% matched the ETP-ALL criteria [43]. ETP-ALL patients are meanwhile categorized as high-risk patients and treated special therapy protocols, as well as the possibility of a stem cell transplantation.

### **1.7. T-ALL treatment**

T-ALL treatment begins immediately after the patient is diagnosed. Based on the current WHO proposal to classify T-ALL as high-risk, containing all ETP-ALL, pro- and pre-T-ALL cases and normal-risk groups, containing cortical- and mature T-ALL. In most cases, malignant lymphocyte reduction is achieved by the induction therapy using glucocorticoids such as prednisolone or dexamethasone, both of which have similar therapeutic success in pediatric T-ALL patients, raising the 5-year OS to approximately 80% [44]. Importantly, dexamethasone appears to be more suitable than prednisolone for the treatment of T-ALL because of its greater efficacy in cases of CNS involvement [45]. However, the therapeutic success is lower if the CNS is involved, because it is associated with a higher relapse incidence [46]. Though, the use of intrathecal chemotherapy and cranial irradiation improved the outcome of CNS involved patients, but the use of these therapies is relatively harmful for patients and can cause severe and long lasting side effects [46]. In general, the use of dexamethasone harbors some risks, ranging from life-threatening infections to neurocognitive impairment, yet the side effects are offset by a relatively high chance of cure [45, 47]. At the end of the therapy induction, one further key prognostic determinant in T-ALL is the minimal residual disease (MRD) response [38]. Patients with persistent MRD negativity are classified as refractory to therapy (TR). In contrast, a patient who initially shows response to therapy and later develops relapse is classified as a relapsed T-ALL case. TR and relapsed T-ALL patients have a generally poorer outcome, which has an important influence on the following treatment options. Like ETP-T-ALL patients, TR and recurrent T-ALL cases belong to a high-risk group whose course of therapy must be

adapted. Therefore, treatment options of TR, relapsed T-ALL or ETP-ALL include poly chemotherapy, which harbor both, toxic side effects at high dosages [48, 49]. As an alternative treatment, nelarabine has been shown to be effective in patients with relapsed and TR T-ALL [50, 51], however this drug also poses severe and irreversible neurotoxic side effects, which requires a well-considered risk-benefit estimation [52, 53]. Still, in children TR T-ALL remains the most common cancer-related cause of death [11, 12]. Current alternative therapy options are neither promising nor harmless for patients. The bone marrow transplantation (BMT) is actually the recommended therapy option for TR or relapsed T-ALL patients, if a suitable stem cell donor matches the criteria. Consequently, many efforts are being made to move away from the use of highly toxic chemotherapeutic agents and to promote the development of drugs that address individual targets. Although T-ALL is a genetically heterogeneous disease, some disease-causing genetic alterations that occur frequently has already been discovered and described.

## **1.8. Genetic landscapes of T-ALL**

A strategy to stratify risk types of leukemia is the identification and the decryption of disease specific gene mutations. T-ALL is a very heterogeneous disease with a few mutations that occur frequently and are therefore linked to play a distinctive role in the appearance of T-ALL. There are two types of genetic abnormalities: first, chromosomal translocations, which are often affecting transcription factors that drive the expression of oncogenes and second, mutations in genes of important proliferation or cell cycle regulators.

### **1.8.1. Translocations**

T-ALL associated translocations are often involved in the relocation of the coding sequence of diverse transcription factors downstream of the TRC receptor, assuming that errors may occur during V(D)J recombination by RAG [54]. In addition, basic helix-loop-helix transcription factors are known to play a major role in the development of T-ALL, such as TAL1, TAL2, LYL1, BHLB1, LMO1, TLX/HOX11, TLX/HOX11L2, and HOXA cluster genes [55-58]. Translocations of the LIM-only domains LMO1 and LMO2 are quite common as well and were identified as T-ALL driving factors [59, 60]. Moreover, the combination of the listed genes that are commonly associated in typical

T-ALL translocations can increase the probability of T-ALL formation. For example, the combination of LMO2 and TAL1 translocation in a genetic engineered mouse model showed stable T-ALL development [61].

### **1.8.2. Mutations**

Point mutations occur even more frequently than translocations and have an important function in the etiology of T-ALL. One of the first highly discussed risk stratification in T-ALL were activating Notch1 mutations that can be observed in more than 50 to 60% of all T-ALL cases [62-67]. Notch signaling is an important regulator for T cell development and regulates proliferation, cell development and thus controls the proper differentiation [68]. However, using activating Notch1 mutations as a risk stratification failed so far due to controversial findings. On the one hand, activating Notch mutations are described to induce proliferation, invasion and chemo resistance [69], and on the other hand, Notch1 mutations were correlated to improved outcomes in T-ALL patients [70, 71]. However, it is interesting to note that increased Notch signaling is also highly related to the stabilization and expression of another important oncogene in the T-ALL, which is MYC [72, 73].

## **1.9. MYC**

The MYC gene (or also known as c-Myc) was first discovered in cells from patients with Burkitt's lymphoma, whereas overexpression of MYC was identified as the driving factor of the disease [74]. It resembled the already known chicken viral myelocytomatosis oncogene (v-Myc, or viral Myc). The human version of the protein was consequently named cellular Myc (c-Myc). Nowadays, the protein is mainly referred to MYC when it is not the N- or L- variant. MYC is a member of the basic helix-loop-helix leucine zipper proteins, which co-interacts together with the MYC associated factor X (MAX) to form a heterodimer that is able to identify enhancer box (E-Box) sequences and induce its transcription [75-77]. The fact that nearly 15% of all human genes are regulated with these E-Box sequences by MYC makes it an important transcription factor [78-80]. Therefore, it is not surprising that among MYC-controlled genes are key cellular functions, including differentiation, proliferation, and apoptosis regulators, to name the most important ones (Figure 4) [80, 81]. Considering the main functions of MYC as a transcription factor, it is not surprising that the vast majority of



all human cancers exhibit dysregulation of MYC. Several downstream genes controlled by MYC are so-called oncogenic drivers, which promote for instance the uncontrolled proliferation by inducing the expression of cell cycle dependent proteins [82, 83] or the tight regulation of apoptosis providing escape mechanisms [84]. Hence, it is unsurprising that the aggressiveness of leukemia such as T-ALL is mainly mediated by MYC and a knockdown lead to significantly higher survival rates in a T-ALL developing transgenic mouse model [85]. Further discussion of the MYC's role in T-ALL is provided below.

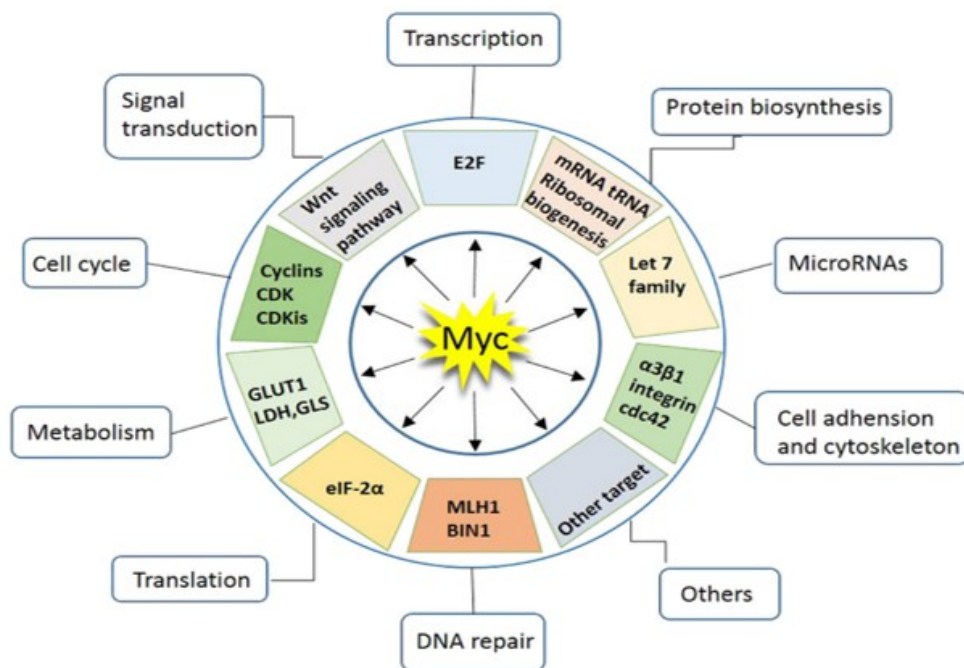


**Figure 4: Overview of MYC-regulated genes and the respective cellular function adopted from [86].**

MYC regulates around 15% of all human genes, which are associated in diverse cell mechanisms. Indicated in this figure are the most prominent genes regulated by MYC and the corresponding cell functions.

### 1.9.1. The role of MYC in T-ALL

In recent years, MYC came into the focus as a potential therapeutic target for pediatric T-ALL, suggesting that overexpression increases the probability for relapse or induction failure [85, 87]. MYC is a global transcription factor during early developmental stages, in a variety of different cell types. Generally, MYC expression is upregulated during T cell development, especially in the late DN CD4<sup>+</sup>CD8<sup>-</sup> stage, where it is regulating T cell proliferation [88]. This time point is crucial for T-ALL

development, if MYC remains dysregulated. Overexpression of MYC can be found in more than 60% of T-ALL patients, supporting the assumption that MYC plays a pivotal role in T-ALL development [89]. Interestingly, translocations that directly affect MYC expression in T-ALL patients are relatively rare at around 1 to 6% [87, 90] and direct targeting via dimer disruptions of MYC failed so far due to low potency and off-target effects of these inhibitors [91]. Thus, increased MYC expression can be explained due to a large extent by indirect MYC regulation via a plethora of regulatory/signaling pathways [92-94]. Consequently, MYC has come to the front as an interesting target for MTT. However, direct targeting of MYC is still a major hurdle due to its hard-accessible protein structure [91]. Therefore, indirect targeting of MYC via inhibition of its regulators seems to be a promising alternative [86].

### **1.9.2. Indirect Targeting of MYC**

Indirect targeting of MYC can take place at different levels. Both upstream signaling pathways that regulate MYC transcription and regulatory signaling pathways that prevent proteasome degradation of MYC are suitable indirect targets, blocking either the transcription of MYC or inducing its degradation, respectively [86]. The major signaling pathways related to MYC with T-ALL are shown in Figure 5 and represent a summary of the approaches discussed in this work to capture successful indirect targets to render MYC harmless.

#### **1.9.2.1. Upstream pathways**

Beginning with upstream signaling pathways, activating Notch1 mutations were the first to be associated with MYC as an important expression-driving factor, as inhibition of Notch1 by gamma secretase inhibitors (GSI) effectively blocked MYC mRNA expression in T-ALL cell line models [73]. Later, the use of GSI was used in clinical trials for T-ALL patients but failed due to the low toxicity against T-ALL and the significant gastrointestinal toxicity derived from Notch1 inhibition in the gut [95]. The search for further indirect target proteins that cause a reduction of the MYC protein by inhibition has continued. Hence, the focus was on an epigenetic modulator BRD4, a member of BET family that is one further known direct upstream regulator of MYC transcription [96, 97]. It turned out to be an effective target initiating the decrease of MYC expression and tumor volume in human squamous carcinoma [97]. The

connection to the use of BET inhibitors in T-ALL was rapidly made, demonstrating that JQ1 had successfully functioned to reduce tumor load with increasing the overall survival in a T-ALL developing mouse model [85]. This success is also reflected in the number of BET inhibitors currently being tested in clinical phases. However, the hope of finding an effective agent is tempered with limited clinical response in terms of relapse and inconsistent effects on MYC expression levels based on alternative MYC regulatory pathways that lead to increased MYC stability and thus induce tumor cell escape mechanisms [98, 99].

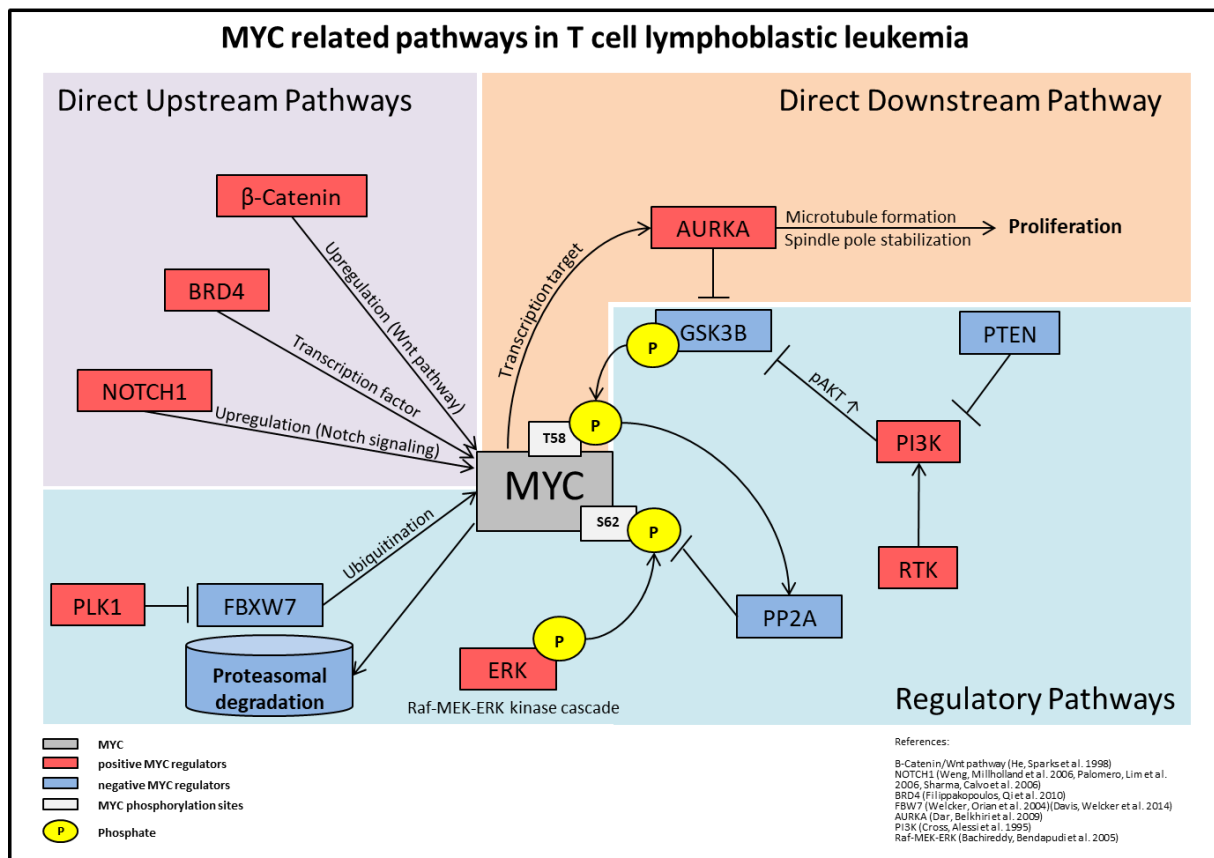


**Figure 5: MYC regulatory pathways in T-ALL.**

Indirect MYC-associated factors are either upstream like the  $\beta$ -catenin/ Wnt-signaling pathway, Notch1 pathway and the transcription factor BRD4 [67, 92, 97, 100, 101]. Direct downstream pathway aurora kinase A (AURKA) is associated to the spindle pole formation during the proliferation and might have an indirect effect on MYC stability due to GSK3 $\beta$  inhibition [102]. GSK3 $\beta$  is an important factor in the regulation of MYC by transferring a phosphate to the T58 site of MYC. Once MYC is phosphorylated at the T58 site, the phosphate at the S62 site, which serves to protect MYC from proteasome degradation, is removed by PP2A. Positive MYC regulators are for example the PI3K/AKT- and the Raf/MEK/ERK pathway [103, 104]. Proteasome degradation is mediated by MYC ubiquitination via FBXW7 as soon as phosphate at site S62 is removed [105].

### 1.9.2.2. Regulatory pathways

Not only upstream targets are suitable for efficient MYC reduction. The fact that MYC is usually tightly regulated by multiple regulatory pathways opens the possibilities for alternative inhibition strategies. MYC regulation at the protein level is mainly under the control of intracellular signaling pathways. Therefore, it is not surprising that mutations in such signaling pathways occur relatively frequently in T-ALL patients. Activating mutations of the PI3K/AKT pathway are the most common mutations, which is mainly caused by mutations in the PTEN (Phosphatase and tensin Homolog) gene that is found in around 14% of T-ALL patients [106-109]. The clinical relevance of PTEN mutations in T-ALL is evident, as survival rates are significantly lower in PTEN-mutated patients compared to PTEN wild-type patients [110, 111]. Moreover, dysfunction of PTEN leads to increased MYC and it can be linked to the reduction of OS and higher relapse rates in T-ALL [93, 110, 112-115]. The main function of PTEN is controlling the PI3K/AKT signaling pathway by dephosphorylating phosphatidylinositol(3,4,5)P3 (PIP3) to phosphatidylinositol(4,5)P2 (PIP2), counteracting AKT phosphorylation and the downstream mechanistic target of rapamycin (mTOR) signaling [116]. Inactivating PTEN mutations lead to increased PI3K/AKT signaling that promote MYC stability due to decreased GSK3 $\beta$  activation, via inhibition by phosphorylated AKT [117, 118]. Usually, GSK3 $\beta$  induce MYC proteolysis by phosphorylation of threonine 58 (T58) and following dephosphorylation of serine 62 (S62) by protein phosphatase 2a (PP2A) [119, 120]. Once the phosphate is removed from S62, FBXW7 binds to MYC and ubiquitinates it for subsequent proteasome degradation (Figure 5) [121, 122]. On the other side, MYC stability is maintained by phosphorylation of the S62 site, which is initiated by the Raf/MEK/ERK pathway. Although mutations in the Raf/MEK/ERK pathway rarely occur in T-ALL, these mutations can have a major impact on MYC stability and should be considered as targets for possible indirect MYC inhibition [104, 123-125].

### 1.9.2.3. Downstream pathways

Another way to suppress the MYC protein is to inhibit the direct downstream targets initiated by MYC. Although MYC has a range of downstream targets that might have an influence on MYC stability the focus here is set on one specific downstream target that plays a pivotal role in proliferation, the AURKA (Figure 5). The particular feature

of AURKA is that it has already been demonstrated that, just like the PI3K/AKT signaling pathway, it also has an influence on GSK3 $\beta$  and could thus contribute to the stabilization of MYC [102]. AURKA and its family member Aurora Kinase B (AURKB) are under the control of MYC and regulate the spindle pol formation, which is essential for the maintenance of the malignant state of the tumors [126]. The use of AURKA inhibitors in combination with other chemotherapeutic agents showed promising *in vitro* and *in vivo* effects and are currently being tested in clinical studies on patients with myeloid leukemia [127, 128]. In T-ALL, the role of AURKB was investigated recently and inhibition showed effective reduction and destabilization of MYC with concomitant cell death, underlining the critical role of aurora kinases in T-ALL [129].

### **1.9.3. Novel approaches to target MYC**

Another possibility of what is currently being investigated to indirectly inhibit MYC, are epigenetic factors such as histone deacetylases (HDACs), and oncogenic chaperone proteins such as heat shock protein 90 (HSP90). The two targets HDACs and HSP90 are currently an exciting topic in cancer science and are addressed as experimental agents next to the commercially available compounds in this work.

#### **1.9.3.1. HDACs and MYC**

The family of HDAC proteins comprise in total 18 members that are grouped into four classes, whereas all classes share the same task to deacetylate  $\epsilon$ -N-acetyl-lysine amino acid residues [130]. HDAC class I include HDAC1, -2, -3, and -8, while HDAC class II, which in turn can be divided into class IIa, consisting of HDAC4, -5, -7, and -9, and class IIb, consisting of HDAC6 and -10. The fourth group is simply referred to as class IV and contains only HDAC11 [130]. HDACs are counteracting epigenetic modulators of histone acetylases (HATs) that provide accessibility from DNA, which can be achieved by acetylation. Deacetylation by HDACs leads to increased condensation of the DNA that suppresses the accessibility of distinctive gene regions ending up with the transcriptional reduction of specific genes [131]. Epigenetic changes initiated by HDACs are a fundamental event in the development and progression of cancer and therefore a rational target for novel cancer therapies [132]. A key role may be performed by the balance between acetylation and deacetylation of various proteins, which are often found to be dysregulated in cancer patients [133]. HDACs

were recently reported to increase cancer cell survival by silencing the proapoptotic protein TRAIL, ensuring the escape of apoptosis mechanisms initiated by death receptor 4- (DC4) or DC5 binding [134-136]. Interestingly, MYC is a marker of TRAIL sensitivity in cancer cells, as demonstrated by several studies [137-139]. Hence, MYC binds to the TRAIL promoter region and is thus essential for its silencing. The use of HDAC inhibitors can induce acetylation of MYC at the K323 site, leading to its downregulation and thus releasing TRAIL expression, opening the possibility of inducing apoptosis [140]. Interestingly, in addition to histones, HDAC1-3 also deacetylate the tumor suppressor protein TP53, which is thereby altered in its activity and stability, leading to apoptosis escape mechanisms and increased cell cycle [141, 142] probably due to reduced transcriptional repression of MYC [143]. Another tumor suppressor that can be manipulated by HDACs through modifications of the mTOR pathway is PTEN [142], and thus may lead to increased MYC stability. Another upregulating factor of MYC could be HDAC3, as it is associated with the upregulation of Notch signaling pathways, which could ultimately also be a driving factor for the development of T-ALL [144]. More precisely, HDAC3 controls acetylation of the Notch1 intracellular domain (NICD1), which is known to be a hallmark of the leukemogenic process in T-ALL, taking over regulating tasks like proliferation, survival, and differentiation [145]. Ferrante and her colleagues demonstrated the dependence of Notch signaling on HDAC3 through mutation or inhibition of HDAC3, underscoring the rationale for HDAC inhibitory approaches, particularly with respect to T-ALL. In addition, the numerous links to MYC, either through direct acetylation or regulation of MYC regulators, make it a promising candidate for indirect MYC targeting. A combination of a secondary inhibitor that decreases MYC should increase the therapeutic effect. Therefore, compounds that inhibit HDACs together with BRD4, which are called dual inhibitors, were used in this work. In previous studies, both targets were shown to influence the decrease of MYC, and thus could have an anti-cancer effect [146-149].

The experimental compounds discussed in this thesis are dual HDAC/BRD4 targeting inhibitors, which potentially could be an effective strategy to target MYC, since both HDAC and BRD4 have an impact on the transcription and post-modification of MYC. HDAC inhibition is known to have an impact on the modulation and acetylation of MYC, affecting its stability and function [140]. The combination of HDAC and BRD4 inhibition

has already shown promising results in both pancreatic cancer and leukemia and has therefore attracted much attention, as both targets have an impact on MYC expression or functionality [147, 148, 150, 151].

### **1.9.3.2. HSP90, a MYC chaperone**

HSP90 is a molecular chaperone, which is important for the homeostasis of proteins and plays a central role in *de novo* protein folding, protein translocation and quality control of proteins [152]. Back in 2009, HSP90 was introduced as a new target for cancer therapy, triggering the research efforts to find suitable inhibitors [153]. Since then, knowledge of HSP90 has improved and client proteins have been identified. Interestingly, MYC is next to other oncogenes a major client protein and is therefore dependent upon proper folding by HSP90, making HSP90 even a more rational target for cancer treatment [154]. However, in several clinical trials involving HSP90 inhibitors a large proportion of patients experienced high grade toxicity such as ocular toxicity leading to retinal diseases (e.g. night blindness) [155]. One reason for this could be the heat shock response (HSR) caused by N-terminal inhibition of the HSP90 protein, which counteracts the tumor suppressive effect [156]. A few years later, it was found that inhibition of the CTD region also had an anti-cancer effect but without provoking an HSR [157, 158]. Consequently, the establishment of novel HSP90-CTD inhibitors was initiated to revive HSP90 as a target for targeted cancer therapy. As a heterodimeric protein, HSP90 consists of a  $\alpha$ - and a  $\beta$ -monomer linked by the CTD. The combination of the  $\alpha$ - and  $\beta$ -monomers is required for proper function and thus a weak point that can be exploited for selective inhibition. Inhibition of CTD presents several advantages. First, inhibitors of the CTD have been shown to have lower toxicity and second, they do not induce HSR. Recently, this was demonstrated with a peptidomimetic Aminoxyrone (AX) that disrupts the heterodimerization of HSP90 and thus showed promising anti-cancer effectivity in an *in vitro* study in TKI resistant AML cell lines without any HSR induction [159]. However, AX and other CTD inhibitors of HSP90 are still not potent enough to become interesting for clinical studies. Therefore, novel inhibitors based on the previous published structure of AX were generated with several modifications on the pharmacophore, as well as reduction of the molecular size at the Institute for Pharmaceutical and Medicinal Chemistry under the supervision of Prof. Dr. Thomas Kurz.

## 1.10. Aim of the thesis

The fact that refractory and relapsed T-ALL is still one of the leading causes of cancer-related deaths in children underscores the need for new innovative cancer therapies. Gleevec (imatinib), a tyrosine kinase inhibitor used in CML patients with the difficult-to-treat BCR-ABL gene fusion, also known as Philadelphia chromosome (Ph+), showed promising therapeutic activity, making it a true success story in novel cancer therapy approaches [160, 161]. Such a success story has yet to be achieved for TR and relapsed T-ALL but may be attainable as more disease-driving factors are identified and pharmacology now provides chemical entities for a variety of potential targets. In the search for new therapeutic approaches for T-ALL, researchers have come across the proto-oncogene MYC, which, in addition to its pro-oncogenic properties such as apoptosis induction, proliferation induction and differentiation arrest, causes cancer cells to resist therapy. However, due to its undruggable structure and the location in the nucleus makes it difficult to target directly with small molecules. Therefore, the following aims were addressed:

1. Characterization of indirect pathways associated to MYC in T-ALL cell models and patient derived xenograft (PDX) cells.
2. Dependent upon these findings respective targets will be chosen to create a high throughput drug screening (HTDS) library.
3. Using the HTDS-library will indicate drug sensitivity profiles that will be matched with the molecular characteristics.
4. In vivo validation of compounds using a xenograft mouse model.
5. Investigation of novel MYC targeting inhibitors (dual HDAC-BRD4 and HSP90) provided by Prof. Dr. Finn K. Hansen and Prof. Dr. Thomas Kurz, respectively.



## 2. Materials and methods

### 2.1. Used machines and devices

Table 1: List of used machines and devices

Device	Company
-20°C Freezer	Liebherr (Kirchdorf an der Iller, Germany)
37°C Incubator	Thermo Fisher Scientific (Schwerte, Germany)
-80°C Ultra Freezer	Thermo Fisher Scientific (Schwerte, Germany)
Centrifuge Heraeus Fresco 21	Thermo Fisher Scientific (Schwerte, Germany)
Centrifuge Pico Microcentrifuge	Thermo Fisher Scientific (Schwerte, Germany)
CFX384 Touch Real-Time PCR Detection System	Bio-Rad (Düsseldorf, Germany)
Chemie Doc	Bio-Rad (Düsseldorf, Germany)
CO <sub>2</sub> -Incubator	Binder (Tuttlingen, Germany)
CytoFLEX Flow Cytometer	Beckman Coulter (Krefeld, Germany)
D300e Digital Dispenser	Tecan (Crailsheim, Germany)
GeneAMP PCR System 2700	Applied Biosystems (Schwerte, Germany)
IVIS Spectrum	PerkinElmer (Rodgau, Germany)
Laminar Flow Hood	Thermo Fisher Scientific (Schwerte, Germany)
LAS-300 Imaging System	Fujifilm (Düsseldorf, Germany)
Maxwell RSC Instrument	Promega (Mannheim, Germany)
Mini Centrifuge	Bio-Rad (Düsseldorf, Germany)
Multidrop Combi Reagent Dispenser	Thermo Fisher Scientific (Schwerte, Germany)
NanoDrop Spectrophotometer ND-1000	Peqlab (Erlangen, Germany)
PCR Cycler 2720	Thermo Fisher Scientific (Schwerte, Germany)
Power Supply Consort EV231	Sigma-Aldrich (Taufkirchen, Germany)
Precision balance	KERN & SOHN (Balingen, Germany)
ProteinSimple Jess	Bio-Techne (Wiesbaden, Germany)
Roller Mixer	Ratek (Victoria, Australia)
See-saw rocker SSM4	Stuart (Staffordshire, UK)
Spark 10M Multimode microplate reader	Tecan (Crailsheim, Germany)
Stir Heater IKA RET	Thermo Fisher Scientific (Schwerte, Germany)
Thermo Block	Eppendorf (Hamburg, Germany)
Vi-Cell-XR	Beckman Coulter (Krefeld, Germany)
Vortex Genie 2	neoLab (Heidelberg, Germany)
Water Bath	GFL (Burgwedel, Germany)

## 2.2. Consumables for cell culture

Unless otherwise listed, plastic consumables from the companies Sarstedt, Nümbrecht, Eppendorf, Hamburg and Greiner Bio-One, Frickenhausen were used.

### 2.2.1. Cell lines

All used cell lines were frequently tested by STR-analysis to avoid cross contaminations.

**Table 2: List of used cell lines**

Cell line name	Cell entity	Distributor
CCRF/CEM	T-ALL	DSMZ (Braunschweig, Germany)
DND41	T-ALL	DSMZ (Braunschweig, Germany)
HEK293T	Kidney Cell	DSMZ (Braunschweig, Germany)
HPBALL	T-ALL	DSMZ (Braunschweig, Germany)
HSB1	T-ALL	DSMZ (Braunschweig, Germany)
JURKAT	T-ALL	DSMZ (Braunschweig, Germany)
K562	AML	DSMZ (Braunschweig, Germany)
KCL22	AML	DSMZ (Braunschweig, Germany)
KOPTK1	T-ALL	DSMZ (Braunschweig, Germany)
KOPTK1	T-ALL	DSMZ (Braunschweig, Germany)
LOUCY	T-ALL	DSMZ (Braunschweig, Germany)
MOLT4	T-ALL	DSMZ (Braunschweig, Germany)
MSC	Mesenchymal Stem Cell	DSMZ (Braunschweig, Germany)
P12 ICHIKAWA	T-ALL	DSMZ (Braunschweig, Germany)
PEER	T-ALL	DSMZ (Braunschweig, Germany)
SUPT1	T-ALL	DSMZ (Braunschweig, Germany)
TALL1	T-ALL	DSMZ (Braunschweig, Germany)

### 2.2.2. Media and supplements for cell culture

**Table 3: List of consumables used for cell culture**

Consumable	Company
Annexin V Buffer	BD Biosciences (Heidelberg, Germany)
CD45 MicroBeads, human	Milteniy Biotec (Bergisch Gladbach, Germany)
Cell strainer	pluriSelect (Leipzig, Germany)
Dimethyl sulfoxide (DMSO)	Sigma-Aldrich (Taufkirchen, Germany)

<b>Consumable</b>	<b>Company</b>
<b>DMEM GlutaMAX</b>	Thermo Fisher Scientific (Schwerte, Germany)
<b>Doxycycline</b>	Thermo Fisher Scientific (Schwerte, Germany)
<b>Dulbecco's phosphate buffered saline (PBS)</b>	Sigma-Aldrich (Taufkirchen, Germany)
<b>Erythrocyte lysis buffer (ACK)</b>	In-house production (Apotheke)
<b>Heat Inactivated Fetal Calf Serum (FCS)</b>	Sigma-Aldrich (Taufkirchen, Germany)
<b>MACS buffer</b>	Milteniy Biotec (Bergisch Gladbach, Germany)
<b>Magnetic columns MS</b>	Milteniy Biotec (Bergisch Gladbach, Germany)
<b>Magnetic stand</b>	Milteniy Biotec (Bergisch Gladbach, Germany)
<b>Penicillin (10.000 U/mL)-Streptomycin (10 mg/mL) (P/S)</b>	Sigma-Aldrich (Taufkirchen, Germany)
<b>Puromycin</b>	Thermo Fisher Scientific (Schwerte, Germany)
<b>RPMI 1640 GlutaMAX</b>	Thermo Fisher Scientific (Schwerte, Germany)
<b>TrypLE Express Phenol Red</b>	Thermo Fisher Scientific (Schwerte, Germany)

Full medium was composed of the main medium with addition of 20% FCS and 1% P/S. For selection of transfected cells puromycin in a concentration of 2 µg/ml was added to complete medium. The promoters of cells transduced with doxycycline inducible shRNA expression were activated with doxycycline in a concentration of 2 µg/ml by adding to the complete medium.

### 2.3. Chemicals

Unless otherwise described, standard chemicals were purchased from VWR (Darmstadt, Germany).

<b>Consumable</b>	<b>Company</b>
<b>Acidified Water</b>	Sigma-Aldrich (Taufkirchen, Germany)
<b>Ammonium persulfate (APS)</b>	Merck (Darmstadt, Germany)
<b>Bromophenol blue</b>	Carl Roth (Karlsruhe, Germany)
<b>BSA powder</b>	Carl Roth (Karlsruhe, Germany)
<b>DTT</b>	Sigma-Aldrich (Taufkirchen, Germany)
<b>Glycerol</b>	Sigma-Aldrich (Taufkirchen, Germany)
<b>Glycine</b>	Sigma-Aldrich (Taufkirchen, Germany)
<b>KH<sub>2</sub>PO<sub>4</sub></b>	Sigma-Aldrich (Taufkirchen, Germany)
<b>Na<sub>2</sub>HPO<sub>4</sub></b>	Sigma-Aldrich (Taufkirchen, Germany)
<b>NaCl</b>	Thermo Fisher Scientific (Schwerte, Germany)

Consumable	Company
Normal saline	G-Biosciences (St. Louis, USA)
PEG 300	Merck (Darmstadt, Germany)
SDS	Carl Roth (Karlsruhe, Germany)
TEMED	VWR (Darmstadt, Germany)
Tris	Sigma-Aldrich (Taufkirchen, Germany)
Triton X-100	Thermo Fisher Scientific (Schwerte, Germany)
Triton X-100	Carl Roth (Karlsruhe, Germany)
TWEEN 20	Sigma-Aldrich (Taufkirchen, Germany)

## 2.4. Buffers and solutions

Buffer/Solution	Composition
Stack buffer	<ul style="list-style-type: none"> <li>• 0.5 M Tris/HCL pH 6.8</li> <li>• 0.4 % (w/v) SDS</li> <li>• In dH2O</li> </ul>
Separation buffer	<ul style="list-style-type: none"> <li>• 1.5 M Tris/HCL pH 8.8</li> <li>• 0.4 % (w/v) SDS</li> <li>• in dH2O</li> </ul>
SDS gel running buffer	<ul style="list-style-type: none"> <li>• 0.05 M Tris</li> <li>• 0.2 M Glycin</li> <li>• In dH2O</li> </ul>
Transfer buffer (WB)	<ul style="list-style-type: none"> <li>• 25 mM Tris</li> <li>• 150 mM Glycin</li> <li>• 10 % MeOH</li> <li>• 0.05 % SDS</li> <li>• In dH2O</li> </ul>
Laemmli buffer 5X	<ul style="list-style-type: none"> <li>• 20% SDS</li> <li>• 1M Tris/HCL pH 6.8</li> <li>• 0.25 % Bromophenol blue</li> <li>• 0.5 M DTT</li> <li>• 50 % Glycerol</li> <li>• In dH2O</li> </ul>
TBS-T	<ul style="list-style-type: none"> <li>• 13.7 mM NaCl</li> <li>• 2.7 mM KCL</li> <li>• 80.9 mM Na2HPO4</li> <li>• 1.5 mM KH2PO4</li> <li>• pH 7.4</li> <li>• In dH2O</li> <li>• 0.5 % Tween 20</li> </ul>
Nicoletti buffer	<ul style="list-style-type: none"> <li>• 0.1 % Sodium citrate</li> <li>• 0.1 % Triton X-100</li> <li>• 50 µg/ml propidium iodide</li> <li>• In dH2O</li> </ul>
Blocking buffer	<ul style="list-style-type: none"> <li>• TBS-T</li> <li>• 5 % BSA</li> </ul>

## 2.5. Consumables for transfection

**Table 4: List of consumables used for transfection**

Consumable	Company
Xfect transfection reagent	Takara (Göteborg, Sweden)
Lenti-x concentrator	Takara (Göteborg, Sweden)
Retronectin	Takara (Göteborg, Sweden)

### 2.5.1. Plasmids and lentiviral packaging system

**Table 5: List of plasmids used for transfection**

Name	Description	Selection	Source
pCDH-Flag-c-Myc	MYC overexpression	GFP	Addgene ID: 102626
125	Lentiviral packaging	-	
126	Lentiviral packaging	-	
127	Lentiviral packaging	-	
pS-luc-GFP-W	Luciferase	GFP	[160]

For downmodulation of the targets, distinct PTEN targeted small hairpin RNA (shRNA) were cloned into SMARTvector inducible lentiviral shRNA vector, with inducible TRE3G promoter activated by Tet-On-3G protein after exposure of doxycycline (Horizon Discovery, Lafayette, USA).

**Table 6: List of doxycycline inducible shRNA plasmids used for transfection**

Name	shRNA sequence
PTEN sh1	TGAACATTGGAATAGTTTC
PTEN sh2	TCAAGTCTAAGTCGAATCC
PTEN sh3	ACAACAAGCAGTGACAGCG

## 2.6. Consumables for RNA isolation and RT-qPCR

**Table 7: List of consumables used for RNA analysis**

Consumable	Company
0.5 mL PCR Tubes	Promega (Mannheim, Germany)
96-Well rt-qPCR Plate white, clear bottom	Bio-Rad (Düsseldorf, Germany)
dNTPs 25 µmol	Promega (Mannheim, Germany)
Maxwell® RSC simplyRNA Cells Kit	Promega (Mannheim, Germany)
Nuclease free water	Thermo Fisher Scientific (Schwerte, Germany)
PCR Strip-Tubes 0.1 mL	Eppendorf (Hamburg, Germany)
Power SYBR Green Mastermix	Thermo Fisher Scientific (Schwerte, Germany)

Consumable	Company
Reverse Transcriptase Kit	Qiagen (Hilden, Germany)
RNase away	Thermo Fisher Scientific (Schwerte, Germany)
RNasin plus, Rnase inhibitor 40 u/μL	Promega (Mannheim, Germany)

### 2.6.1. Primer Mix

**Table 8: List of primer mixes purchased from Qiagen (Hilden, Germany)**

Primer Mix	GeneGlobe Id
ABCA5	QT00051660
B2M	QT00088935
GAPDH	QT00079247
MYC	QT00035406

## 2.7. Consumables for drug screening

**Table 9: List of consumables used for drug screening**

Consumables	Company
Cell Titer Glo 2.0	Promega (Mannheim, Germany)
D4+ cassette	Tecan (Crailsheim, Germany)
Multidrop tubing	Thermo Fisher Scientific (Schwerte, Germany)
Multidrop tubing small	Thermo Fisher Scientific (Schwerte, Germany)
Parafilm	Bemis (Oshkosh, USA)
T8+ cassette	Tecan (Crailsheim, Germany)
White 1536 well plates, sterile, TC treated	Corning (Wiesbaden, Germany)
White 384 well plates, sterile, TC treated	Corning (Wiesbaden, Germany)

### 2.7.1. Compound library for high throughput drug screening

**Table 10: Selection of compounds for leukemia-specific high throughput drug screening**

#	INHIBITOR	TARGET	FDA APPROVED	EMA APPROVED
1	DMSO			
2	5-Azacytidine	Antimetabolites	Yes	Yes
3	5-Fluorouracil	Antimetabolites	Yes	Yes
4	6-Mercaptopurine (Monohydrate)	Antimetabolites	Yes	Yes
5	6-Thioguanine	Antimetabolites	Yes	Yes
6	Clofarabine	Antimetabolites	Yes	Yes
7	Cytarabine (Hydrochlorid)	Antimetabolites	Yes	Yes
8	Cyclocytidine HCL	Antimetabolites	No	No
9	Fludarabine (phosphate)	Antimetabolites	Yes	Yes

Materials and methods

#	INHIBITOR	TARGET	FDA APPROVED	EMA APPROVED
10	Nelarabine	Antimetabolites	Yes	Yes
11	Gemcitabine	Antimetabolites	Yes	Yes
12	Methotrexate	Antimetabolites	Yes	Yes
13	Pentostatin	Antimetabolites	Yes	Yes
14	Cladribine	Antimetabolites	Yes	Yes
15	Dacarbazine	Antimetabolites/ DNA alkylator/crosslinker;	Yes	Yes
16	Vinblastine (sulfate)	Antimitotics	Yes	Yes
17	Vincristine (sulfate)	Antimitotics	Yes	Yes
18	Busulfan	Alkylating agents	Yes	Yes
19	Carmustine	Alkylating agents	Yes	Yes
20	Cyclophosphamide (Clafen) (Monohydrate)	Alkylating agents	Yes	Yes
21	Lomustine	Alkylating agents	Yes	Yes
22	Cisplatin	Alkylating agents	Yes	Yes
23	Oxaliplatin	Alkylating agents	Yes	Yes
24	Procarbazine (Hydrochloride)	Alkylating agents	Yes	Yes
25	Thio-TEPA	DNA alkylator/crosslinker;	Yes	Yes
26	Temozolomide	Alkylating agents	Yes	Yes
27	Chlorambucil	Alkylating agents	Yes	Yes
28	Bendamustine (hydrochloride)	Alkylating agents	Yes	Yes
29	Mechlorethamine hydrochloride	DNA alkylator/crosslinker;	Yes	Yes
30	Epirubicin (hydrochloride)	Topoisomerase inhibitors	Yes	Yes
31	Etoposide	Topoisomerase inhibitors	Yes	Yes
32	Idarubicin (hydrochloride)	Topoisomerase inhibitors	Yes	Yes
33	Mitoxantrone (dihydrochloride)	Topoisomerase inhibitors	Yes	Yes
34	Teniposide	Topoisomerase inhibitors	Yes	Yes
35	Daunorubicin (Hydrochloride)	Topoisomerase inhibitors	Yes	Yes
36	Doxorubicin (hydrochloride)	Topoisomerase inhibitors	Yes	Yes
37	Amsacrine (Hydrochlorid)	Topoisomerase inhibitors	Yes	Yes
38	Dexamethasone	GC/GCR complex	Yes	Yes
39	Prednisone	GC/GCR complex	Yes	Yes
40	Prednisolone (Acetate)	GC/GCR complex	Yes	Yes
41	Belinostat	HDACi	Yes	Yes
42	DMSO			
43	CI-994 (Tacedinaline)	HDACi	No	No
44	Panobinostat	HDACi	Yes	Yes
45	Romidepsin	HDACi	Yes	Yes
46	Quisinostat	HDACi	No	No
47	Tubastatin A (Hydrochloride)	HDAC6i	No	No
48	Givinostat (ITF2357)	HDACi	No	Yes

Materials and methods

#	INHIBITOR	TARGET	FDA APPROVED	EMA APPROVED
49	Vorinostat	HDACi	Yes	No
50	Entinostat	HDACi	No	Yes
51	Ricolinostat	HDAC6i	No	No
52	Pracinostat	HDACi	Yes	Yes
53	Abexinostat	HDACi	No	No
54	MPK544	HDACi	No	No
55	EPZ-6438 (Tazemetostat)	EZH2i/HMTasei	No	Yes
56	GSK126	EZH2i/HMTasei	No	No
57	GSK343	EZH2i/HMTasei	No	No
58	GSK 525762A	BET bromodomain;	No	No
59	Paclitaxel	Antimetabolites		
60	JQ1	BET bromodomain	No	No
61	Bortezomib	Proteasome inhibitor	Yes	Yes
62	MLN-9708 (Citrate)	Proteasome inhibitor	No	No
63	Carfilzomib	Proteasome inhibitor	No	No
64	Ganetespib	HSP90i	No	No
65	PUH71	HSP90i	No	No
66	AUY922 (LUMINESPIB)	HSP90i	No	No
67	NVP-HSP990	HSP90i	No	No
68	EC144	HSP90i	No	No
69	PF-04929113	HSP90i	No	No
70	BIIB021	HSP90i	No	No
71	VWK627	HSP90i	No	No
72	VWK603	HSP90i	No	No
73	Alisertib	Aurora Kinase A	No	Yes
74	Aurora A Inhibitor I	Aurora Kinase A inhibitor	No	No
75	MLN8054	Aurora Kinase A inhibitor	No	No
76	MK-5108 (VX-689)	Aurora Kinase A inhibitor	No	No
77	Danusertib	Aurora Kinase A	No	No
78	Barasertib	Aurora kinase B	No	No
79	Volasertib	Polo-like Kinase (PLK);	Yes	Yes
80	BI2536	PLK	No	No
81	LEE011 (Ribociclib)	CDK;	Yes	Yes
82	LY2835219 (Abemaciclib)	CDK;	Yes	Yes
83	Dinaciclib	CDK;	No	Yes
84	SY-1365-THZ1	cdk7i	No	No
85	Cabozantinib (S-malate)	VEGFR	Yes	Yes
86	Erlotinib	EGFR	Yes	Yes
87	Gefitinib (Hydrochlorid)	EGFR	Yes	Yes
88	Sunitinib (malate)	PDGFR; VEGFR	Yes	Yes
89	Axitinib	VEGFR	Yes	Yes
90	Midostaurin	PKC, vegfr2, pdgfr, FLT3	Yes	Yes
91	Foretinib	VEGFR2; c-MET	No	No
92	Dovitinib	FLT3; PDGFR; VEGFR; c-Kit;	No	No
93	Crenolanib	FLT3; PDGFR	No	Yes



Materials and methods

#	INHIBITOR	TARGET	FDA APPROVED	EMA APPROVED
94	Pexidartinib	FLT3, KIT, CSF1R	Yes	Yes
95	Lestaurtinib	FLT3	No	No
96	Quizartinib	FLT3;	No	No
97	KW-2449	FLT3	No	No
98	Pacritinib	FLT3; JAK;	No	No
99	Gilteritinib	FLT3/AXL	Yes	Yes
100	Buparlisib	PI3K	No	No
101	Idelalisib	PI3K;	Yes	Yes
102	Pictilisib GDC-0941	Pi3K	No	No
103	GSK2636771	PI3K/AKT	No	No
104	Alpelisib	PI3K/AKT	Yes	No
105	Dactolisib (BEZ235)	PI3K, mTOR	No	No
106	GSK2110183 (Afuresertib)	AKT;	No	No
107	Ro 08-2750			
108	ARQ-092 (Miransertib)	AKT	No	Yes
109	Ipatasertib (GDC-0068)	AKT;	Yes	No
110	Deforolimus	mTOR;	Yes	No
111	Everolimus	mTOR;	Yes	Yes
112	Rapamycin	mTOR;	Yes	Yes
113	Temsirolimus	mTOR;	Yes	Yes
114	PF-04691502	mTOR; PI3K;	No	No
115	INK 128 (MLN0128)	mTORC1/2	No	No
116	BMS-911543	JAK;	No	No
117	AT9283	JAK;	No	No
118	Baricitinib (phosphate)	JAK;	Yes	Yes
119	CYT387 (Momelotinib)	JAK;	Yes	Yes
120	Ruxolitinib	JAK;	Yes	Yes
121	Tofacitinib (citrate)	JAK;	Yes	Yes
122	Fedratinib (TG101348)	JAK; FLT3	Yes	No
123	Gandotinib	JAK mutant (JAK2V617F)	No	No
124	Tipifarnib	Farnesyl Transferase; Ras inhibitor	Yes	Yes
125	Lonafarnib	Rasi	No	Yes
126	Salirasib	Rasi	Yes	No
127	Dabrafenib (Mesylate)	Raf inhibitor	Yes	Yes
128	Sorafenib (Tosylate)	Raf inhibitor	Yes	Yes
129	Regorafenib (Monohydrate)	Raf inhibitor	Yes	Yes
130	Vemurafenib	Raf inhibitor	Yes	Yes
131	LGX818 (Encorafenib)	Rafi	Yes	Yes
132	Cobimetinib	MEK;	Yes	Yes
133	MEK162 (Binimetinib)	MEK;	Yes	Yes
134	Selumetinib	MEK;	No	Yes
135	Trametinib	MEK;	Yes	Yes
136	PD0325901	MEK	No	No
137	PD184352	MEK	No	No

Materials and methods

#	INHIBITOR	TARGET	FDA APPROVED	EMA APPROVED
138	Pimasertib	MEK	No	No
139	SHP099 (Dihydrochloride)	Ras-ERK	No	No
140	SCH772984	ERK1/2	No	No
141	GDC-0994	ERK	No	No
142	Losmapimod	p38 MAPK;	No	No
143	Zanubrutinib	BTKi	Yes	Yes
144	Tirabrutinib	BTKi	No	No
145	Spebrutinib	BTKi	No	No
146	Ibrutinib	(Ibruvica) 'Btk;	Yes	Yes
147	Imatinib (Mesylate)	Bcr-Abl inhibitor	Yes	Yes
148	Radotinib	Bcr-Abl inhibitor	No	No
149	Nilotinib (Hydrochlorid)	Bcr-Abl;	Yes	Yes
150	Ponatinib	Bcr-Abl; FGFR; FLT3; VEGFR;	Yes	Yes
151	Bosutinib	Bcr-Abl; Src;	Yes	Yes
152	Dasatinib (Hydrochlorid)	Bcr-Abl; Src;	Yes	Yes
153	Rebastinib (DCC- 2036)	Bcr-Abl	No	No
154	Saracatinib	Src; Abl	No	No
155	Bafetinib	Bcr-Abl; Src;	Yes	No
156	Staurosporin	Multiple non-selective inhibitor of protein kinases	No	No
157	BSI-201 (Iniparib)	PARP;	No	No
158	Olaparib	PARP;	Yes	Yes
159	Rucaparib (phosphate)	PARP;	Yes	Yes
160	Veliparib (dihydrochloride)	PARP;	Yes	Yes
161	ABT-199 (Venetoclax)	Bcl-2 Family;	Yes	Yes
162	Obatoclax (Mesylate)	Bcl-2 Family;	No	No
163	Y-27632 (Dihydrochloride)	ROCK	No	No
164	QNZ (EVP4593)	NF-κBi	No	No
165	Omaveloxolone	NF-κBi	No	Yes
166	Enasidenib	isocitrate dehydrogenase type 2 (IDH2)	Yes	Yes
167	Ivosidenib	IDH1	Yes	Yes
168	Birinapant	XIAPi and cIAP1i	No	No
169	Tariquidar	P-glycoprotein;	No	No
170	Enzastaurin	PKC;	Yes	Yes
171	KYA1797K	wnt/catenin	No	No
172	Selinexor	CRM1 inhibitor	Yes	Yes
173	AZD6738	ATM/ATRi	No	No
174	Omacetaxine Mepesuccinate (Homoharringtonine)	Ribosom Inhibtor	Yes	No
175	Actinomycin D	Antibacterial	Yes	Yes
176	DMSO			
177	Bexarotene	Retinoid Inhibitor	Yes	Yes

#	INHIBITOR	TARGET	FDA APPROVED	EMA APPROVED
178	PND-1186	FAK inhibitor	No	No
179	Nintedanib (BIBF1120)	LCK inhibitor	Yes	Yes
180	BAY 80-6946 (Copanlisib)	PI3K	Yes	Yes
181	Palbociclib	cdki	Yes	Yes
182	DMSO			

## 2.8. Consumables for protein analysis

Table 11: List of consumables used for protein analysis

Consumables	Company
Blottingmembrane Amersham Hybound P, PVDF, 0.45 µm	GE Healthcare (Solingen, Germany)
Blottingmembrane Amersham Protran, Nitrocellulose, 0.45 µm	GE Healthcare (Solingen, Germany)
Gel Blotting paper Whatman	GE Healthcare (Solingen, Germany)
MYC Activity assay	Active Motif (Carlsbad, CA, USA)
Nuclear extraction kit	Active Motif (Carlsbad, CA, USA)
PhosphoSTOP	Roche (Mannheim, Germany)
Protein ladder (PageRuler Prestained)	Thermo Fisher Scientific (Schwerte, Germany)
RIPA buffer	Thermo Fisher Scientific (Schwerte, Germany)

### 2.8.1. Antibodies and chemicals for flow cytometry

Antibodies for flow cytometry were purchased from BD Biosciences (Heidelberg, Germany).

Table 12: List of fluorochrome-conjugated antibodies and chemicals used for flow cytometry

Name	Conjugate	Species	Dilution	Order NR
CD45 – APC	APC	Human	1:100	555485
CD45 – APC-AF700	AF700	Mouse	1:100	560693
Annexin V – APC	APC	Human	1:40	550474
Annexin V – FITC	FITC	Human	1:40	556419
CD3	APC	Human	1:100	561804
CD7	APC	Human	1:100	561604
Propidium Iodide	-	-	-	556463

## 2.8.2. Antibodies for Western Blot

**Table 13: List of primary- and HSR-conjugated secondary antibodies used for Western Blot**

<b>Name</b>	<b>Species</b>	<b>Dilution</b>	<b>Order NR</b>	<b>Company</b>
<b>Ac-Alphatubulin</b>	Rabbit	1:1000	5335S	Cell Signaling Technology (Frankfurt, Germany)
<b>Acetyl Histone H3</b>	Rabbit	1:2000	9677S	Cell Signaling Technology (Frankfurt, Germany)
<b>AKT</b>	Rabbit	1:1000	4691S	Cell Signaling Technology (Frankfurt, Germany)
<b>Alpha Tubulin</b>	Rabbit	1:1000	2144S	Cell Signaling Technology (Frankfurt, Germany)
<b>Beta-actin</b>	Mouse	1:10000	A5316	Sigma-Aldrich (Taufkirchen, Germany)
<b>BRD4</b>	Rabbit	1:1000	13440S	Cell Signaling Technology (Frankfurt, Germany)
<b>c-Myc</b>	Rabbit	1:1000	13987S	Cell Signaling Technology (Frankfurt, Germany)
<b>GAPDH</b>	Rabbit	1:1000	2118S	Cell Signaling Technology (Frankfurt, Germany)
<b>GSK-3beta</b>	Rabbit	1:2000	9315S	Cell Signaling Technology (Frankfurt, Germany)
<b>HDAC1</b>	Mouse	1:1000	5356S	Cell Signaling Technology (Frankfurt, Germany)
<b>HDAC6</b>	Rabbit	1:1000	7558S	Cell Signaling Technology (Frankfurt, Germany)
<b>Histone H3</b>	Rabbit	1:2000	2650	Cell Signaling Technology (Frankfurt, Germany)
<b>HSP27</b>	Mouse	1:1000	2402S	Cell Signaling Technology (Frankfurt, Germany)
<b>HSP40</b>	Rabbit	1:1000	4871P	Cell Signaling Technology (Frankfurt, Germany)
<b>HSP70</b>	Rabbit	1:2000	4872S	Cell Signaling Technology (Frankfurt, Germany)
<b>HSP90</b>	Rabbit	1:1000	4877S	Cell Signaling Technology (Frankfurt, Germany)
<b>MEK</b>	Rabbit	1:1000	9126S	Cell Signaling Technology (Frankfurt, Germany)
<b>p44/42 MAPK (ERK1/2)</b>	Rabbit	1:1000	4695S	Cell Signaling Technology (Frankfurt, Germany)
<b>P-AKT (S473)</b>	Rabbit	1:2000	4060P	Cell Signaling Technology (Frankfurt, Germany)
<b>P-AKT (T308)</b>	Rabbit	1:1000	2965P	Cell Signaling Technology (Frankfurt, Germany)
<b>PARP</b>	Rabbit	1:1000	9542	Cell Signaling Technology (Frankfurt, Germany)
<b>P-c-Myc (S62)</b>	Rabbit	1:1000	13748S	Cell Signaling Technology (Frankfurt, Germany)
<b>P-GSK-3beta (S9)</b>	Rabbit	1:1000	9323P	Cell Signaling Technology (Frankfurt, Germany)
<b>p-MEK</b>	Rabbit	1:1000	9154S	Cell Signaling Technology (Frankfurt, Germany)

Name	Species	Dilution	Order NR	Company
<b>p-MYC (S62)</b>	Rabbit	1:1000	13748S	Cell Signaling Technology (Frankfurt, Germany)
<b>p-MYC (T58)</b>	Rabbit	1:1000	46650S	Abcam (Cambridge, UK)
<b>P-p44/42 MAPK (T202/Y204)</b>	Rabbit	1:1000	4370S	Cell Signaling Technology (Frankfurt, Germany)
<b>PTEN</b>	Rabbit	1:1000	9188P	Cell Signaling Technology (Frankfurt, Germany)

Table 14: List of secondary, HRP-linked antibodies

Name	Species	Dilution	Order NR	Company
<b>Anti-rabbit</b>	Goat	1:5000	7074S	Cell Signaling Technology (Frankfurt, Germany)
<b>Anti-mouse</b>	Horse	1:5000	7076S	Cell Signaling Technology (Frankfurt, Germany)

## 2.9. *In vivo* experiments

### 2.9.1. Mouse strain

The mouse strain was purchased from The Jackson Laboratory by Dr. Johannes Stegbauer, who shared the mouse strain with our working group. The mice were allocated to both working groups based on their sex. The working group of Dr. Stegbauer used exclusively male mice and our working group used female mice for the experiments. Thus, optimal experimental animal use could be arranged.

International name of the mouse strain: **NOD.Cg-Prkdcscid H2-K1tm1Bpe H2-D1tm1Bpe Il2rgtm1Wjl/SzJ** (Cg = NSG, C57BL/6J, 129P2 und B6;129).

### 2.9.2. consumables for *in vivo* experiments

Table 15: List of consumables used for *in vivo* experiments

Consumable	Company
<b>Afuresertib (GSK2110183) 200 mg</b>	MedChemExpress (Monmouth Junction, USA)
<b>Birabresib (OTX-015) 200 mg</b>	MedChemExpress (Monmouth Junction, USA)
<b>Copanlisib (BAY80-6946) 100 mg</b>	MedChemExpress (Monmouth Junction, USA)
<b>D-Lightning Luciferin</b>	PerkinElmer (Rodgau, Germany)
<b>JQ1 100 mg</b>	MedChemExpress (Monmouth Junction, USA)
<b>Li-Heparin tubes (Microtainer)</b>	BD Biosciences (Heidelberg, Germany)
<b>Oral gavage tubes</b>	Thermo Fisher Scientific (Schwerte, Germany)
<b>Syringe Micro-fine+ U40</b>	BD Biosciences (Heidelberg, Germany)

## 2.10. Software

**Table 16: List of software used in this thesis**

Software	Company
CFX Manager	Bio-Rad Laboratories (Düsseldorf, Germany)
Living Image	PerkinElmer (Rodgau, Germany)
Combenefit (version 2.021)	Cancer Research UK Cambridge Institute (downloaded from <a href="http://www.sourceforge.net">www.sourceforge.net</a> )
CytExpert	Beckman Coulter (Krefeld, Germany)
D300e control and merge	Tecan (Crailsheim, Germany)
GraphPad Prism 7	GraphPad Software (San Diego, USA)
Spark control	Tecan (Crailsheim, Germany)

## 2.11. Cell culture methods

### 2.11.1. Thawing cells

The original inoculation cultures were stored in liquid nitrogen. The thawing process was performed by thawing the cryo-tube in a water bath in 37°C warm water for a few seconds. The thawed cells were immediately transferred into fresh media to reduce the DMSO concentration that was used for the freezing process. By removing the supernatant after centrifuging the cells at 1500 rpm and 20 C° for 5 min, most of the toxic DMSO was removed. Afterwards, the cells need up to 7 days for recovery.

### 2.11.2. Culturing leukemic cell lines

To prevent the cell lines from genetically changing over a longer period, the cell lines were kept in culture for a maximum of 30 days. The cell culture procedures followed the standard requirements of experimental cell culture. All used leukemic cell lines and leukemic cells from patients were cultured in RPMI-full medium. Suspension culture cells were cultured in T25, T75 or T150 flasks vertically and split twice weekly up to 1:50 to avoid overgrowth and to ensure sufficient nutrient supply. Adherent cells (LOUCY and CCRF/CEM) were cultured in T75 bottle horizontally until confluence of 95% was reached. TrypLE was used to detach the cells. Overgrowth was prevented by splitting cells 1:10 two times a week. To prevent a contamination of the cells with mycoplasma a PCR-based test was performed frequently using the supernatant of cell lines in culture. Only mycoplasma-free cells were used. For experiments, cells were kept in the exponential growth phase, which increases the reproducibility and the

comparability between other cell lines. To create equal conditions before the experiments, the cells were cultivated in a concentration of  $1 \times 10^6$  cells per ml in fresh medium for 24h. Freezing of the cells was achieved by resuspending up to 10 million cells per cryo-tube in 1 ml freezing medium and then cooling them down to  $-80^\circ\text{C}$  in a cell-protecting manner using a freezing container. To avoid cross contaminations of used cell lines STR analysis were performed before freezing the cells.

#### **2.11.3. Culturing HEK293T (Human Embryonic Kidney 293T)**

The adherent growing cell line HEK293T is a highly transfectable variant of the human embryonic renal epithelial cell line 293, which constitutively expresses the simian virus 40(SV40) large T antigen. The cells were cultivated in DMEM-full medium.

#### **2.11.4. Culturing primary patient cells**

Primary patient- or patient derived xenograft (PDX) cells were cultured either with or without the presence of feeder mesenchymal stem cells (MSCs), depending on the health status of the cells. In general, the duration of cultivation of the cells differed from donor to donor. RPMI-full medium was used for cultivation and the cells were viable for up to 4 weeks.

#### **2.11.5. Culturing doxycycline inducible target knock down cells**

Cells carrying the plasmid for inducible PTEN knockdown are resistant to puromycin according to the resistance marker on the plasmids and are therefore cultivated in RPMI-full medium with  $2\mu\text{g/ml}$  puromycin as a supplement to ensure a stable population of transduced cells. To activate the RNA interference (RNAi)  $2\mu\text{g/ml}$  doxycycline was added into the culture media and incubated for 48h. Doxycycline activates the promoter of the plasmid and the transcription of the target small hairpin RNA (shRNA) begins. To identify the efficacy of the shRNA expression, GFP will be co-expressed that can be validated by flow cytometry.

### **2.11.6. Determination of cell count**

The determination of the total cell number as well as the proportion of vital cells was performed using the trypan blue method either by using the cell count machine or the Neubauer counting chamber.

#### **2.11.6.1. Automated cell count**

The cells are mixed with trypan blue solution and dead cells are stained blue, since the dye can penetrate their perforated cell membrane. Vital cells with an intact cell membrane do not absorb the dye, thus a clear distinction between living and dead cells is possible. The cell counting device Vi-Cell XR was used for the cell count determination, which automates the manual trypan blue method.

#### **2.11.6.2. Manual cell count**

As an alternative method, the cell count could be determined using a Neubauer counting chamber. A pre-mixture of cell solution with trypan blue was prepared and 10  $\mu$ l transferred to the Neubauer chamber. To determine the cell count, all four big squares of the instrument were counted and added together. The cell number was calculated with the following formula:

$$C_{culture} = \frac{n_{cells} * f * 10000}{(n_{squares} * ml)}$$

$C_{culture}$  = cell concentration

$n_{cell}$  = total cell count

f = dilution factor

$n_{squares}$  = number of counted squares

### **2.11.7. Flow cytometry**

The method of fluorescence-activated cell sorting (FACS) enables the analysis of individual cells from a cell suspension with respect to various parameters. The cells are aspirated with a capillary and pass as single cells a laser beam. Its light is scattered through the cell and the extent and direction of the scattering provide information about the size of the cell, which is measured in forward scattering (FSC), and its granularity,



which is measured inside scattering (SSC). In addition to light scattering, the flow cytometer can also detect emissions of fluorescent dyes. This allows the analysis and quantification of fluorescent-dye conjugated antibodies or fluorescent protein expressing cells.

**Table 17: Absorbance spectrum of used antibodies and chemicals for flow cytometry**

<b>Fluorochrome</b>	<b>Excitation maximum</b>	<b>Emission maximum</b>
<b>PE</b>	496 nm	578 nm
<b>FITC</b>	490 nm	525 nm
<b>APC</b>	650 nm	660 nm
<b>Alexa Fluor 700 (AF700)</b>	702 nm	723 nm

To prepare cells for flow cytometric analysis, the cells were centrifuged at 1500 rpm at 20°C for 5 min and the supernatant was discarded. The pellet was resuspended in 100 µl PBS and transferred into a 96-well plate. Fluorescence-conjugated antibodies or DNA staining chemicals were used at a concentration according to the manufacturer's recommendation and added to the cell solution. After incubation for 15 min in the dark at 20°C, the cells were ready for measurement.

## **2.12. RNA analysis**

### **2.12.1. RNA isolation**

For automated RNA isolation of cells, the Maxwell RSC machine was used following the manufacturer's protocol. Whenever possible,  $5 \times 10^6$  cells were used for RNA isolation. RNA purification is based on the use of paramagnetic particles that bind the nucleic acids. Wash buffers and a combination of DNases and proteases are used to remove impurities from the RNA suspension, which consists mostly of DNA and proteins, as well as cell debris. RNA was finally eluted with RNase/ DNase free ddH<sub>2</sub>O and storage was at -80°C.

### **2.12.2. RNA concentration determination using a spectrophotometer**

The concentration of the RNA samples was determined on a spectrophotometer. For this purpose, RNA was measured at the RNA-specific adsorption spectrum 230 nm. Impurities were indicated by additional measurements of adsorption at 280 nm

(specific for proteins) and 260 nm (specific for DNA). For measurement, 1 µl of RNase/DNase free ddH<sub>2</sub>O was applied as a reference and 1 µl of each sample.

### **2.12.3. cDNA synthesis**

cDNA stands for complementary DNA and is produced with the help of an enzyme found in retroviruses called reverse transcriptase. Single-stranded RNA strands serve as the template. Transcription of the isolated RNA into cDNA was performed using reverse transcription kit from Qiagen (Hilden, Germany) according to the manufacturer's instructions. Oligo-dT primers were used in the procedure, with synthesis of cDNA starting from the poly-A<sup>+</sup> tail of mRNA. Thus, mainly cDNA products were obtained starting from the mRNA matrices. The reaction mixture, consisting of enzyme buffer, reverse transcriptase, oligo-dT primer, RNase-, DNase-free ddH<sub>2</sub>O and a buffer to remove genomic DNA. cDNA samples were stored at -20°C.

### **2.12.4. qPCR**

Real-time quantitative PCR (qPCR) is a method used to quantify a target gene. In general, the method is based on the principles of PCR (polymerase chain reaction). Amplification of the target gene is performed in several cycles consisting of denaturation of the template, attachment of target gene-specific primers, elongation, and synthesis of the new DNA strand. The individual steps depend on temperature and duration. With the use of DNA-binding fluorescent dyes and an appropriate PCR instrument that detects the fluorescent signal, it is possible to determine the amount of amplicon. The values given by a PCR instrument are called Ct (cycle of threshold) values. These values correspond to the cycle time of the PCR, when the fluorescence signal just stands out clearly from the background signal. The lower the Ct value, the more copies of the target gene were present in the sample at the beginning. With additional determination of the quantity of a constantly expressed reference gene, a so-called housekeeping gene, the transcript quantity of the target gene can be normalized to the transcript quantity of the reference gene. This allows comparability between other samples. GAPDH was selected as the reference gene. GAPDH is a ubiquitous and constantly synthesized enzyme involved in energy production by glycolysis and is therefore optimally suited as a reference gene.

For real-time qPCR, following qPCR mix was used:

**Table 18: qPCR Mix for one well of 96-well plates**

Volume	Reagent
10 $\mu$ L	Power SYBR Green Mastermix
1 $\mu$ L	Primer Mix
7 $\mu$ L	H <sub>2</sub> O
2 $\mu$ L	cDNA

The following approach was used with appropriate instrument setup:

**Table 19: Machine settings for RT-qPCR**

Step	Temperature	Time
1	50°C	2 min
2	95°C	10 min
3	95°C	15 s
4	60°C	1 min
Go to step 3, 39x		

## 2.13. Protein analysis

### 2.13.1. Protein isolation

Cells were lysed and protein was extracted using lysis-buffer, supplemented with protease and phosphatase inhibitor cocktail for 20 min on ice. The cell debris and DNA were sedimented by centrifugation at 14.000 g for 20 min at 4°C. The clear supernatant, containing protein was then quantified by BSA assay according to manufacturer's instructions.

### 2.13.2. Western Blotting (WB)

#### 2.13.2.1. Preparation of the SDS polyacrylamide gel

The SDS-polyacrylamide gel consists of two different gels, the stacking gel, and the separation gel. The stacking gel has a low pH and triggers the proteins to accumulate before they are separated according to their molecular size in the separation gel.

The following approaches are used for collection gels and separation gels:

Stacking gel (for four gels):

**Table 20: Recipe for stacking gel**

Substance	Acrylamide	dH <sub>2</sub> O	Stack buffer	APS	TEMED
Quantity	1.5 mL	6.0 mL	2.5 mL	0.2 mL	0.05 mL

Separation gel (for four gels):

**Table 21: Recipe for separation gel**

Substance	Acrylamide	dH <sub>2</sub> O	Separation buffer	APS	TEMED
Quantity	6.7 mL	8.4 mL	5.0 mL	0.2 mL	0.07 mL

TEMED is added just before pouring the respective batch, as this starts the polymerization.

A gel chamber was tightly clamped in a setting fixture and checked with dH<sub>2</sub>O for leakage. The separating gel batch is poured quickly and kept free of air bubbles with isopropanol. After the separating gel batch has polymerized, the isopropanol is thoroughly washed out with dH<sub>2</sub>O. The collection gel batch is poured in next. A Teflon-coated comb is used to form pockets. The gel can be stored at 4°C for a few days in plastic bags containing water to prevent the gel from drying out.

### 2.13.2.2. SDS-polyacrylamide gel electrophoresis (SDS-PAGE)

Protein samples are mixed with a 5x Laemmli-buffer and, unless otherwise described, and denatured at 95°C for 5 min and cooled down to 4°C before it was loaded in the gel pockets for SDS-PAGE or frozen at -80°C for storage.

In SDS-PAGE, protein samples are separated from each other according to their size. The detergent SDS surrounds the proteins in solution and leads to a negative charge. The intrinsic charge of the proteins can be neglected due to the negative charge of SDS; thus, the negative charge is proportional to the protein size. In a static field, the proteins migrate towards the positive pole, with small molecules migrating faster through the gel than larger ones. Electrophoresis was performed at 200 V and approximately 50 mA for 1 h and 20 min.

### **2.13.3. WB analysis**

Separated proteins in the SDS gel were transferred to a Polyvinylidenfluorid (PVDF)- or nitrocellulose membrane for immobilization. These membranes can be used for antibody binding and staining in the further course.

#### **2.13.3.1. Set-up of the blot apparatus:**

Whatman papers are cut to size and placed in transfer buffer for 10 min so that they become saturated with it. Other than the nitrocellulose membrane, the PVDF membrane must be activated first in pure methanol for 10 seconds and then transferred to transfer buffer and incubated in it for 1 min. The membrane was then placed on the fully soaked filter paper. The SDS gel was carefully placed on the membrane and pressed with a roller to remove air bubbles. A second fully soaked Whatman paper was placed on top. The construct is again pressed free of air bubbles with a roller. The whole construct was fixed in the according cassettes and transferred into the blotting apparatus. The blotting apparatus was set as follows: 120 min at 100 V and a maximum of 25 watts.

#### **2.13.3.2. Antibody staining on PVDF- or nitrocellulose membrane**

To avoid unspecific binding, the membrane was blocked in 5% BSA containing T-BST buffer for 15 min in a plastic tray on a shaker. The respective primary antibody (Table 12) was added in a 50 ml tube diluted in 10 ml 5% BSA in TBS-T. The membrane was then transferred to this tube on a rolling platform to bring the membrane into continuous contact with the antibody solution. Either overnight at 4°C or at 20°C for at least 2 h. Unbound primary antibodies were then washed away by TBS-T. The addition of a secondary antibody was done in the next step and is similar to the previous step. The secondary antibody was coupled with horse radish peroxidase (HRP) that is subsequently required for staining with the ECL solution.

### **2.13.4. Digital quantitative WB**

For the MYC protein quantification, the cell lysates were analyzed by digital quantitative Western Blotting (WB) platform (JESS, Simple Western systems), along with a housekeeping control (Figure 9a). As a housekeeper, HDAC1 was chosen as it is also

localized in the nucleus like MYC. The area under the curve of the protein intensities were measured and indicated by JESS. Relative MYC expression were calculated using the area under the curve values from MYC and HDAC1.

Nuclear extracts were performed using the nuclear extract kit, following manufacturer's instructions. Fluorescent 5x master mix, DTT and biotinylated ladder were prepared following manufacturer's instructions. Lysates were diluted with 0.1x sample buffer and mixed 5:1 with fluorescent 5x master mix to obtain a target sample concentration of 0.40 µg/µl per well. Samples were then denatured for 5 min at 95°C in a PCR cycler. The assay plate was loaded as per manufacture's instruction and centrifuged at 1500 rpm for 5 min at 20°C to remove bubbles. The immunoassay was performed using a 12-230 kDa separation module with 25 cartridges. Lysates were separated 25 min at 375 V, blocked for 5 min with antibody diluent. Subsequently, lysates were incubated (30 min each) with primary and secondary antibodies. Primary antibody multiplex mix consisted diluted in antibody Diluent 2. Signals were detected using an anti-rabbit detection module for Jess multiplexed with an anti-mouse secondary NIR antibody.

#### **2.13.5. MYC Activity Assay**

DNA-based ELISA method was employed to measure the transcriptional activity of MYC. The method was based on ability of MYC on heterodimer formation with MAX, which is required for it binding to the E-box motif CAC(GA)TG to activate transcription. Nuclear extract of T-ALL cell lines was measured with the MYC TransAm binding ELISA, following manufacturer's instructions. 2.5 µg of nuclear extract was used for MYC binding assay using a 96-well format.

#### **2.14. Lentiviral transduction**

The lentiviral transduction allows to add, remove, or manipulate genetic information in a host cell using a commercially available third generation lentiviral vector system. To produce lentiviral viruses, packaging systems of the third generation were chosen, which guarantee a particularly high biosafety, since the viruses produced in the packaging cell line HEK293T are able to stably integrate the insert into the host cell genome but are replication incompetent.

### **2.14.1. Virus production in HEK293T**

HEK293T cells were seeded in Ø 5 cm dishes and cultivated until cells reach confluency of 70 – 80 %. Helper plasmids (virus packaging) and target plasmid were substituted in Xfect transfection reagent, a polymer containing buffer in a total volume of 600 µl and incubated on room temperature for 15 min. The plasmid-polymer solution was added subsequently, dropwise into the cell medium. Careful swirling was used to mix the plasmid solution with the cell medium. The cells were incubated for 24h. The supernatant was removed to avoid toxicity emanating from the polymer. Fresh medium was added, and cells were incubated for 48h for virus production. For virus harvest, the cell debris containing supernatant must pass a 0.45 µm filter. Then the Lenti-X concentrator was added in a 1:3 dilution to bind the virus and concentrate it for subsequent centrifugation at 1500 g at 4°C for 30 min. The supernatant was discarded and the virus containing pellets were resuspended in RPMI-full media, for following cell transduction.

### **2.14.2. Transduction of cells**

For the cell transduction, 12 well plates were prepared using retronectine-coating (20 µg/ml) to ensure the virus binding on the bottom, to keep the subsequently added cells and the virus at a close distance. To avoid cell death due to the high viral load, cells were incubated for a maximum of 24h. Cells were then washed three times with PBS, with centrifugation and discarding the supernatant. Finally, cells were resuspended in complete RPMI medium. The next step was to select the positively transduced cells.

### **2.14.3. Selection of positively transduced cells**

The used plasmids contain a selection marker to get rid of non-transduced cells. If the plasmids contain a puromycin selectin marker, the addition of puromycin in the culturing media leads to the death of the non-transduced cells. The transduced cells can handle the puromycin and stay alive. In other plasmids, where GFP was chosen as a selection marker, the separation was performed by FACS system, performed by Katharina Raba at the Institute of Transplantation Diagnostics and Cell Therapeutics (ITZ), Düsseldorf. In the case of the doxycycline driven shRNA constructs, a combination of both selections was performed. First, the cells were selected for their

puromycin resistance and second, after doxycycline addition the shRNA was produced accompanied by GFP expression, the cells were selected using FACS.

## **2.15. Gene expression analysis**

Expression data of T-ALL samples with PTEN mutation status contained in the Cancer Cell Line Encyclopedia (CCLE) project (GSE36133) was downloaded from the R2: Genomics analysis and visualization platform (<https://hgserver1.amc.nl/cgi-bin/r2/main.cgi>). Samples in the R2 platform are processed as follows: data is extracted from .cel-files, normalized according to MAS5.0 and log<sub>2</sub> transformed. A t-test was performed comparing PTEN mutated (PTEN<sup>mut</sup>) versus wildtype (PTEN<sup>wt</sup>) cell lines and considered significant if  $p < 0.05$  and fold change  $\pm 2$ . Heatmap visualization and unsupervised hierarchical clustering was performed using all significant, differentially regulated genes after normalizing mean expression to 0 with a standard deviation of 1 and using Pearson's dissimilarity algorithm and average linkage in Partek Genomics Suite. Clustering of upregulated and downregulated gene sets were performed by using the web-based program STRING (<https://string-db.org>). Gene expression analysis were kindly performed by Daniel Picard.

## **2.16. Drug screening**

To evaluate the biological activity of selected compounds, drug screening plays a major role. The heterogeneity of tumor diseases, especially when using targeted therapies, leads to a variety of possible reactions, ranging from inhibition of growth to complete killing or even increased growth.

### **2.16.1. Compound screening for IC<sub>50</sub> determination**

Inhibitors to be tested are brought into solution in a concentration of 10 mM using DMSO. Different concentrations of the compound are added to cells in a concentration of  $1 \times 10^6$  cells/ml. Accordingly, the IC<sub>50</sub> value, which indicates the concentration required to achieve 50% viability, can be determined more reliably the more concentrations are used. The read-out will be performed after 72h cell treatment using cell-titer glo for viability measurement.



### **2.16.2. Compound library**

A library containing 178 compounds was created for *ex vivo* high throughput drug screening of leukemic cell lines and patient samples. DMSO dissolved compound library was purchased from MedChemExpress (Uppsala, Sweden). The compound selection involves majority of FDA/EMA approved routinely used chemotherapeutic and targeting drugs involved in the treatment protocols (Table 10).

### **2.16.3. High throughput drug screening**

High throughput drug screening (HTDS) was performed on human T-ALL cell lines, PDX cells and healthy control peripheral blood mononuclear cells (PBMCs). Briefly, the DMSO dissolved compound library was dispensed with increasing concentrations of the inhibitors in 6 dilution steps (0.008 - 25  $\mu$ M) on a white 1536-well plate using digital dispenser, which ensures precise and robotic compound application in randomized fashion. The printed plates were sealed with parafilm, followed by packing in vacuum-sealed bags to avoid evaporation during storage at -80°C. The cells (>95% viability) were seeded on the thawed pre-dispensed inhibitor plates using an automated Multidrop Combi Reagent Dispenser. Differential responses were monitored with ATP-dependent CellTiter-Glo (CTG) luminescent cell viability kit after 72h of inhibitor exposure using microplate reader Spark 10M. The outer three wells of the plate were excluded from analysis to circumvent the evaporation effect on the plate edges. For validation of the interesting hits, 384-well plates were used, and screens were proceeded in a similar fashion as described above with more different concentrations in a logarithmic scale and in triplicates. Dose response curves (n=3) for the inhibitors were determined by plotting raw data (normalized to controls) with non-linear regression (log(inhibitor) vs. normalized response) variable slope function.

### **2.16.4. Synergy drug screening**

The compounds were printed on white 384-well plates with increasing concentrations in a dose-response 8 by 8 matrices by using a digital dispenser D300e, as described above. For birabresib and afuresertib, the concentration range was 0.01  $\mu$ M up to 5  $\mu$ M in a logarithmic distribution. Cell viability was monitored after 72h using CTG

luminescent assay measured by microplate reader Spark 10M. The Bliss synergy scores were determined using the Combenefit synergy analysis software [161].

## **2.17. Molecular biological techniques**

The effectiveness of an inhibitor can be assessed only to a certain extent by drug screening. Further investigations of biological mechanisms of action need to be validated using methods that indicate apoptosis or cell cycle analysis.

### **2.17.1. Apoptosis assays**

#### **2.17.1.1. Annexin V**

Annexin V is a protein that binds on phosphatidylserine (PS), which is found normally on the intracellular side of the plasma membrane in healthy cells. In the case of early apoptotic however, the symmetry of the plasma membrane gets lost and the PS swaps on the outside of the membrane together with the bound Annexin V. The quantification of Annexin V on the cell surface by flow cytometry provides information about the stage of apoptosis and how far it has progressed. In combination with propidium iodide (PI) the apoptotic cells can be separated into early apoptotic and late apoptotic groups. The mechanism behind is that late apoptotic cells start to get a perforated membrane, which let the PI passes inside the cell and bind the DNA. Thus, it can be used to differentiate between early apoptotic stage (Annexin V positive / PI negative) and late apoptotic stage (Annexin V positive / PI positive). For the Annexin V staining, cells were centrifuged at 400 g at 20°C for 5 min and the supernatant was discarded. The pellet was resuspended in 100 µl 1x Annexin V buffer and transferred in a 96-well plate. Fluorescence-conjugated Annexin V antibody together with PI were added according to the manufacturer's instructions into the cell suspension. The plate was incubated in the dark for 15 min before the cells were measured by flow cytometry.

#### **2.17.1.2. Caspase 3/7**

The proteins caspase 3 and caspase 7 are members of the caspase family, which play an important role in apoptosis [162]. By quantification of these proteins, the degree of apoptosis can be determined. For caspase 3/7 measurement the Caspase-Glo® 3/7 Assay system was used according to manufacturer's instructions. For the apoptosis

measurement, cells were counted and a total number of 10000 cells in 100  $\mu$ l medium were transferred into a well of a white 96 well plate with flat bottom. By adding 100  $\mu$ l of the Caspase-Glo 3/7 Assay solution to the well, the lysis of the cells was initiated, and the caspase 3/7 dependent luciferase reagent gets cleaved by the caspase that generates a luminescent signal. This reaction reaches after 40 min the maximum luminescence. After the incubation the luminescence was measured by the Tecan Spark 10M.

### 2.17.2. Cell cycle assay

The Nicoletti assay [163] is a modified cell cycle assay based on the fluorescent dye PI, which is used to detect and quantify the amount of DNA in a single cell. The percentage of cells that are in each cell cycle phase can be determined by the PI signal intensity. Apoptotic cells have a characteristic DNA content of less than  $2n$  ("sub-G0/G1 cells"). Thus, cells undergoing apoptosis initiate degradation of their DNA by cellular endonucleases. A decreased number of dividing cells (n-phase or G2-phase) indicates decreased proliferation activity of the cells. If an increased number of G2-phase cells is present, this may be due to impaired division activity resulting, for example, from defects in the spindle apparatus.

To quantify the DNA amount, cells were centrifuged at 1500 rpm at 20°C for 5 min and the supernatant was discarded. The pellet was resuspended in 100  $\mu$ l Nicoletti buffer and transferred in a 96 well plate. The plate was incubated in the dark for 30 min before the cells were measured by flow cytometry.

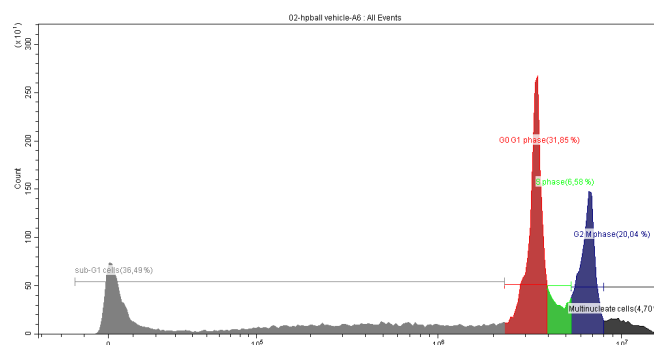


**Figure 6: Example for Nicoletti Assay analysis**

Flow cytometric measurement of an untreated leukemia cell (HPBALL) as control is shown. The PE-fluorescence intensities are shown on the y-axis and the cell number on the x-axis. The signal intensities characteristic of each cell cycle was divided into sub-G1 cells, G0/G1 phase, S phase G2/M phase and multinucleate cells.

## **2.18. *In vivo* methods**

### **2.18.1. Laboratory Animal Facility**

The mouse line used was kept and bred in the conventional animal facility of the ZETT (Heinrich-Heine University Düsseldorf). Inbreeding was performed to keep the genotype stable. Each animal was registered and set down with the help of an ear tag according to their individual number. Tail tip biopsies were performed regularly to determine the genotype, which was performed by the group of Dr. Stegbauer. All experiments performed were approved by the North Rhine-Westphalia State Office for Nature, Environment and Consumer Protection (LANUV) (Aktenzeichen 81-02.04.2017.A441) and were conducted in compliance with German animal welfare laws.

### **2.18.2. PDX cell enrichment**

Patient cells obtained from the clinic (University Hospital Düsseldorf) were thawed and washed twice with PBS.  $1 \times 10^5$  to  $1 \times 10^6$  cells in 100  $\mu$ l PBS were injected in the tail vein of mice. Monitoring of the engraftment was performed weekly by analyzing blood samples via flow cytometry using anti-mouse CD45-AF700 and anti-human CD45-APC. After the cells reached a percentage of 60 or higher in the blood, the cells were harvested from the spleen and bone marrow. Mouse cells were separated from human cells by using CD45 mouse magnetic beads and the appropriate columns. The flow-through containing the non-touched, enriched human cells were used further for *in vitro* drug screening and functional assays.

### **2.18.3. *In vivo* optical imaging**

Engraftment and disease progress of human leukemia cell line models was performed by bioluminescence imaging of stable luciferase expressing cell lines. The bioluminescence was initiated by intraperitoneal (i.p.) injection of 10  $\mu$ l/kg D-Luciferin potassium salt in a concentration of 15 mg/ml solved in PBS. Between 10 and 15 min the highest signal intensities were expected. In case of a positive engraftment, the leukemic cells enter the mouse bloodstream and settle in the bone marrow. Accordingly, a high signal of bioluminescence is found in the hind legs but also in the

spinal cord and spleen cells are rapidly affected by cell infiltration. The signal intensities become stronger the later the disease progress. Measurements were performed using the IVIS Spectrum *in vivo* imaging system. Three images of different exposure times were made; 60 sec, 30 sec and 5 sec to avoid saturation in late diseased mice with higher signal intensities. The images were subsequently analyzed using the software Living Image.

#### 2.18.4. *In vivo* testing of copanlisib and JQ1

$5 \times 10^6$  MOLT4-luciferase expressing (stably transduced) cells were injected intravenously (i.v.) in the tail vein of mice. Engraftment was monitored after 7 days via *in vivo* optical imaging. Positively engrafted mice were separated into four different groups  $n=3$ . Mice were injected i.v. either with vehicle or inhibitors copanlisib, JQ1 or the combination of both (each 5 mg/kg dose).

Vehicle for JQ1:

**Table 22: Vehicle for iv. injection (5 mg/kg)**

Substitution order	Substance	Percentage
1	DMSO	2%
2	PEG300	30%
3	Tween20	5%
4	ddH <sub>2</sub> O	63%

Vehicle for copanlisib:

**Table 23: Vehicle for iv. injection (5 mg/kg)**

Substitution order	Substance	Percentage
1	0.1 N HCL H <sub>2</sub> O	80%
2	PEG300	20%

Mice were sacrificed on day 40.

#### 2.18.5. *In vivo* testing afuresertib and birabresib

$5 \times 10^6$  HPBALL-luciferase expressing (stably transduced) cells were injected i.v. in the tail vein of mice. Engraftment was monitored after 3 days via i.p. injection of 10  $\mu$ l/g D-Luciferin, firefly, potassium salt. The luminescence measurements were performed after an incubation time of 12 min, using the Caliper IVIS Lumina II Multispectral Imaging System and the Living Image Software. Inhibitors (50 mg/kg dose) or vehicle

was administered starting from the day after the transplantation by oral gavage for up to 15 days (n=5 per group).

The vehicle of the compounds used was composed as follows:

Vehicle for afuresertib:

**Table 24: Vehicle for oral gavage (50 mg/kg)**

<b>Substitution order</b>	<b>Substance</b>	<b>Percentage</b>
1	DMSO	2%
2	PEG300	30%
3	Tween 20	5%
4	Normal saline	63%

Vehicle for birabresib:

**Table 25: Vehicle for oral gavage (50 mg/kg)**

<b>Substitution order</b>	<b>Substance</b>	<b>Percentage</b>
1	DMSO	2%
2	PEG300	30%
3	Tween 20	5%
4	Normal saline	63%

Mice were sacrificed on Day 40.

### 3. Results

#### 3.1. Characterization of MYC in T-ALL cell line models

The oncoprotein MYC plays a crucial role in the development of future therapies for refractory or relapsed T-ALL patients. MYC is a key player in the development of leukemia initiating cells (LIC). Since dysregulation of MYC is frequently observed in T-ALL patients, the following section focuses on the characterization of T-ALL cell lines and patient-derived T-ALL cells based on their MYC expression and MYC activity. The additional aim of this section is to identify the signaling pathways involved in deregulation of MYC expression for further drug screening experiments.

##### 3.1.1. Identification of MYC expression on mRNA and protein level in T-ALL cell line models

To start, the MYC expression on mRNA and protein level was investigated in nine different T-ALL cell line models, including DND41, HPBALL, HSB2, JURKAT, KOPTK1, MOLT4, P12 ICHIKAWA, PEER and TALL1. The expression of MYC mRNA in cell line models was normalized to MYC mRNA levels of T cells from a healthy donor (Figure 7a). Heterogeneously upregulated MYC mRNA expression was measured in all screened cell lines with HPBALL as the one with the highest expression ( $\Delta\Delta\text{ct}$  6.6) and JURKAT with the lowest determined amount ( $\Delta\Delta\text{ct}$  0.5). Next, MYC protein expression values quantified from WB (Figure 8b) were compared to the cell line specific mRNA values (Figure 7a). A Pearson correlation was performed with the mRNA and protein values to determine the correlation coefficient (Figure 7b). No significant correlation was found when comparing MYC mRNA expression with protein expression ( $r=0.2017$ ,  $p=0.2252$ ). In line with these results, previous studies on human patient samples have shown that the expression of the MYC mRNA does not correlate with the protein content of the patients either [93]. Based on these facts, the next step was to investigate possible MYC regulatory signaling pathways.

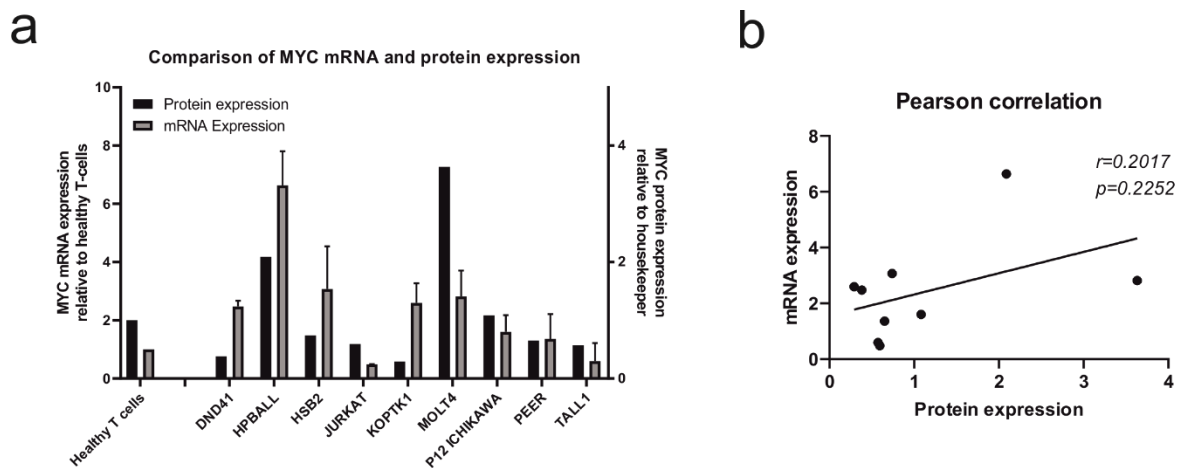


### Figure 7: Analysis of MYC expression on mRNA and protein level

a) Correlation of MYC mRNA fold expression relative to healthy T cells with protein expression relative to healthy T cells in T-ALL cell line models. b) Pearson correlation between MYC- MYC mRNA fold expression relative to healthy T cells with protein expression relative to healthy T cells.

#### 3.1.2. Characterization of post-transcriptional MYC regulatory pathways

In order to investigate potential MYC regulators, several previously discussed pathways, related to MYC were further investigated by WB from cell lysates of nine different T-ALL cell lines (Figure 8a). Prominent pathways described in connection with MYC, include MEK/ERK- and PI3K/AKT pathway as stability regulators and AURKA as a direct downstream target. Two characteristics attracted attention when analyzing the WB results. Firstly, half of the cell lines, including HPBALL, JURKAT, MOLT4 and SUPT1 showed no or only a weak PTEN signal and secondly, there were two cell lines with strongly increased MEK phosphorylation, including DND41 and HSB2. No obvious correlation was made with cell lines DND41 and HSB2, the increased phosphorylation of MEK and MYC expression. However, the analysis of protein expression, especially with regard to the PI3K/AKT pathway, revealed an interesting relationship between the presence or absence of PTEN, the phosphorylation of AKT and the total amount of MYC. MYC protein expression was quantified relative to housekeeper  $\beta$ -actin (Figure 8b). It was noticed that the amount of MYC correlated with the absence of PTEN. When all PTEN-positive cell lines were compared with PTEN-negative cells, a high tendency of a correlation between the absence of PTEN and increased MYC expression was observed with a mean normalized MYC expression of 0.53 for PTEN<sup>wt</sup> and 1.85 for PTEN<sup>mut</sup> ( $p=0.0625$ ) (Figure 8c). Consequently, cell lines lacking PTEN protein bands were designated PTEN<sup>mut</sup>, including HPBALL, JURKAT, MOLT4, and additionally cell



lines CCRF/CEM and P12 ICHIKAWA examined later. All cell lines that showed PTEN expression at the protein level, including DND41, HSB2, KOTK1, PEER, and TALL1, were designated as PTEN<sup>wt</sup>. To investigate the correlation between the absence of PTEN and the expression of MYC proteins, further protein quantification analyses were performed in a highly quantitative manner using digital WB.

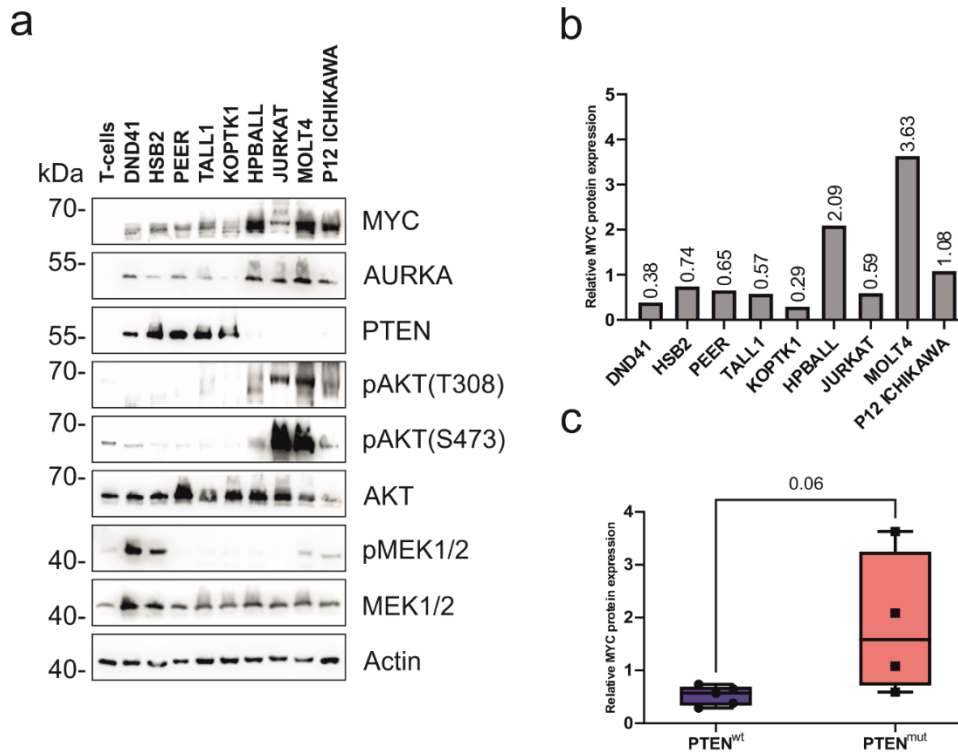


### Figure 8: Characterization of MYC related signaling pathways

a) Representative WBs of T-ALL cell lines, assessing MYC associated proteins. b) MYC protein expression values relative to  $\beta$  Actin c) MYC expression comparison between PTEN<sup>mut</sup> and PTEN<sup>wt</sup> cell lines,  $p=0.06$ , significance was determined by student's t-test.

The evaluation of the MYC values by digital quantitative WB method showed that the expression in PTEN<sup>mut</sup> cell lines appeared to be significantly increased (Figure 9a and b). Here, P12 ICHIKAWA cell line showed the highest amount of MYC (relative expression of 2.78) in the PTEN<sup>mut</sup> group, followed by MOLT4 (relative expression of 2.44), HPBALL (relative expression of 1.67), CCRF/CEM (relative expression of 1.58), and JURKAT (relative expression of 0.89). DND41 showed the highest amount of MYC in the group of PTEN<sup>wt</sup> cell lines (relative expression of 1.34), followed by HSB2 (relative expression of 0.96), PEER (relative expression of 0.84), KOPTK1 (relative expression of 0.78), and TALL1 (relative expression of 0.77), respectively (Figure 9a). Taken together, the MYC expression was significantly higher in PTEN<sup>mut</sup> compared to PTEN<sup>wt</sup> (relative expression of 1.97 vs. 1.07,  $p=0.0206$ ).

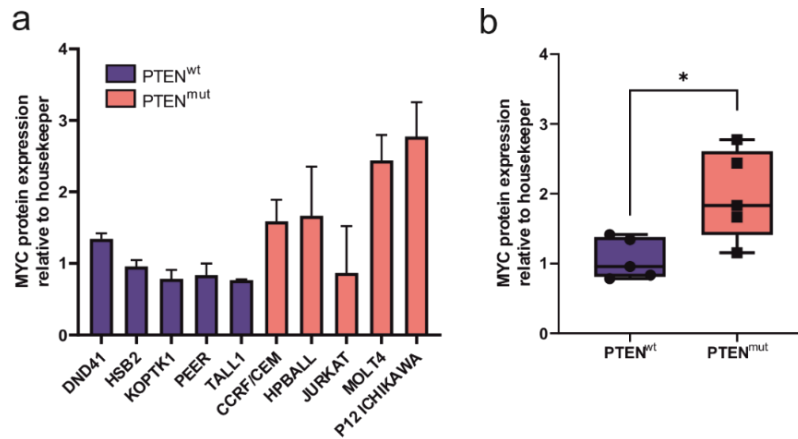


**Figure 9: Correlation of MYC protein level between PTEN<sup>wt</sup> and PTEN<sup>mut</sup>**

a) MYC quantification by quantitative WB using values of biological triplicates, cell lines were separated by the previous classified pre- or absence of PTEN. b) Boxplots of grouped quantitative WB values PTEN<sup>wt</sup> vs. PTEN<sup>mut</sup>. \*, p<0.05; \*\*, p<0.01; \*\*\*, p<0.001 (student's t-test).

To determine whether not only the expression but also the activity of MYC is affected by PTEN, an ELISA-based assay was performed. The activity of MYC from the nucleus extracts of the cell lines was examined by its binding affinity to E-box sequences bound to the bottom of the ELISA plates (Figure 10a). The activity of MYC was slightly but not significantly increased in the PTEN<sup>mut</sup>, as shown in the box plot figure 10b when compared to PTEN<sup>wt</sup> (relative activity of 0.81 vs. 0.68, p=0.1566).

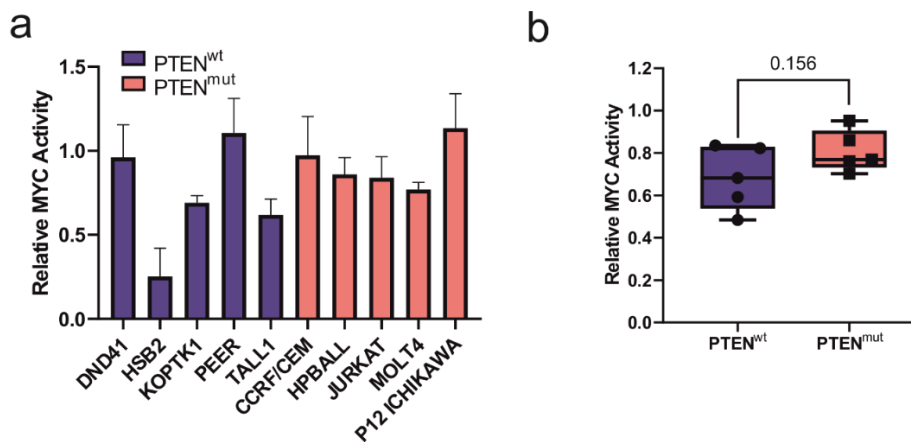


**Figure 10. Correlation of MYC activity between PTEN<sup>wt</sup> and PTEN<sup>mut</sup>**

a) MYC activity of PTEN<sup>wt</sup> and PTEN<sup>mut</sup> cell lines was measured with an ELISA based assay with E-Box sequence coated plates. The more MYC binding on the E-Box sequences on the plate, the higher the relative MYC activity was measured. b) Boxplot of grouped MYC activity values for PTEN<sup>wt</sup> and PTEN<sup>mut</sup>, p=0.156, significance was determined by student's t-test.

To investigate the molecular mechanism behind the increased protein stability and activity of MYC, the PTEN- and MYC-associated signaling pathways in the cell lysates

were investigated by WB (Figure 11a). Since PTEN is a negative regulator of the PI3K/AKT signaling pathway, the expression and phosphorylation of AKT and GSK3 $\beta$  was studied in detail. The phosphorylation of MYC at the known sites T58 (marker for degradation) and S62 (marker for stability) were also investigated to find out whether the absence of PTEN influences the MYC balance as it is hypothesized in figure 11b.

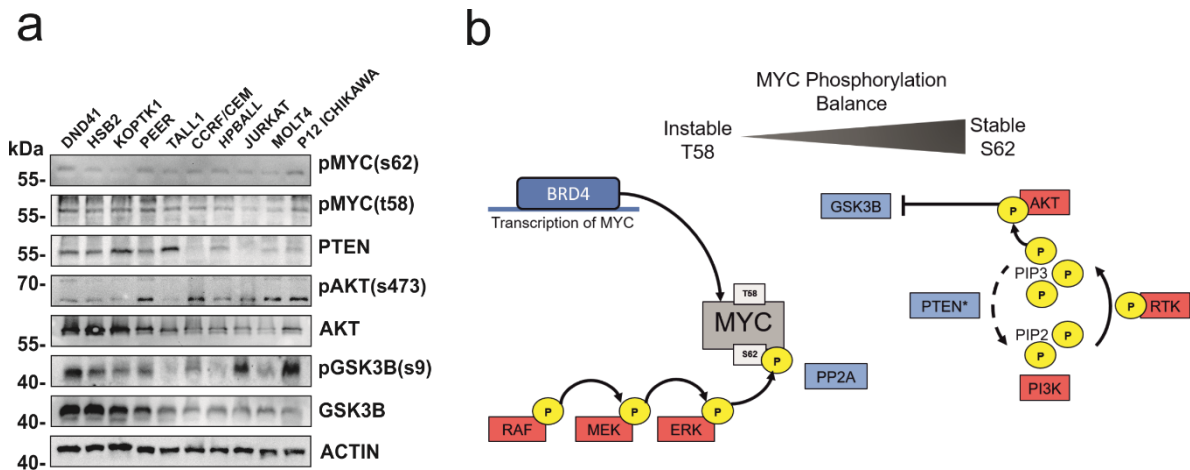


**Figure 11: The role of PI3K/AKT pathway in MYC stability regulation**

a) Representative WB of T-ALL cell lines focused on the PI3K/AKT-GSK3 $\beta$  axis and examined phosphorylation status. b) Schematic figure of MYC stability enhancement due to dysregulated PI3K/AKT pathway caused by PTEN loss of function.

Slightly higher MYC expressions were examined in PTEN<sup>mut</sup> cell lines, CCRF/CEM, HPBALL, MOLT4 and P12 ICHIKAWA with JURKAT again as an exception, matching to the previous results of the protein quantification. The phosphorylation on site T58 was slightly lower in PTEN mutant cell lines as compared to the wild types. At the protein level, AKT is generally more highly phosphorylated in PTEN<sup>mut</sup>, and in some cases GSK3 $\beta$  phosphorylation is increased (JURKAT and P12 ICHIKAWA), resulting from its inhibition by the increased inhibitory activity of AKT. Considering the total amount of GSK3 $\beta$  protein, it was found that more GSK3 $\beta$  protein was present at PTEN<sup>wt</sup> compared with the mutants. However, no differences in the phosphorylation of MYC at site S62 could be found between the two groups.

### 3.1.3. Characterization of T-ALL Patient derived xenograft cells

To confirm these results in patients, samples from the bone marrow of four T-ALL patients were enriched by xenotransplantation in NGS mice. Four of five injected patient cells engrafted successfully in mice and were obtained soon as the number of human cells in the peripheral blood reached over 60%. Cell pellets were harvested

and lysed for target assessment by WB (Figure 12). It was found that half of the patients had no visible PTEN expression at the protein level, which will be hereafter referred as PTEN<sup>mut</sup>.

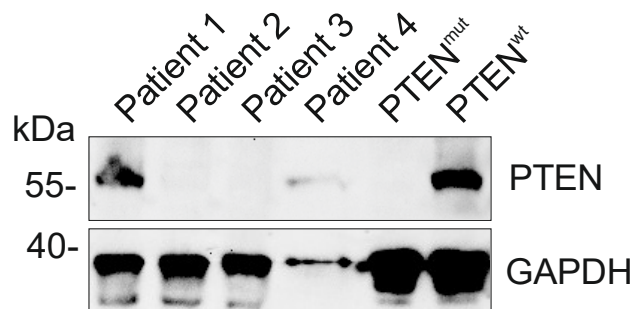


**Figure 12: PTEN protein detection of T-ALL patient cells**

Representative WBs of lysates taken from T-ALL patient samples enriched in a xenograft mouse model to investigate PTEN expression on protein level.

**3.1.4. Establishment of an inducible PTEN knock down cell line model**

To validate the impact of the absence of PTEN on MYC protein, findings overserved in PTEN<sup>mut</sup> vs. PTEN<sup>wt</sup> T-ALL cell lines, a PTEN positive cell line DND41 was transduced with a doxycycline inducible shRNA targeting PTEN mRNA. Three PTEN shRNA constructs were used and one non-target (NT) shRNA. PTEN reduction with shRNA construct 2 was successful (herein referred as shPTEN). The non-target shRNA (herein referred as shNT) was used as a control. The decrease of PTEN was visibly correlated with a slight increase of phosphorylated AKT, GSK3 $\beta$  and the of total amount of MYC protein level, according to the WB results (Figure 13a). Quantitative digital WB analysis has shown that the decrease of PTEN lead to an increase in the total amount of MYC significantly (relative expression of 1.78 for shNT vs. 2.11 for shPTEN,  $p=0.007$ ) (Figure 13b). Interestingly, when looking at the mRNA expression of MYC no differences were detected ( $\Delta\Delta\text{ct}$  1.00 shNT vs.  $\Delta\Delta\text{ct}$  1.17 shPTEN) (Figure 13c).

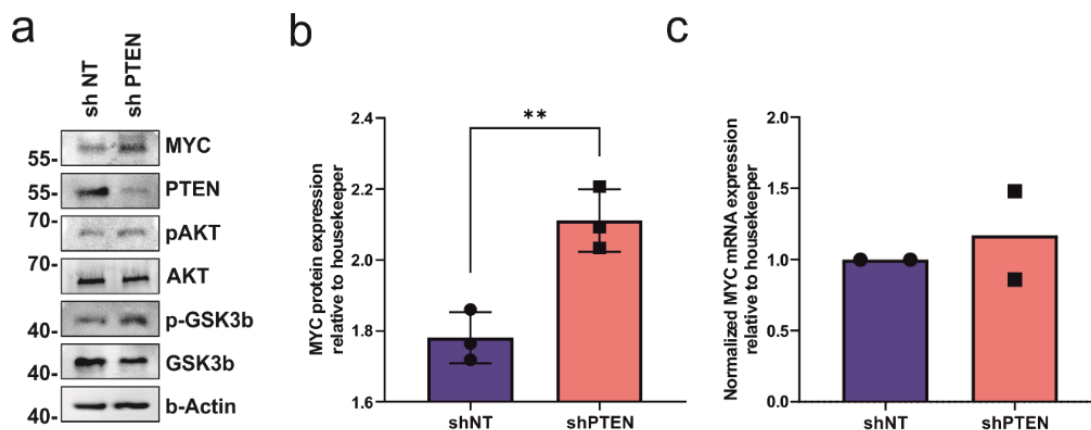


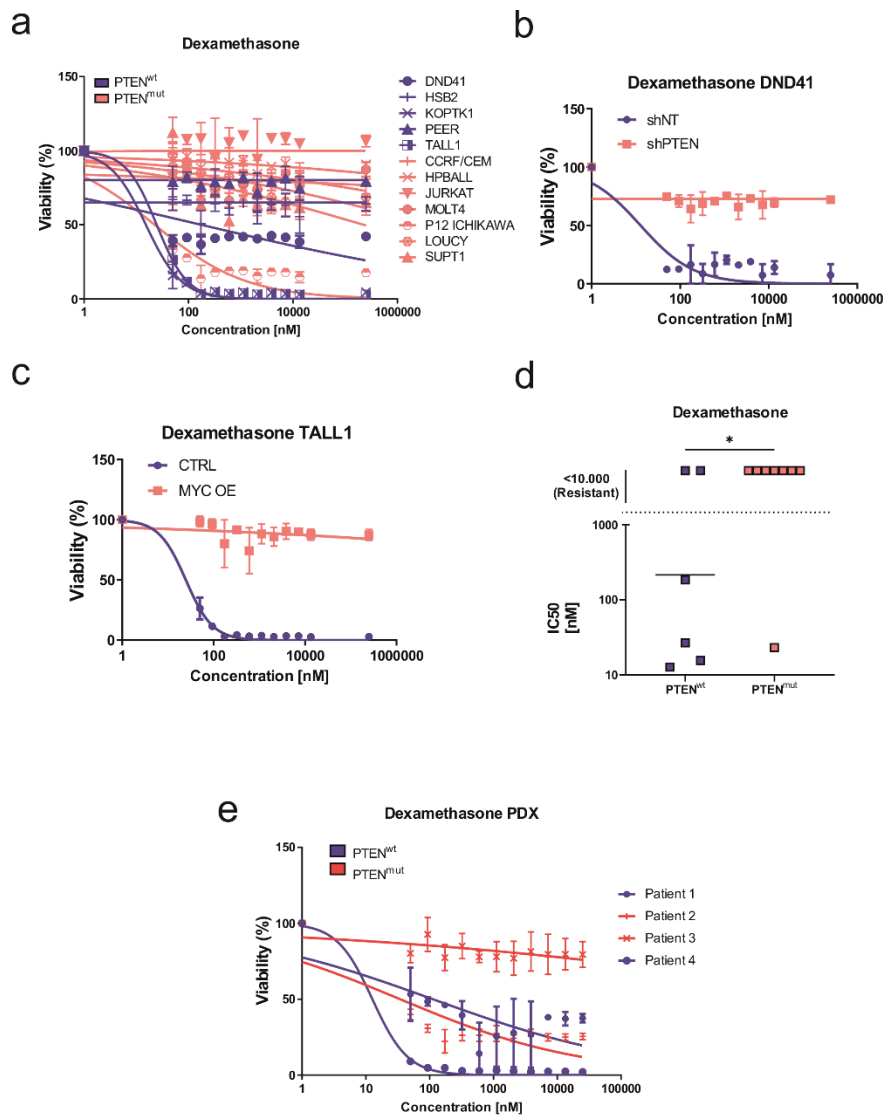
**Figure 13: Investigation of an inducible PTEN knockdown cell model DND4**

a) Representative WB of transduced DND41 cells with either inducible non-target knockdown (shNT) or PTEN (shPTEN) by the expression of respective shRNA. b) Quantitative WB values of MYC compared between shNT and shPTEN. c) Normalized MYC mRNA expression comparison between shNT and shPTEN. \*,  $p < 0.05$ ; \*\*,  $p < 0.01$ ; \*\*\*,  $p < 0.001$  (student's t-test).

### 3.1.5. Investigation of glucocorticoid therapy resistance

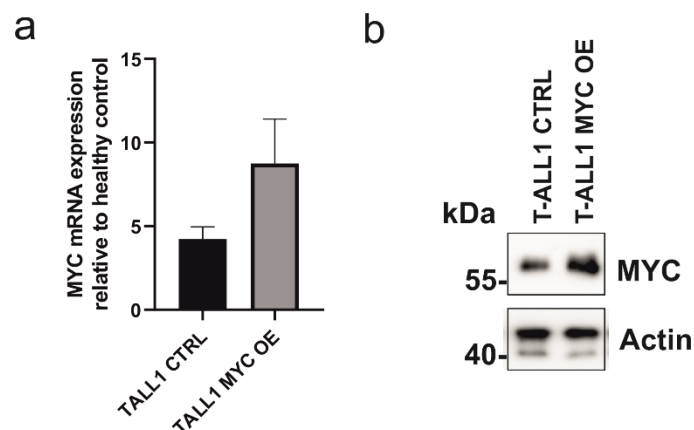
In connection with PTEN mutations, previous studies have shown resistance to glucocorticoids (GC) [164, 165]. Therefore, a drug screening with dexamethasone in a concentration range from 5 to 10000 nM in a total number of 5 PTEN<sup>wt</sup> and 7 PTEN<sup>mut</sup> T-ALL cell lines was performed (Figure 14a). T-ALL cell lines surviving at 10000 nM dexamethasone were categorized as GC resistant. Interestingly, 6 of 7 PTEN<sup>mut</sup> cell lines tested were significantly resistant to GC except for P12 ICHIKAWA with an IC<sub>50</sub> value of 23.17 nM, whereas 3 of 5 of the PTEN<sup>wt</sup> cell lines had IC<sub>50</sub> values ranging from 15.29 to 177.50 nM, and the remaining two cell lines (PEER and HSB2) were considered as GC resistant (Figure 14a). The same drug screening was performed with the inducible PTEN knock down model in DND41 cell line (Figure 14b). Interestingly, when PTEN was knocked down (shPTEN), the DND41 cells were resistant to dexamethasone treatment, as compared to control (shNT) with an IC<sub>50</sub> value of 12.70 nM. In order to find out, whether this effect is caused by the increased MYC protein level or not, the cell line T-ALL1 with the lowest MYC protein (amount measured by digital WB) was transduced with a MYC overexpression plasmid that was validated by mRNA and WB (Figure 15a and b). The additional increase of MYC in T-ALL caused indeed a resistance against dexamethasone treatment (Figure 14c). IC<sub>50</sub> values of dexamethasone treatment were taken together and compared between PTEN<sup>wt</sup> and PTEN<sup>mut</sup> (Figure 14d). PTEN<sup>mut</sup> were significantly resistant against

dexamethasone treatment ( $p=0.0379$ ). Next, the resistance to dexamethasone in PDX T-ALL cells was investigated (Figure 14e). Based on the result of PTEN protein assay (Figure 12), patient samples were classified into either PTEN wild-type or mutant. Drug screening with dexamethasone revealed that one PTEN<sup>mut</sup> PDX sample was resistant to dexamethasone. The other three, which included one PTEN<sup>mut</sup> and two PTEN<sup>wt</sup> PDX cells, showed sensitivity to dexamethasone. Due to the small number of samples, no statistics analysis was conducted.



**Figure 14: Correlation between PTEN mutation and glucocorticoid resistance (Dexamethasone)**

a) Drug response curves of dexamethasone in T-ALL cell lines, b) PTEN knock down cell model DND41 and c) Drug response curves of MYC overexpressing cell model TALL1. d) Comparison of the dexamethasone IC<sub>50</sub> values between PTEN<sup>mut</sup> and PTEN<sup>wt</sup> e) Drug response curves of dexamethasone in T-ALL PDX samples. \*,  $p<0.05$ ; \*\*,  $p<0.01$ ; \*\*\*,  $p<0.001$  (student's t-test).

**Figure 15: Molecular validation of MYC overexpression cell model T-ALL1**

a) Normalized MYC mRNA values in TALL1 transduced with an empty vector (ctrl) and a MYC overexpression vector (MYC OE). b) Representative WB of TALL1 MYC overexpression cell model to validate MYC overexpression on molecular level.

To figure out the genetic mechanism behind the GC resistance, a public available gene expression dataset of diverse T-ALL cell lines was analyzed [166]. All significant up- and downregulated genes in  $PTEN^{wt}$  and  $PTEN^{mut}$  cell lines were analyzed and are shown in a non-supervised clustered heatmap (Figure 16a). In fact, a lot of genes were differently expressed, which cluster both groups  $PTEN^{wt}$  and  $PTEN^{mut}$ . To find out whether there is a correlation between the up- and down-regulated genes in  $PTEN^{mut}$ , the genes were matched with a MYC target gene database from hallmark gene sets (HALLMARK\_MYC\_TARGETS\_V1 and HALLMARK\_MYC\_TARGETS\_V2). Matching genes are shown in Figure 16b sorted by decreasing significance from left to right. The highest and most significant expressed gene in  $PTEN^{mut}$  was ARNTL2 ( $p=0.0024$ ), which is a transcriptional activator that plays a major role as a transcriptional activator, that forms a core component of the circadian clock [167, 168]. The second most significant upregulated gene was ABCA5 ( $p=0.0034$ ), a member of the ABC transporter molecule family. ABC proteins transport different molecules across extra- and intracellular membranes. Interestingly, ABCA5 has been previously implicated in resistance mechanisms to small inhibitors [169]. Although ARNTL2 expression appears to be higher and more significant in the  $PTEN^{mut}$  cell lines, the next step was to focus on the ABC transport molecule ABCA5, as a link to a resistance mechanism would be more likely in this case.



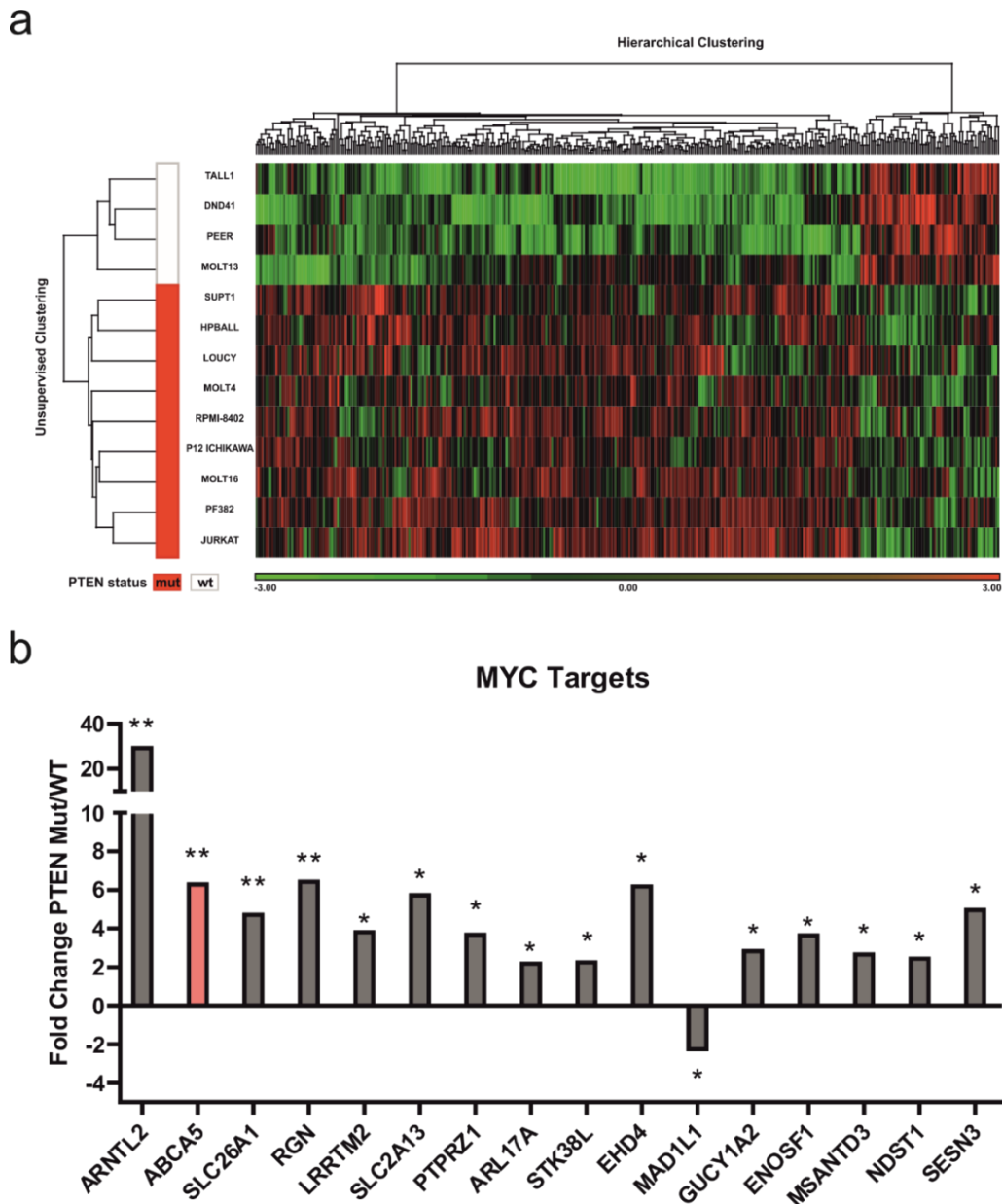


**Figure 16: Genetic hallmarks of PTEN mutant cell lines**

a) Heatmap of up- and downregulated genes dependent on the PTEN pre- or absence. b) Most significant up- and downregulated MYC-target genes in PTEN<sup>mut</sup> cell lines, significance is decreasing from left to right. \*, p<0.05; \*\*, p<0.01; \*\*\*, p<0.001 (student's t-test).

To validate the expression of ABCA5 in T-ALL cell line models used in this thesis, the mRNA expression of ABCA5 was measured by rt-qPCR. Interestingly, all the PTEN<sup>mut</sup> cell lines exposed a higher normalized fold expression of ABCA5 with ranging  $\Delta\Delta$ ct values from 0.42 to 4.03, compared to the PTEN<sup>wt</sup> cell lines with  $\Delta\Delta$ ct ranging from 0.01 to 0.31 (Figure 17a). By comparing both groups, significant differences in ABCA5 expression were mentioned dependent on the PTEN pre- or absence (p<0.001) (Figure 17b).



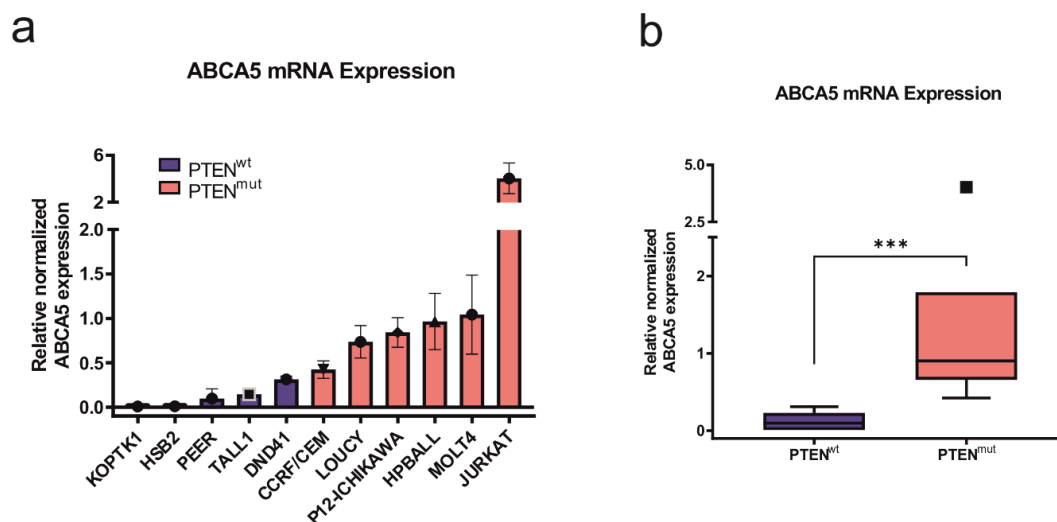


**Figure 17: Validation of increased ABCA5 expression in T-ALL cell lines**

a) Normalized fold ABCA5 expression relative to zero of T-ALL cell lines sorted by increased values from left to right. b) Boxplot of grouped normalized fold ABCA5 mRNA expression in PTEN<sup>wt</sup> vs. PTEN<sup>mut</sup>. \*, p<0.05; \*\*, p<0.01; \*\*\*, p<0.001 (student's t-test). (outlier excluded).

### 3.2. High-Throughput drug screening of T-ALL cell lines

A high-throughput drug screening was performed to identify appropriate inhibitors for MYC-dependent and GC resistant cells by tackling several signaling pathways that might be involved in MYC stabilization, modification, or transcription. Therefore, a compound library was established, harboring 178 compounds, including several compound groups like conventional chemotherapeutics, antimetabolites, Kinase-, HDAC-, TKI inhibitors (Table 21). T-ALL cell lines were seeded in a conc. of  $0.5 \times 10^6$  cells/ml in the prepared wells of the drug screening library and were incubated for 72h before CTG was added to analyze the viability. The log IC<sub>50</sub> value of every compound was calculated using non-linear calculations. Log IC<sub>50</sub> values are compared between the cell lines dependent on their PTEN status. A heatmap of calculated IC<sub>50</sub> values was generated using R. Non-supervised clustering sorted the compounds by efficacy and differences in the pre-clustered cell subsets (Figure 18b). Compounds that are efficient in both groups are clustered on the left side whereas selective compounds are clustered on the right-side dependent upon the PTEN status. Less-efficient compounds are indicated in the middle area. When examining the clusters formed in the heatmap, it was noticed that some compounds were particularly effective in the group of PTEN<sup>mut</sup> cell lines, the PI3K and AKT inhibitors. These compounds show a selective effectiveness only in the group of PTEN<sup>mut</sup>. Among these compounds, two are

particularly noteworthy, the reversible pan PI3K inhibitor copanlisib (FDA approved) and the AKT inhibitor afuresertib.

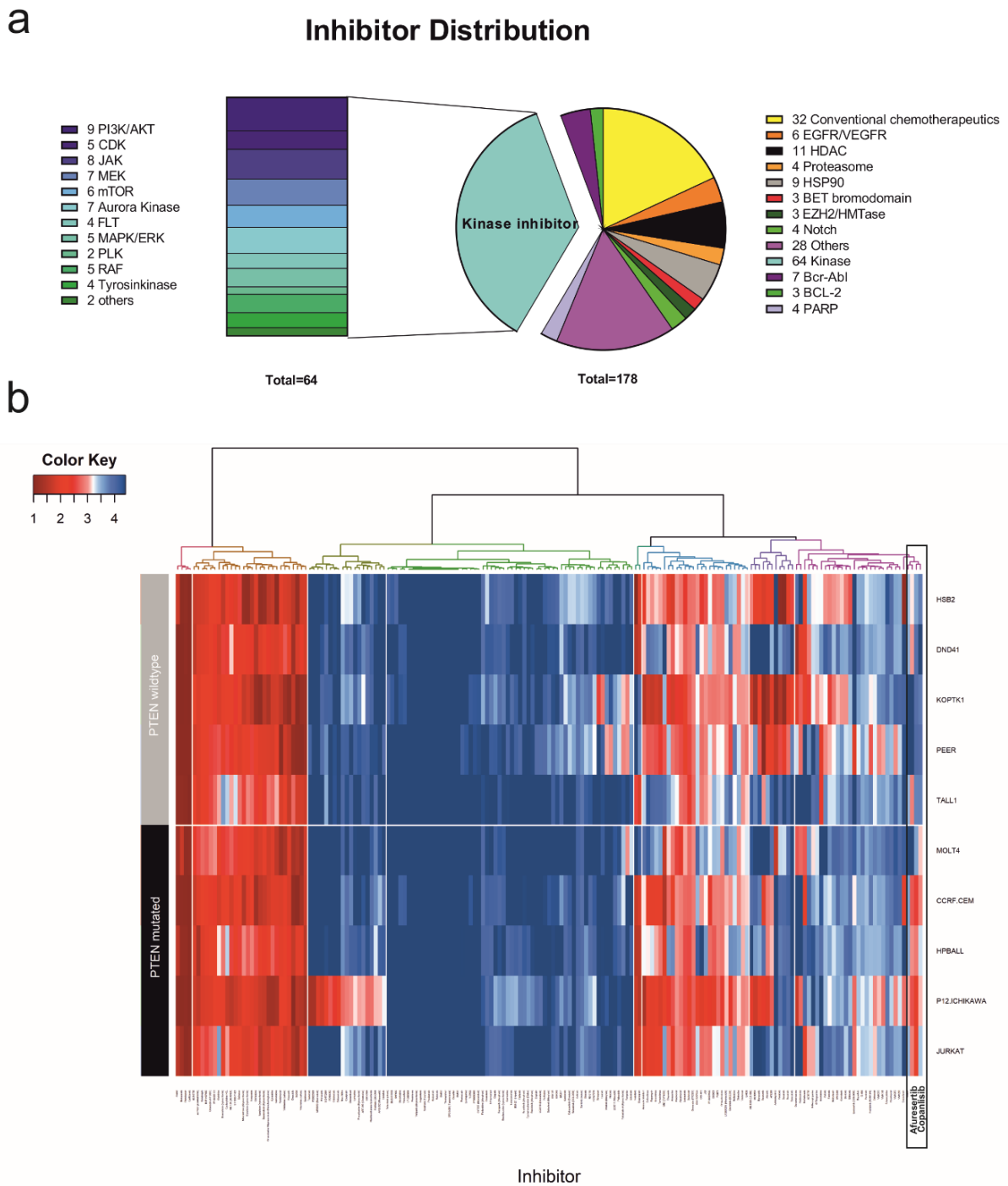


**Figure 18: High throughput drugscreening pipeline for leukemia**

a) Summary of different inhibitor groups. b) Heatmap of determined  $IC_{50}$  values form different T-ALL cell lines separated in groups  $PTEN^{wt}$  and  $PTEN^{mut}$ . Non-supervised clustering was performed on the inhibitors to demonstrate similar effectivity on the right side and more group specific activity on the right side.

To better illustrate this, another heat map was generated using R, which contains only the inhibitors of the PI3K and AKT signaling pathways (Figure 19). Copanlisib showed the most selective activity in both groups with  $IC_{50}$  values ranging from 0.84 to 2.40  $\mu\text{M}$ , with a mean of 1.57  $\mu\text{M}$  in  $PTEN^{\text{mut}}$  and 1.20 to 23.99  $\mu\text{M}$  with a mean of 9.15  $\mu\text{M}$  in  $PTEN^{\text{wt}}$ . Afuleresertib showed similar selectivity but higher efficacy in  $PTEN^{\text{mut}}$  cell lines with  $IC_{50}$  values of 0.20 to 3.60  $\mu\text{M}$  with a mean of 0.99  $\mu\text{M}$  compared with  $IC_{50}$  values of 3.29 to 9.75  $\mu\text{M}$  with a mean of 6.50  $\mu\text{M}$  for  $PTEN^{\text{wt}}$ . Dactolisib and buparlisib, two other PI3K inhibitors, showed less selective efficacy in  $PTEN^{\text{mut}}$  with mean values of 2.11  $\mu\text{M}$  and 2.77  $\mu\text{M}$ , respectively. The compounds pictilisib (mean of 11.2  $\mu\text{M}$ ), miransertib (mean of 8.57  $\mu\text{M}$ ) and idelalisib (mean of 17.08  $\mu\text{M}$ ) had even poorer selectivity or efficacy. The decision was made to continue with more focused drugs testing with the most potent and selective compounds copanlisib and afuleresertib.

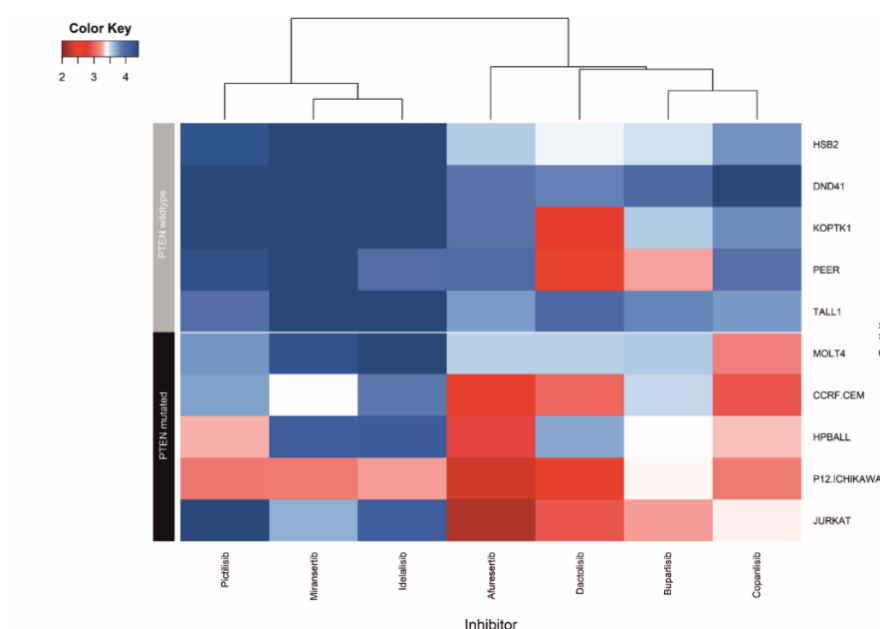


**Figure 19: Focused heatmap of PI3K and AKT inhibitors**

A section of the selectively acting PI3K and AKT inhibitors is shown in Figure 18.

### 3.2.1. Investigation of PI3K/AKT inhibitors

To prevent inhibition of the target signaling pathways from damaging healthy cells, peripheral blood derived mononuclear cells (PBMCs) from three healthy donors were treated with selected compounds (Figure 20). The results show that the compound copanlisib has a very low effect on healthy PBMCs without reaching an  $IC_{50}$  value and afuleresertib only affects healthy cells at very high concentrations ( $IC_{50}$  22.35  $\mu\text{M}$ ), whereas staurosporine, the control for killing had an  $IC_{50}$  of 0.98  $\mu\text{M}$ .

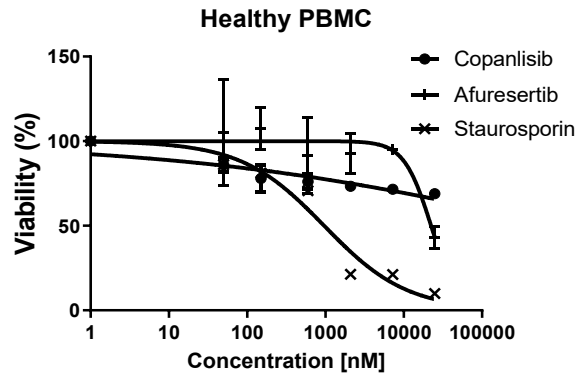


**Figure 20: Drug response curves of PBMCs from three different healthy donors**  
 Drug response curves of copanlisib, afuresertib and staurosporin as killing control tested on healthy PBMCs from three different donors after 72h treatment of 6 different concentrations.

Subsequently, an in-depth drug screen with a higher number of concentrations and triplicates for 10 cell lines comprising 5 PTEN<sup>wt</sup> and 5 PTEN<sup>mut</sup> cell lines was performed with afuresertib and copanlisib to validate the findings of the high throughput drug screening (Figure 21a and c).

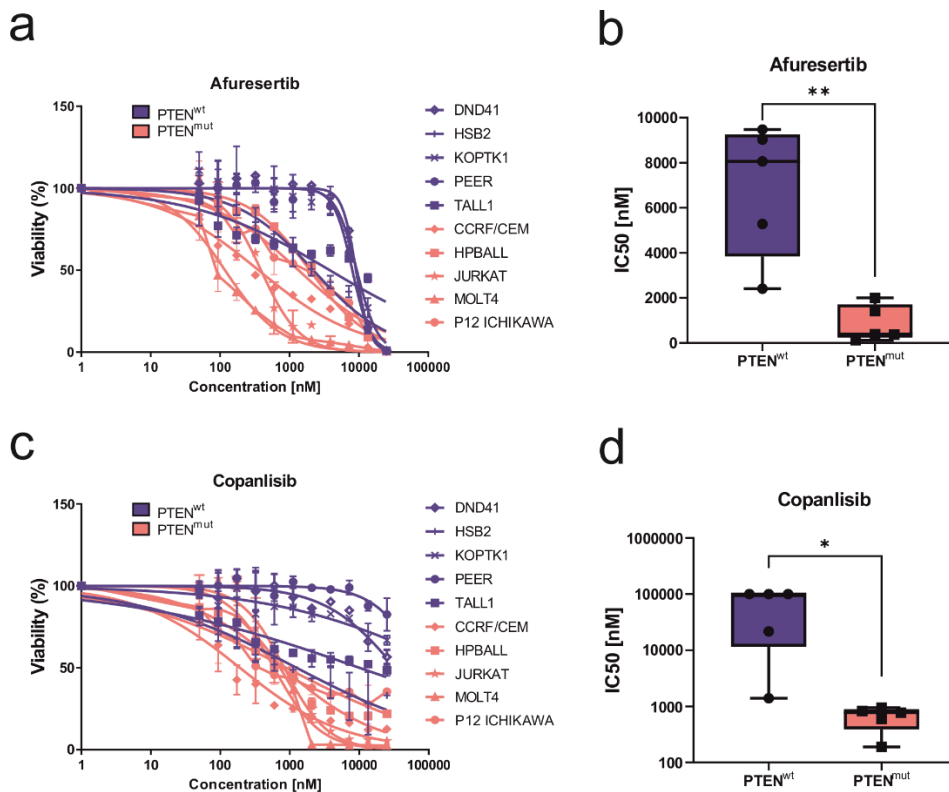


**Figure 21: Focused drug screening of PI3K and AKT inhibitors**

a) Drug response curves of afuresertib. b) Boxplots of IC<sub>50</sub> values compared between PTEN<sup>wt</sup> and PTEN<sup>mut</sup> cell lines. c) Drug response curves of copanlisib. d) Boxplots of IC<sub>50</sub> values compared between PTEN<sup>wt</sup> and PTEN<sup>mut</sup> cell lines. \*, p<0.05; \*\*, p<0.01; \*\*\*, p<0.001 (student's t-test).

The IC<sub>50</sub> values of the two compounds afuresertib and copanlisib were calculated for each T-ALL cell line used and presented in Table 26. IC<sub>50</sub> values for copanlisib varied in the group of PTEN<sup>wt</sup> between 1.17 to 34.32 μM with two cell lines (KOPTK1 and PEER) that did not reach the IC<sub>50</sub>. Considerably lower IC<sub>50</sub> values were measured in the PTEN<sup>mut</sup> cell lines varying between 0.19 to 0.91 μM. Similar trends were observed using afuresertib where PTEN<sup>wt</sup> IC<sub>50</sub> varied between 2.25 to 9.36 μM and PTEN<sup>mut</sup> between 0.12 to 1.96 μM. Comparing both groups PTEN<sup>wt</sup> and PTEN<sup>mut</sup> showed significant differences in sensitivity using the PI3K inhibitor copanlisib (p=0.0193) and even higher significant differences with the AKT inhibitor afuresertib (p=0.0024) (Figure 21b and d). In both cases, the PTEN<sup>mut</sup> cell lines showed more sloping linear regression curves than the PTEN<sup>wt</sup> cell lines.

**Table 26: IC<sub>50</sub> values of copanlisib and afuresertib in T-ALL cell lines**

	IC <sub>50</sub> [μM]									
	PTEN wildtype					PTEN mutant				
	DND41	HSB2	KOPTK1	PEER	TALL1	CCRF/CEM	HPBALL	JURKAT	MOLT4	P12 ICHIKAWA
Afuresertib	9.04 ± 0.01	2.25 ± 0.42	9.36 ± 0.07	8.05 ± 0.09	3.81 ± 0.64	0.36 ± 0.01	1.96 ± 0.08	0.39 ± 0.03	0.12 ± 0.02	1.34 ± 0.35
Copanlisib	34.32 ± 4.53	1.17 ± 0.22	n.e.	n.e.	10.38 ± 2.50	0.19 ± 0.03	0.79 ± 0.13	0.83 ± 0.11	0.60 ± 0.08	0.91 ± 0.21

Subsequently, the effectivity of afuresertib was tested in T-ALL PDX patient samples based on previous findings where PTEN was expressed or absent (Figure 22a). The linear regression curves of both PTEN<sup>mut</sup> PDX samples showed a lower slope of the curve and thus higher inhibitor efficacy in the mutants. The IC<sub>50</sub> values were determined and compared (Figure 22b). An IC<sub>50</sub> mean value of 14.9 μM for PTEN<sup>wt</sup> is compared to the value of 1.3 μM for PTEN<sup>mut</sup>. However, due to the small number of PDX samples and the high standard deviation, there is no significance (p=0.3135).

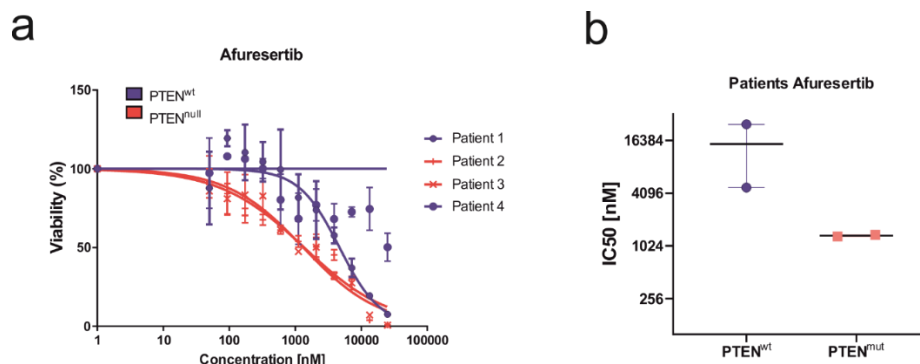


**Figure 22: Validation of AKT inhibition efficacy in T-ALL PDX samples.**

a) Drug response curves of afuresertib in T-ALL PDX samples and b) comparison of the respective IC<sub>50</sub> values.

Next, the sensitivity to PI3K/AKT inhibitors was investigated with the inducible PTEN knock out model DND41, described above. When PTEN was knocked down in DND41, sensitivity to PI3K inhibition was substantially increased ( $IC_{50}$  not reached for shNT vs.  $3.03 \mu\text{M}$  for shPTEN) with copanlisib and slightly improved ( $0.52 \mu\text{M}$  for shNT vs.  $0.13 \mu\text{M}$  for shPTEN) in the case of afuresertib (Figure 23a and b).

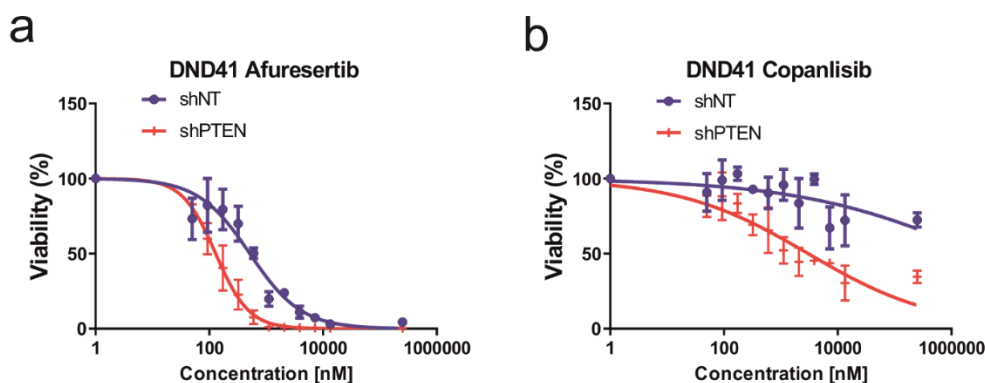


**Figure 23: Drug response curves of selected inhibitors of the inducible PTEN knockdown cell model DND41**

a) Drug response curve of afuresertib and b) copanlisib in cell line model DND41 with shNT and shPTEN expression.

### 3.3. *In vitro* validation of inhibitors

*In vitro* validation methods in this thesis include synergy screenings, apoptosis assays, cell cycle analysis and protein analysis. With combinatorial drug screening, enhanced killing activity can be achieved at lower concentration of the inhibitors, which is beneficial to reduce toxicity effects coming from single compounds used at high concentrations. A combination of different methods is needed to validate a drug for subsequent *in vivo* experiments.

#### 3.3.1. *In vitro* validation of copanlisib and JQ1

The PI3K inhibitor copanlisib showed a remarkable specific effect in  $PTEN^{mut}$  cell lines. To determine whether the use of an additional target increases efficacy in eradicating MYC-dependent tumor cells, synergy screens were performed with JQ1, a BRD4 inhibitor that has shown high potency in reducing MYC protein levels and thus an anti-tumor effect in recent publications [85, 97]. The strategy behind this approach is to deactivate MYC by inhibiting two different axes, thereby withdrawing the important properties of the malignant cell. Therefore, both compounds, Copanlisib and JQ1, were tested against each other in an 8 by 8 matrix at different concentrations based on the

individual IC<sub>50</sub> values previously determined. The synergy screen was performed with three PTEN<sup>mut</sup> cell lines MOLT4, HPBALL and JURKAT (Figure 24). In fact, the combination of copanlisib and JQ1 in tests with MOLT4 showed high synergistic ranges (blue) at relatively low concentrations between 0.05  $\mu$ M to 0.50  $\mu$ M for copanlisib and 1.00  $\mu$ M to 3.00  $\mu$ M for JQ1. In the case of HPBALL synergistic areas were detected at concentrations between 1.00  $\mu$ M to 5.00  $\mu$ M for copanlisib, and between 0.05  $\mu$ M to 1.00  $\mu$ M for JQ1, though the synergy was less intense as it was the case with MOLT4. However, no synergy at all was detected in JURKAT.

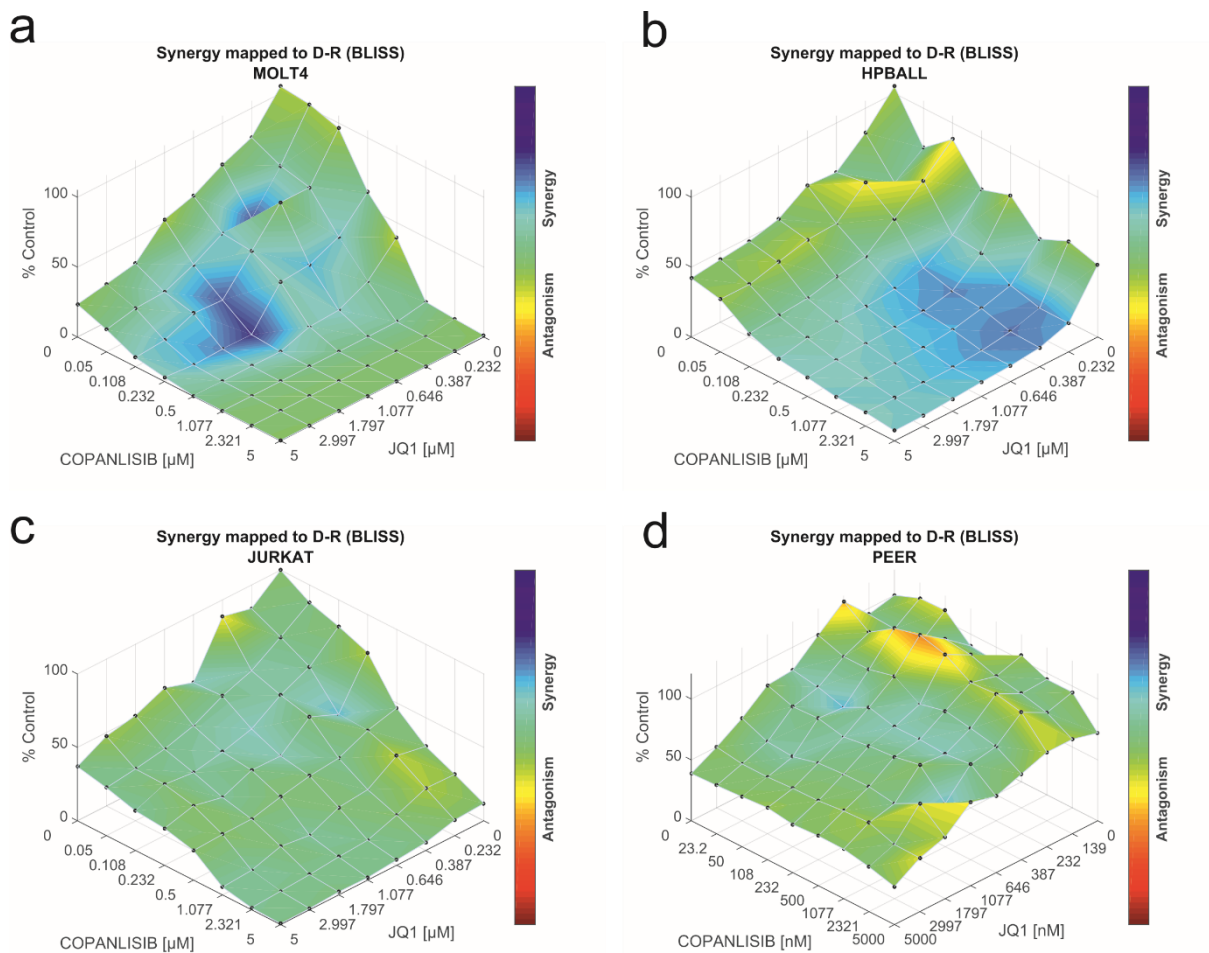


**Figure 24: Synergy matrices of copanlisib with JQ1**

a) 3D drug response plot of copanlisib with JQ1 for MOLT4, b) for HPBALL, c) for JURKAT and d) for PEER. Synergism was predicted by BLISS independence model and high synergy is indicated as blue areas, whereas additive effect is indicated as green areas and antagonism in red.

To determine whether the effect of the drug combination can be detected by apoptosis induction, the PTEN<sup>mut</sup> cell line MOLT4 was treated with Copanlisib, JQ1 and the combination of both for 24h, followed by Annexin V/PI staining (Figure 25a). Even with



a very low concentration, the compound copanlisib induced significant apoptosis with 10.20% compared to the vehicle treated control with 6.72% ( $p < 0.001$ ). In combination with JQ1 however, the measured amount of apoptosis was even higher with 13.04%, although the single treatment with JQ1 did not induced apoptosis in the same manner with 8.09%. Moreover, the combination treated cells had a significantly higher number of apoptotic cells compared to the copanlisib alone treated cells (10.20% vs 13.04%,  $p < 0.001$ ). Similar trends were observed after 48h and 72h. Interestingly, only the combination of copanlisib and JQ1 increased the proportion of apoptotic cells in a time dependent manner (20.65% after 48h and 38.24% after 72h,  $p < 0.001$ ). Next, the molecular processes affected by the inhibition of the compounds were investigated using WB (Figure 25b). The effect of the PI3K inhibitor was demonstrated by phosphorylation of GSK3 $\beta$ . The use of this compound resulted in a reduction of pGSK3 $\beta$ . In addition, the use of copanlisib alone did not affect the expression of MYC in contrast to the use of JQ1 alone. Interestingly, small amounts of both compounds in combination reduced the amount of MYC more effectively than fourfold higher concentration of JQ1 alone. Cleaved PARP, the marker for apoptosis, appeared only in samples treated with the combination and already at the lowest concentrations used.

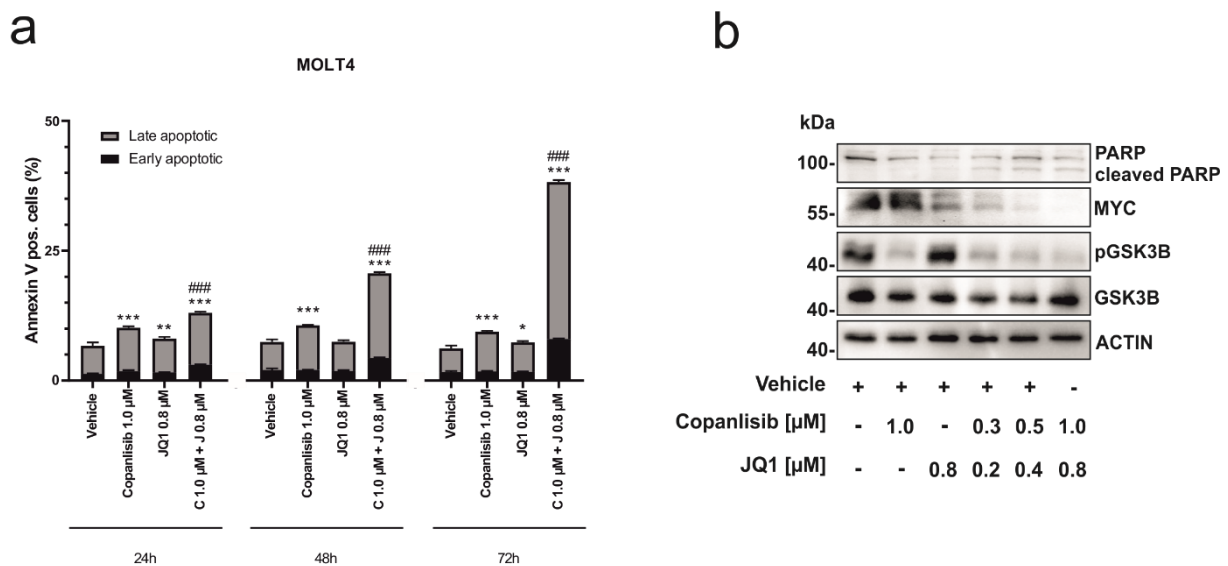


**Figure 25: Biological validation of compound effectivity in MOLT4**

a) Annexin V/PI staining of MOLT4 after 24h, 48h and 72h treatment with the indicated doses based on the determined  $IC_{50}$  values ( $n=3$ ). Based on the co-appearance of PI with Annexin V cells were separated in late and early apoptotic stages. Differences were measured using total apoptosis values (early apoptosis plus late apoptosis) with vehicle control as reference (\*) and copanlisib alone treatment (#). \*, #,  $p < 0.05$ ; \*\*, ##,  $p < 0.01$ ; \*\*\*, ###,  $p < 0.001$  (Two-way ANOVA test). b) WB analysis of MOLT4 cells after 24h treatment with compounds at the indicated doses.



### 3.3.2. *In vitro* validation of afuresertib and birabresib

The next inhibitors studied *in vitro* were the AKT inhibitor afuresertib and the BRD4 inhibitor birabresib. Birabresib is of greater clinical relevance compared to JQ1, as it is already approved for clinical trials and is actually in a phase 2 clinical trial (NCT02303782), whereas JQ1 is solely an experimentally available compound. The combination of these inhibitors was tested in an 8 by 8 matrix with different concentrations in four PTEN<sup>mut</sup> and two PTEN<sup>wt</sup> cell lines and synergism was predicted using BLISS independence model (Figure 26).

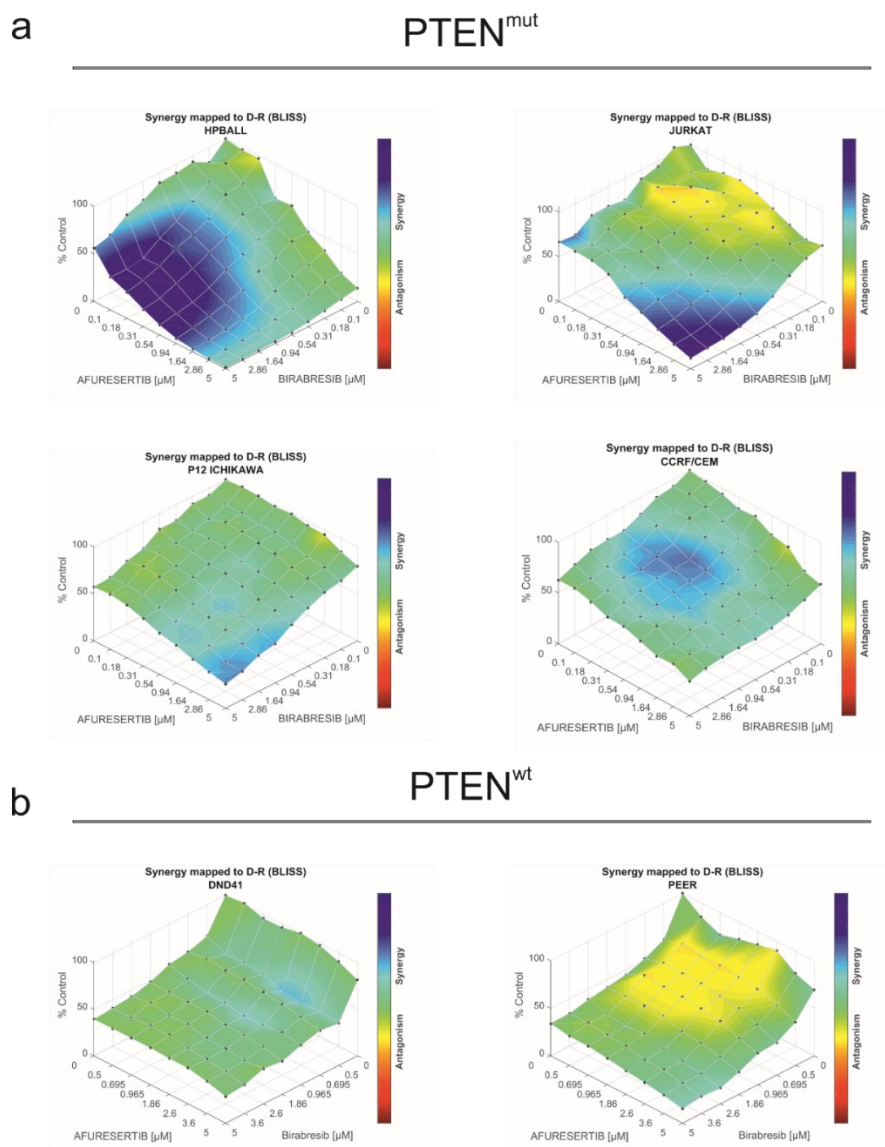


**Figure 26: Synergy matrices of afuresertib with birabresib**

a) 3D drug response plot of afuresertib with birabresib for PTEN<sup>mut</sup> cell lines HPBALL, JURKAT, P12 ICHIKAWA, CCRF/CEM and b) PTEN<sup>wt</sup> cell lines DND41 and PEER. Synergism was predicted by BLISS independence model and high synergy is indicated as blue areas, whereas additive effect is indicated as green areas and antagonism in red.

Highly synergistic areas (indicated in dark blue) were observed with HPBALL, CCRF/CEM and JURKAT (Figure 26a) and low synergism (light blue) was seen in combination of high concentrations with P12 ICHIKAWA cell line (Figure 26a). HPBALL and CCRF/CEM showed the highest synergism when afuresertib was used at low concentrations between 0.1 and 0.5  $\mu\text{M}$  and birabresib at higher concentrations between 0.5 and 5.0  $\mu\text{M}$ . However, in the JURKAT and P12 ICHIKAWA cell lines, synergism was observed to be evident only when high concentrations of both inhibitors (5.0  $\mu\text{M}$ ) were combined. The combination of birabresib and afuresertib showed an even higher synergism in HPBALL cells compared to the previously tested combination of JQ1 with copanlisib. However, no synergism but only additivity was observed in the PTEN<sup>wt</sup> cell line DND41, and a slight antagonistic (yellow) effect was observed in PEER (Figure 26b).

Encouraged by the synergistic efficacy of the AKT inhibitor afuresertib in combination with the BRD4 inhibitor birabresib shown in PTEN<sup>mut</sup> cell lines, further *in vitro* validations were performed to identify apoptosis by annexin V/PI staining with HPBALL, JURKAT, and P12 ICHIKAWA (Figure 27). Examination of apoptosis induction by the three cell lines tested showed similar efficacy of the compounds. In all cases, afuresertib alone induced apoptosis more potently than birabresib at all time points examined. However, the combination of both compounds showed even higher apoptosis induction compared to afuresertib alone at all time points tested ( $p < 0.001$  for all cell lines tested). Interestingly, even using half concentrations of afuresertib and birabresib in HPBALL showed significant differences in apoptosis after 48h (32.3% for afuresertib at 5  $\mu\text{M}$  vs. 42.4% for a + b in combination at 2.5  $\mu\text{M}$ ,  $p < 0.01$ ) and after 72h (32.6% for afuresertib 5  $\mu\text{M}$  vs. 47.8% for a + b in combination 2.5  $\mu\text{M}$ ,  $p < 0.001$ ), supporting the predicted synergy results (Figure 27a). In JURKAT, the observed results were similar to HPBALL, with one exception: birabresib alone induced significant apoptosis compared to vehicle at 24h (16.6% vs. 23.9%,  $p < 0.01$ ), 48h (9.7% vs. 18.8%,  $p < 0.001$ ), and 72h (5.1% vs. 20.0%,  $p < 0.001$ ) (Figure 27b). The combination of both compounds in a concentration of 5  $\mu\text{M}$  induced again significantly higher apoptosis after 48h and 72h compared to afuresertib alone induced apoptosis (both  $p < 0.001$ ). Hence, the use of half of the concentrations (2.5  $\mu\text{M}$  afuresertib and 2.5  $\mu\text{M}$  birabresib) induced apoptosis similar to afuresertib alone at a concentration of 5  $\mu\text{M}$ . The third tested cell line P12 ICHIKAWA showed the lowest predicted synergism

in the Bliss independence model and the results were in line with the minimal apoptosis induction during Annexin V/PI assay (Figure 27c). However, the apoptosis induction of the combination increased in a time-dependent manner and reached its peak after 72h. Interestingly, afuresertib alone did not induce significantly higher apoptosis in P12 ICHIKAWA compared with birabresib at 24 and 48h. However, after 72h, birabresib showed higher apoptotic activity compared to afuresertib (14.7% vs. 8.2%,  $p < 0.001$ ). The combination of both agents showed the highest efficacy especially after 72h 46.8% in cells treated with a + b in combination at 5  $\mu\text{M}$  vs. 14.7% in cells treated with birabresib alone at 5  $\mu\text{M}$ ,  $p < 0.001$ .

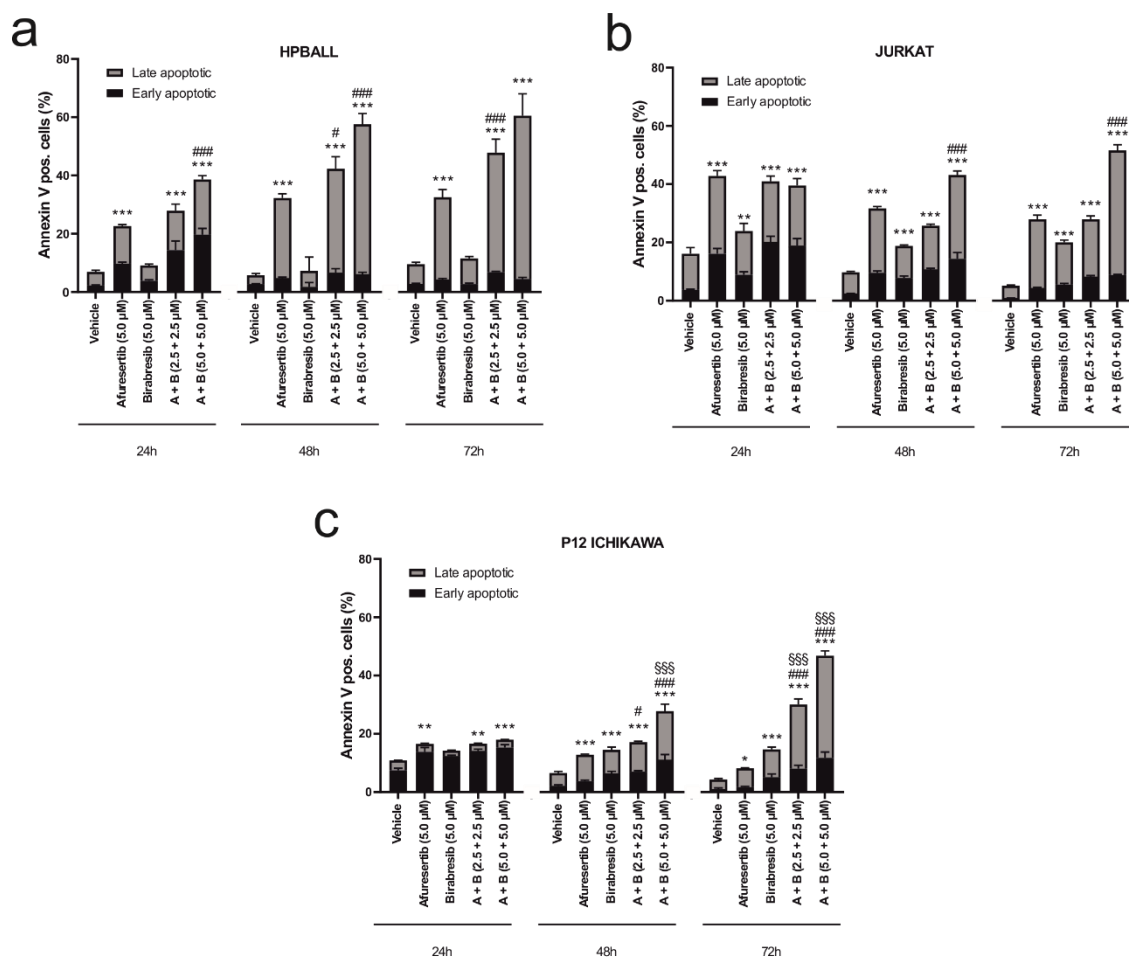


**Figure 27: Apoptosis measurement of three different PTEN<sup>mut</sup> cell lines treated with afuresertib, birabresib and the combination of both**  
a) Annexin V/PI staining of HPBALL, b) JURKAT and c) P12 ICHIKAWA after 24h, 48h and 72h treatment with the indicated doses based on the determined IC<sub>50</sub> values (n=3). Based on the co-appearance of PI with Annexin V, cells were separated in late and early apoptotic stages. Differences were measured using total apoptosis values (early apoptosis plus late apoptosis) with vehicle control as reference (\*), afuresertib alone treatment (#) and birabresib alone treatment (§). \*, #, §,  $p < 0.05$ ; \*\*, ##, §§,  $p < 0.01$ ; \*\*\*, ###, §§§,  $p < 0.001$  (Two-way ANOVA test).

To validate the apoptosis assessed by Annexin V/PI measurements, two additional apoptosis assays were performed, the cell cycle assay by Nicoletti-Assay [163] and the measurement of caspase 3/7 complex (Figure 28a and b). The increase of cells in the sub-G1 phase was found to be higher in afuresertib alone treated cells compared to vehicle after 24h treatment (59.6% +/- 2.4% vs. 38.4% +/- 2.9%,  $p < 0.001$ ) and indicates an increase in apoptosis. In combination of both compounds the values were even higher, matching the previous results (66.5% +/- 0.7% vs. 38.4% +/- 2.9%,  $p < 0.001$ ). The induction of caspase 3/7 expression was performed after 48h treatment with the compounds alone and in combination. The exposure of the compounds in HPBALL cells showed again significant differences between the combination and single treatments, even when half the concentration of the combination was used ( $p < 0.001$ ).

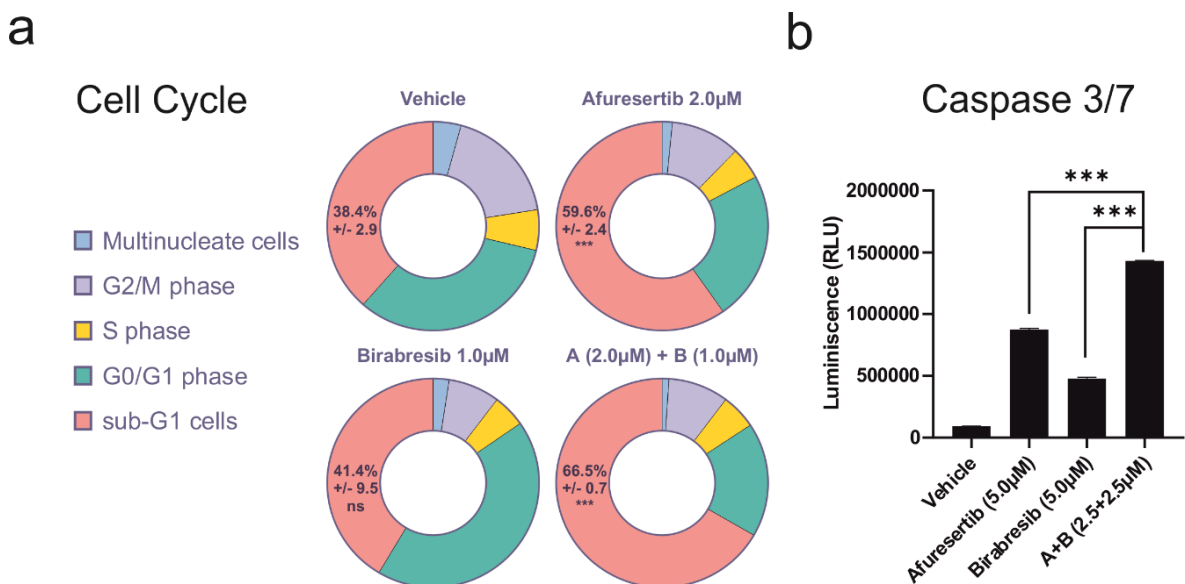


**Figure 28: Biological validation of afuresertib and birabresib with regard to cell cycle and caspase**

a) HPBALL Cell cycle measurement by PI based Nicoletti Assay after 24h treatment. Different stages were determined based on the measured intensities of detected PI signals and indicate a specific cell cycle stage (n=3). Sub-G1 phase indicates apoptosis and was compared with vehicle control. b) Caspase 3/7 bioluminescence assay with HPBALL after 48h treatment (n=3). The combination values of afuresertib and birabresib was compared with values of single compounds in double higher concentrations. \*,  $p < 0.05$ ; \*\*,  $p < 0.01$ ; \*\*\*,  $p < 0.001$  (student's t-test).

To investigate the molecular mechanisms of the combination treatment with afuresertib and birabresib, relevant targets were assessed by WB after 24h treatment at indicated doses (Figure 29a). MYC was decreased after afuresertib treatment and completely

diminished after birabresib and combination treatments. In addition, pGSK3 $\beta$  was only lower in samples treated with afuresertib, indicating its function as an AKT inhibitor (Figure 29b). Phosphorylation of the MYC degradation site T58, was correlated with the phosphorylation of GSK3 $\beta$ . The stability site S62 was reduced in afuresertib treated cells but increased in birabresib single treated cells.

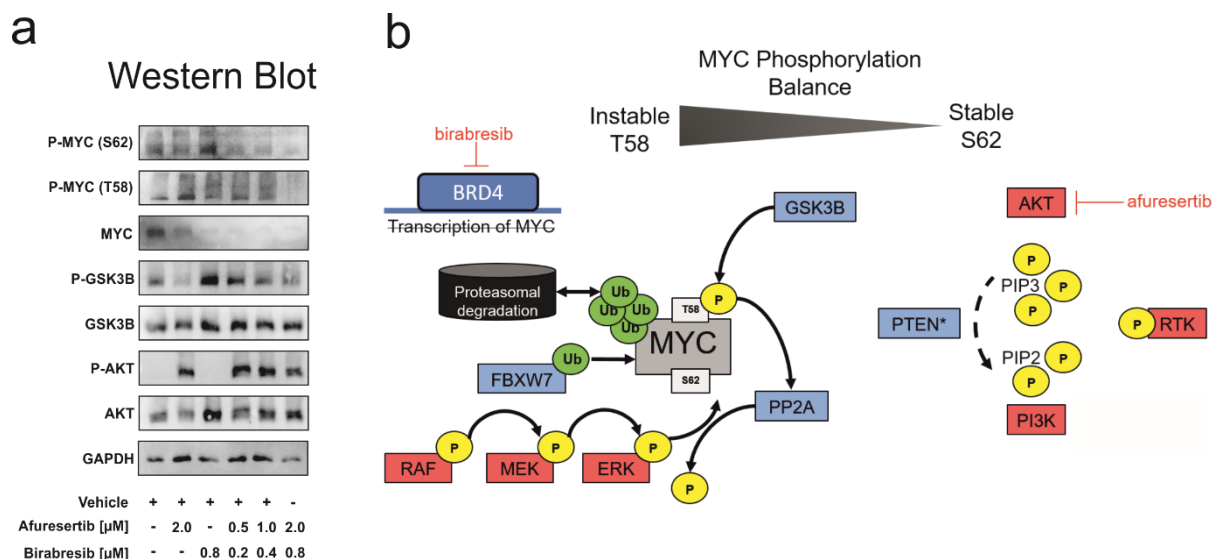


**Figure 29: Targeting strategy on molecular level**

a) Protein biochemical analysis by WB. Representative WBs prove the compound effects on molecular level and the resulting dysregulation of MYC stability. b) Schematic representation of compound targets and the resulting molecular interactions shifting the phosphorylation balance of MYC from stable to instable.

### 3.3.3. *In vitro* validation of AURKA inhibitors in MYC dependent cell lines

Semi-automated drug screen of an AURKA inhibitor alisertib showed no distinctive efficacy in cell lines dependent on their PTEN pre- or absence, since the drug response curves were similarly in both groups (Figure 30a). However, the importance of AURKA inhibition was clear when the detected IC<sub>50</sub> values of the MYC overexpressing T-ALL1 cell line was compared to the control (0.59  $\mu$ M vs. 4.62  $\mu$ M, respectively) (Figure 30b). To investigate if AURKA inhibition could be synergistic with PI3K inhibition, the combination of the copanlisib was tested with alisertib in an 8 by 8 matrix. Highly synergistic regions were found with alisertib at concentrations ranging from 0.04 to 0.14  $\mu$ M and copanlisib at concentrations ranging from 0.18 to 0.94  $\mu$ M (Figure 30c). The effectivity of alisertib inhibition on cell cycle was demonstrated using a cell cycle assay (Figure 30d). Whereas alisertib single treated cells get stuck in the G2/M-phase (46,8%,  $p < 0.001$ ), the proportions of copanlisib single treated cells do not differ that

much from the vehicle sample, only showing higher proportions of cells in the G0/G1 phase, indicating an ongoing apoptosis. When both compounds were combined, both effects (increased apoptosis and increased cells remaining arrested in the G2/M phase) were observed, although all compounds had a significant effect on apoptosis induction ( $p < 0.001$ ). However, when investigating the apoptosis by Annexin V/PI measurement we saw that copanlisib induced apoptosis faster than alisertib alone the combination of both was by far more effective in apoptosis induction than single treatments (39.9% combination vs. 19.6% alisertib, and 25.7% copanlisib,  $p < 0.001$ ) (Figure 30e). Further, WB was performed to investigate molecular mechanisms on protein level, driven by the compounds (Figure 30f). During single AURKA inhibition the MYC expression was not directly affected, as it was observed with PI3K inhibition. On the other hand, the use of low doses of the combination of alisertib and copanlisib significantly reduced MYC expression with decreasing phosphorylation of GSK3 $\beta$ .

Prior results were confirmed in an TKI-resistant BCR-ABL1+ B-ALL cell line model (SUP-B15), which was desensitized to imatinib due to continuous exposure to imatinib at steadily increasing concentrations [159]. It has been previously reported that imatinib resistance is often associated with *de novo* PTEN mutations caused by upregulation of DNA methyltransferases and Polycomb group proteins [170]. Therefore, the imatinib resistant (ImR) SUP-B15 cell model attracted attention, since the PTEN mutation was accompanied with a huge increase of MYC that was verified by WB (Figure 31a). When performing inhibitor screening, it was observed that a slightly higher sensitivity to PI3K inhibition by copanlisib was mentioned with an measured IC<sub>50</sub> value at a concentration of 5.50  $\mu$ M with SUPB15 and 1.81  $\mu$ M with the ImR variant (Figure 31b), confirming the previous observations. However, further inhibitor screenings showed that the highest differences were found in the entire group of Aurora Kinase inhibitors, with all inhibitors being more effective in the SUP-B15 ImR cell line compared to the wild type SUP-B15 (Figure 31c).

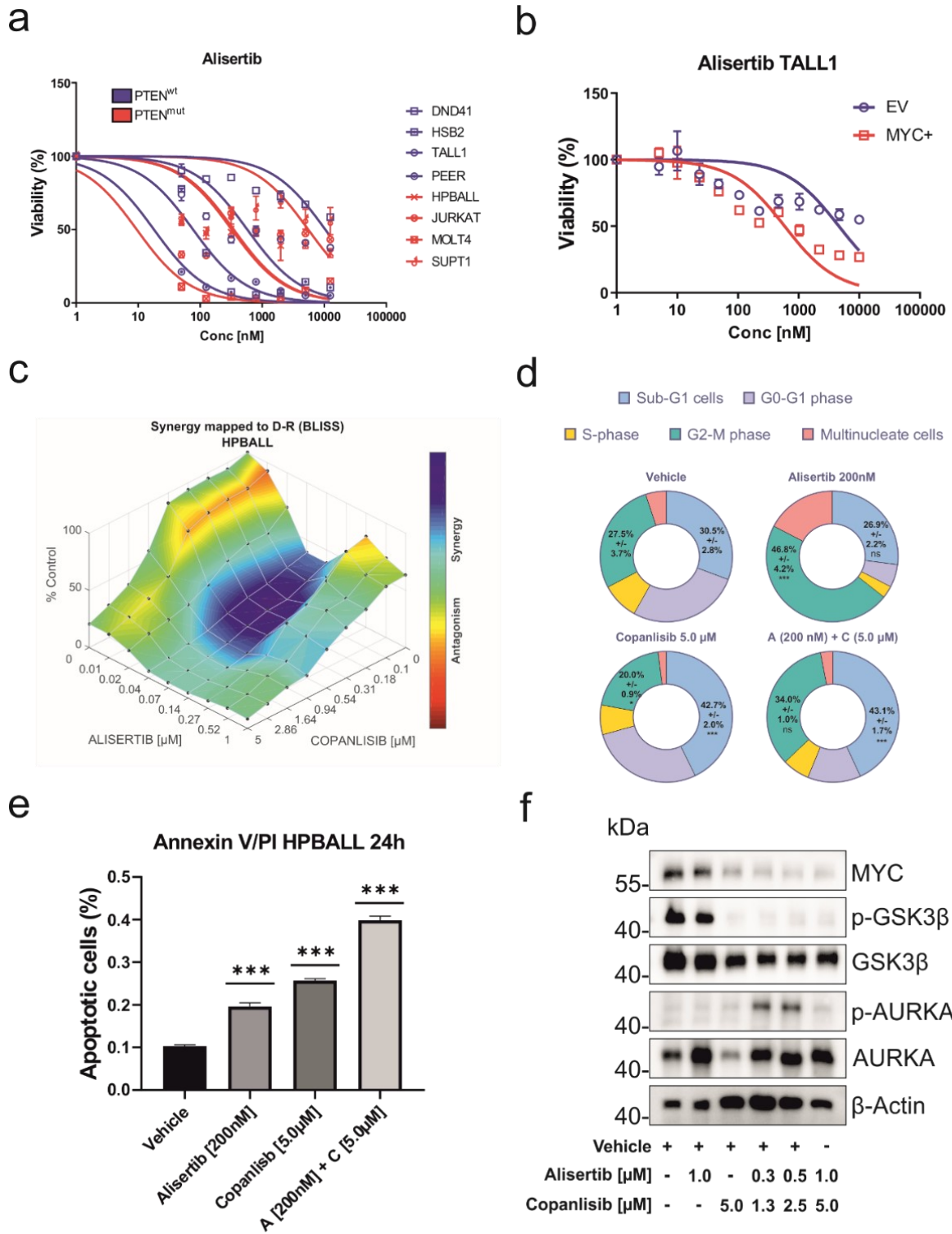


**Figure 30: Biological validation of AURKAi with PI3Ki in PTEN<sup>mut</sup> cell line HPBALL**

a) Drug response curves of AURKAi alisertib in T-ALL cell line models and b) in MYC overexpressing cell model TALL1. c) 3D drug response plot of alisertib with copanlisib in an 8 by 8 matrix. Synergism was predicted by BLISS model and high synergy is indicated as blue areas, whereas additive effect is indicated as green areas and antagonism in red. d) Cell cycle assay of HPBALL after 24h treatment e) Annexin V/PI staining by flow cytometry after 24h treatment. f) Representative WBs of HPBALL cell lysates after 24h treatment. \*, p<0.05; \*\*, p<0.01; \*\*\*, p<0.001 (student's t-test).



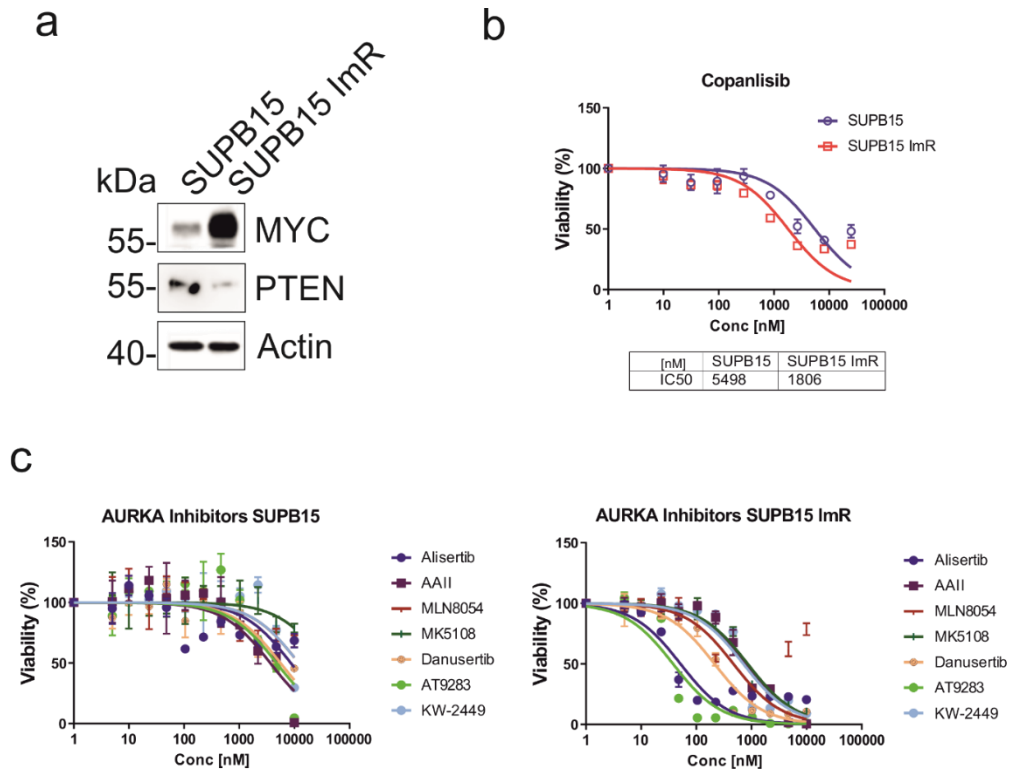


**Figure 31: Introducing the SUPB15 cell line model and its imatinib resistant lineage model SUPB15 ImR**

a) Representative WBs of SUPB15 and SUPB15 ImR, focusing on the correlation between PTEN and MYC. b) Drug response curves of copanlisib and indicated mean IC<sub>50</sub> values below. c) Comparison of different Aurora Kinase inhibitors, drug response curves of SUPB15 and SUPB15 ImR.

### 3.3.4. *In vitro* validation of MEK inhibitors in high MEK phosphorylated T-ALL cell lines

At the end of the *in vitro* analyses, the focus was once again placed on the PTEN knock down model in DND41 T-ALL cell line. Differences in sensitivity against various compounds was screened using high throughput drug screening (Figure 32a). Interestingly, when PTEN was knocked down by shRNA, a set of compounds were more effective than in the shNT control. These agents belonged to the class of MEK/ERK pathway inhibitors, including cobimetinib, binimetinib, selumetinib, trametinib, and PD184352 with a few exceptions such as PD0325901 and pimasertib. For example, for cobimetinib, IC<sub>50</sub> values changed from 17.87  $\mu$ M to 1.52 when PTEN was knocked down by shRNA (Figure 32b).



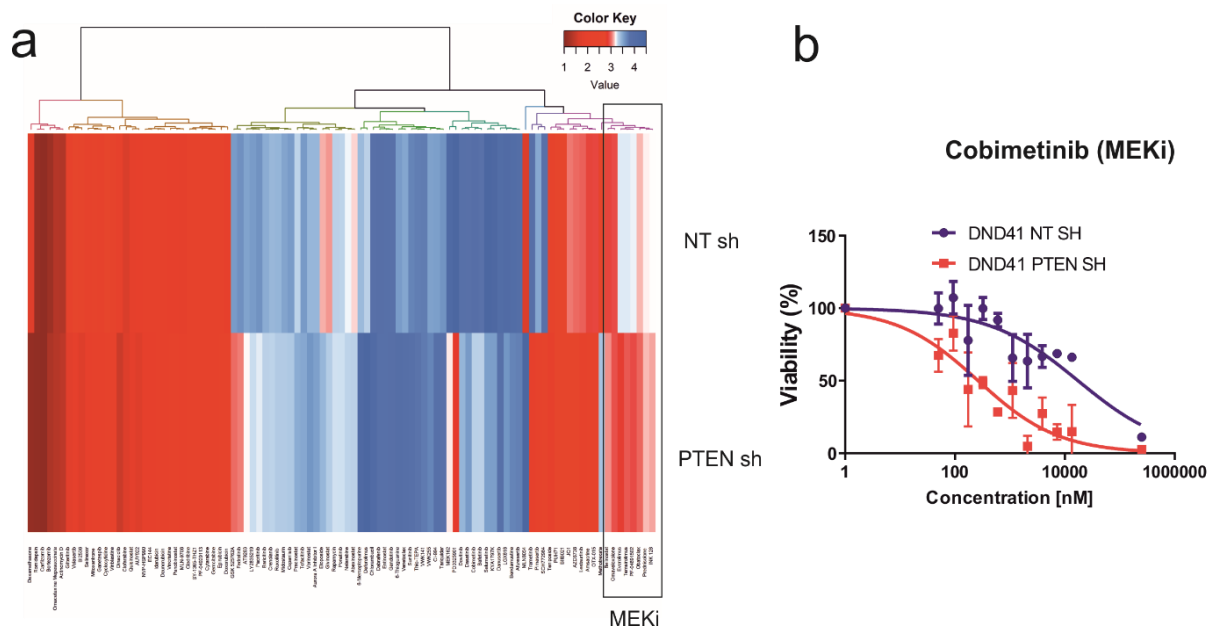


**Figure 32: The role of MEKi in an inducible PTEN knock down model DND41**

a) Heatmap of IC<sub>50</sub> values measured by high throughput drug screening of DND41 shNT and shPTEN cell model. b) Drug response curves of focused screening for cobimetinib (one of the inhibitors that were noticed in high throughput drug screening).

The choice was made to evaluate whether the combinatorial use of the MEK inhibitor cobimetinib is synergistic with the PI3K inhibitor copanlisib in cells with a high level of MEK phosphorylation (DND41 and HSB2) according to previously performed WB analysis (Figure 8a). The compounds were tested in an 8 by 8 matrix with two highly MEK-phosphorylated (p-MEK<sup>high</sup>) cell lines (DND41 and HSB2) and two p-MEK<sup>low</sup> cell lines (PEER and HPBALL), both representing a cell line for PTEN<sup>wt</sup> and PTEN<sup>mut</sup>, respectively (Figure 33). Synergy was evident in the p-MEK<sup>high</sup> cell lines DND41 and HSB2, shown as dark blue areas in the 3D diagram, but not in the p-MEK<sup>low</sup> cell lines, which demonstrated either antagonistic or additive regions. Therefore, this compound combination was investigated further on the molecular level.

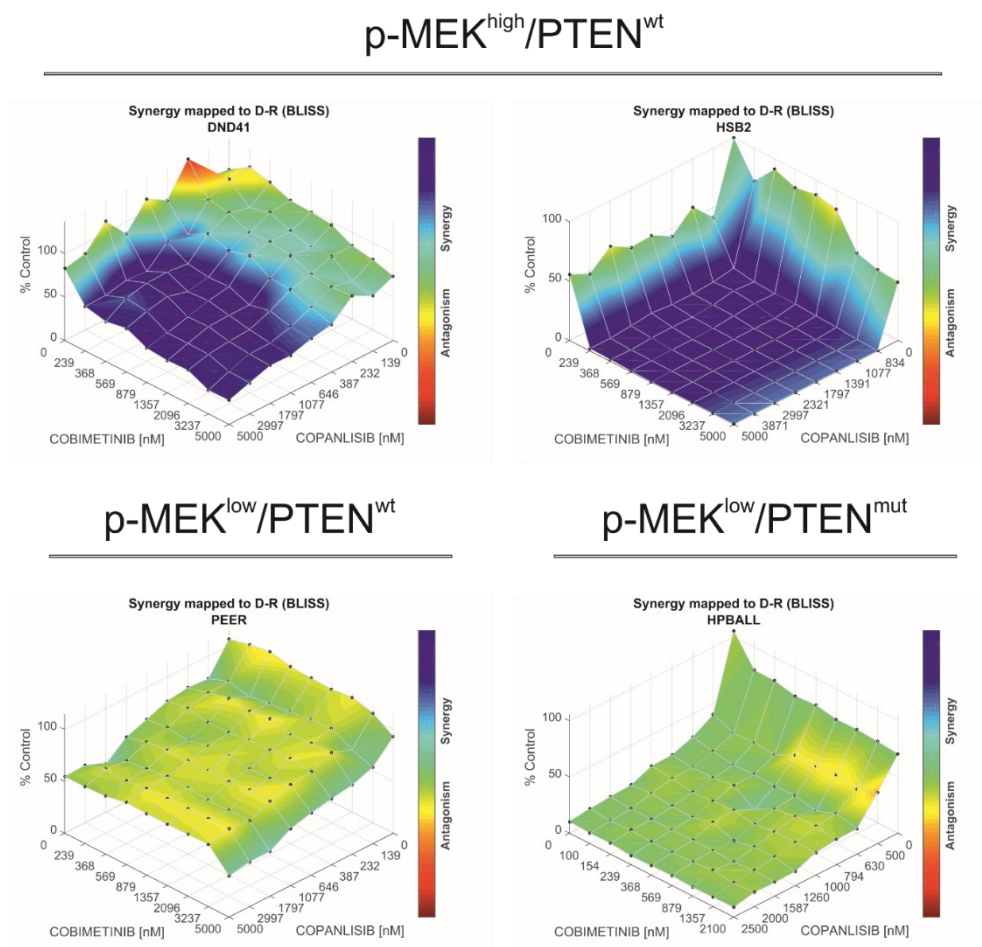
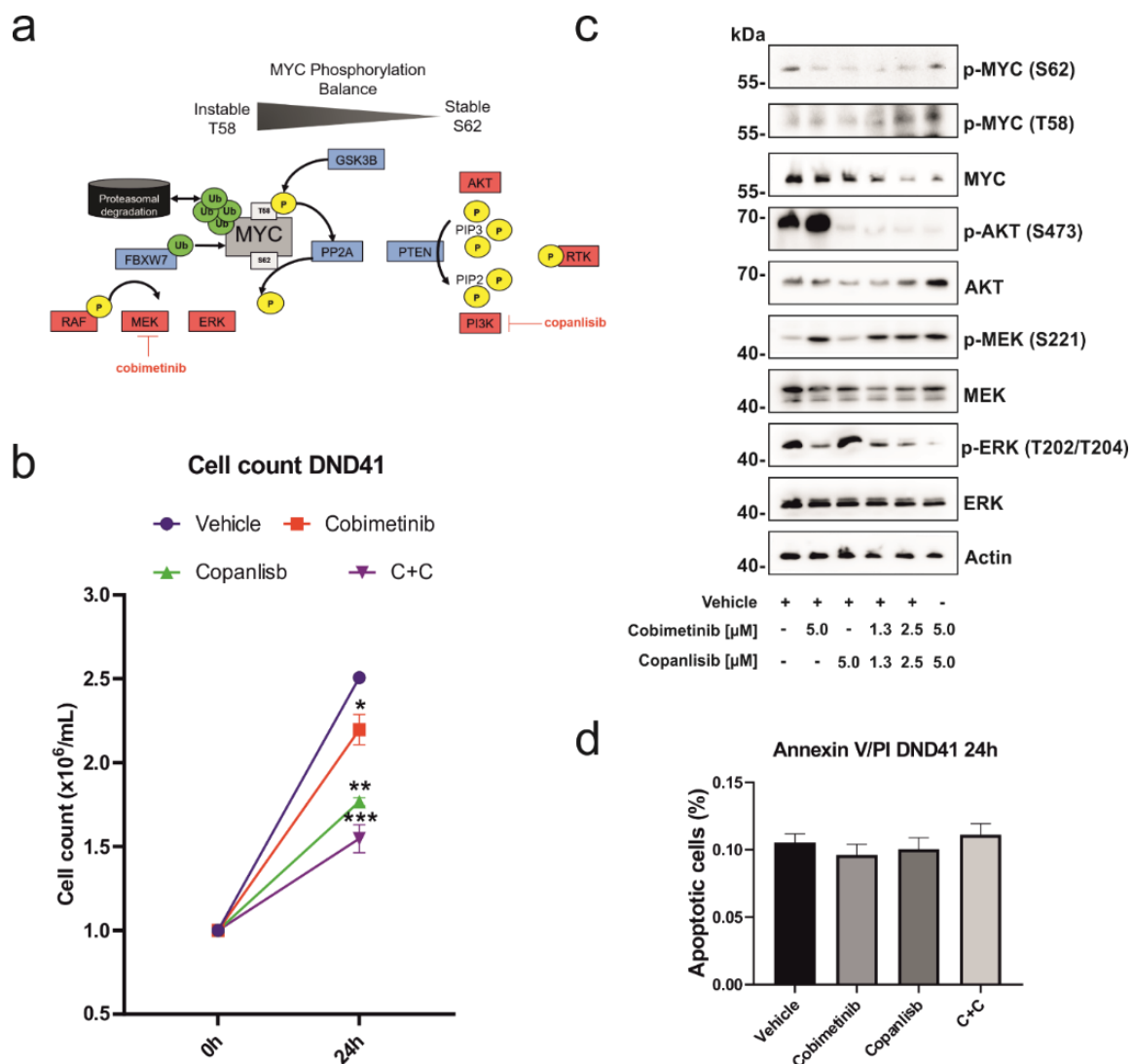


**Figure 33: Synergy analysis of cobimetinib in combination with copanlisib in dependency of different stratification markers**

a) 3D drug response plot of alisertib with copanlisib in an 8 by 8 matrix for  $p\text{-MEK}^{\text{high}}/\text{PTEN}^{\text{wt}}$  cell lines DND41 and HSB2,  $p\text{-MEK}^{\text{low}}/\text{PTEN}^{\text{wt}}$  cell line PEER and  $p\text{-MEK}^{\text{low}}/\text{PTEN}^{\text{mut}}$  cell line HPBALL. Synergism was predicted by BLISS independence model and high synergy is indicated as blue areas, whereas additive effect is indicated as green areas and antagonism in red.

The Raf/MEK/ERK signaling pathway is described to increase the MYC stability due to phosphorylation of MYC on Site S62 counteracting the phosphorylation on site T58 [104]. Therefore, in this case, the strategy chosen was to inhibit the Raf/MEK/ERK pathway using cobimetinib and simultaneously inhibit the PI3K/AKT pathway using copanlisib, as indicated in schematic Figure 34a. Initially, it was found that DND41 cells showed decreased cell proliferation after being treated with the inhibitors cobimetinib and copanlisib and the combination of both for 24h (Figure 34b). The highest difference was observed with the combination of cobimetinib and copanlisib ( $1.55 \times 10^6$  cells treated with combination vs.  $2.51 \times 10^6$  cells treated with vehicle,  $p < 0.001$ ). It was then examined whether there were differences in the phosphorylation and expression of MYC at the protein level after the cells were treated with the inhibitors. Therefore, a

WB of DND41 cell lysates after 24h treatment was performed, and proteins of interest were assessed regarding the MYC stability (Figure 34c). The combination treatment with copanlisib and cobimetinib solely decreased the total level of MYC. In addition, of both inhibitors showed an increase of the MYC phosphorylation on site T58, leading to an enhanced degradation that can be observed by the decreasing total amount of MYC with increasing concentrations of the used inhibitors. Interestingly, no apoptosis was detected after inhibition, neither in the single treated cells nor in the combination treatment (Figure 34d).



### 3.4. *In vivo* validation of compound combinations

#### 3.4.1. *In vivo* validation of PI3K inhibitor copanlisib and BRD4 inhibitor JQ1

After the previously performed *in vitro* validation (Figure 24 and 25), the first compounds to be tested *in vivo* were the PI3K inhibitor copanlisib and the BRD4 inhibitor JQ1, both available for intravenous (i.v.) injections. Therefore, luciferase transduced MOLT4-luc cells were injected i.v. into 12 mice. After one week, the engraftment was verified in all mice by measuring radiance of the luciferase-transduced cells in the mouse body. Subsequently, the treatment induction with vehicle control, copanlisib (5 mg/kg) or JQ1 (5 mg/kg) alone or in combination (both 5 mg/kg) was started by i.v. injection. The treatment scheme is shown in Figure 35a. After each week, all mice were pictured individually (Figure 35b) and ROIs were measured consequently for each mouse after 7, 14, 21 and 28 days (Figure 35c). Treatment started after 7-days post injection. Differences in the individual groups were observed after 14 days. The measured mean radiance of the mice treated with the combination was  $1.4 \times 10^8$  p/s/cm<sup>2</sup>/sr and was significantly different from the mean radiance of the vehicle-treated group at  $8.2 \times 10^8$  p/s/cm<sup>2</sup>/sr ( $p=0.0301$ ). One mouse in the copanlisib-treated group showed delayed engraftment with a mean radiance of  $3.6 \times 10^6$  p/s/cm<sup>2</sup>/sr, while the other two mice in the group had values similar to the vehicle-treated mice ( $6.6 \times 10^8$  and  $4.8 \times 10^8$  p/s/cm<sup>2</sup>/sr), indicating no significant differences from the vehicle group. The mean value of JQ1-treated mice was  $2.2 \times 10^8$  p/s/cm<sup>2</sup>/sr and tended to be, but was not significantly, lower than the mean value of vehicle ( $p=0.0612$ ). However, one week later, at day 21, no further differences could be detected between the different treated groups. Only the mouse from the Copanlisib-treated group continued to show delayed engraftment and reduced signal intensities with  $4.2 \times 10^7$  p/s/cm<sup>2</sup>/sr, well below the signals of the remaining mice, which averaged between 2 to  $4 \times 10^9$  p/s/cm<sup>2</sup>/sr. Notably, the mice of the vehicle-treated group and the combination-treated group did not survive until the next measurement day (day 28). One mouse from the JQ1-treated group and the copanlisib-treated group also died before. Interestingly, on day 28, signal intensity in a Copanlisib-treated mouse was even lower than the week before ( $4.8 \times 10^9$  p/s/cm<sup>2</sup>/sr on day 21 and  $1.7 \times 10^8$  p/s/cm<sup>2</sup>/sr on day 28). However, this mouse had lost so much weight on day 30, which lead to the initiation of the termination criteria, and this mouse was sacrificed. The JQ1 treated mice showed a continuous

increase in signal intensity and were significantly higher than the copanlisib treated group with values ranging from  $2.6$  to  $7.4 \times 10^9$  p/s/cm<sup>2</sup>/sr. These mice died on the same day (day 28) after measurement. Besides, it was remarkable that most of the mice showed a strongly bundled bioluminescence signal in the abdomen and in the head region. When the termination criteria were reached, the mice were autopsied, and the organs were examined more closely, and biopsies were taken for flow cytometric analysis (Figure 35d). It turned out that MOLT4 cells migrated in most cases besides the CNS also in the ovaries.

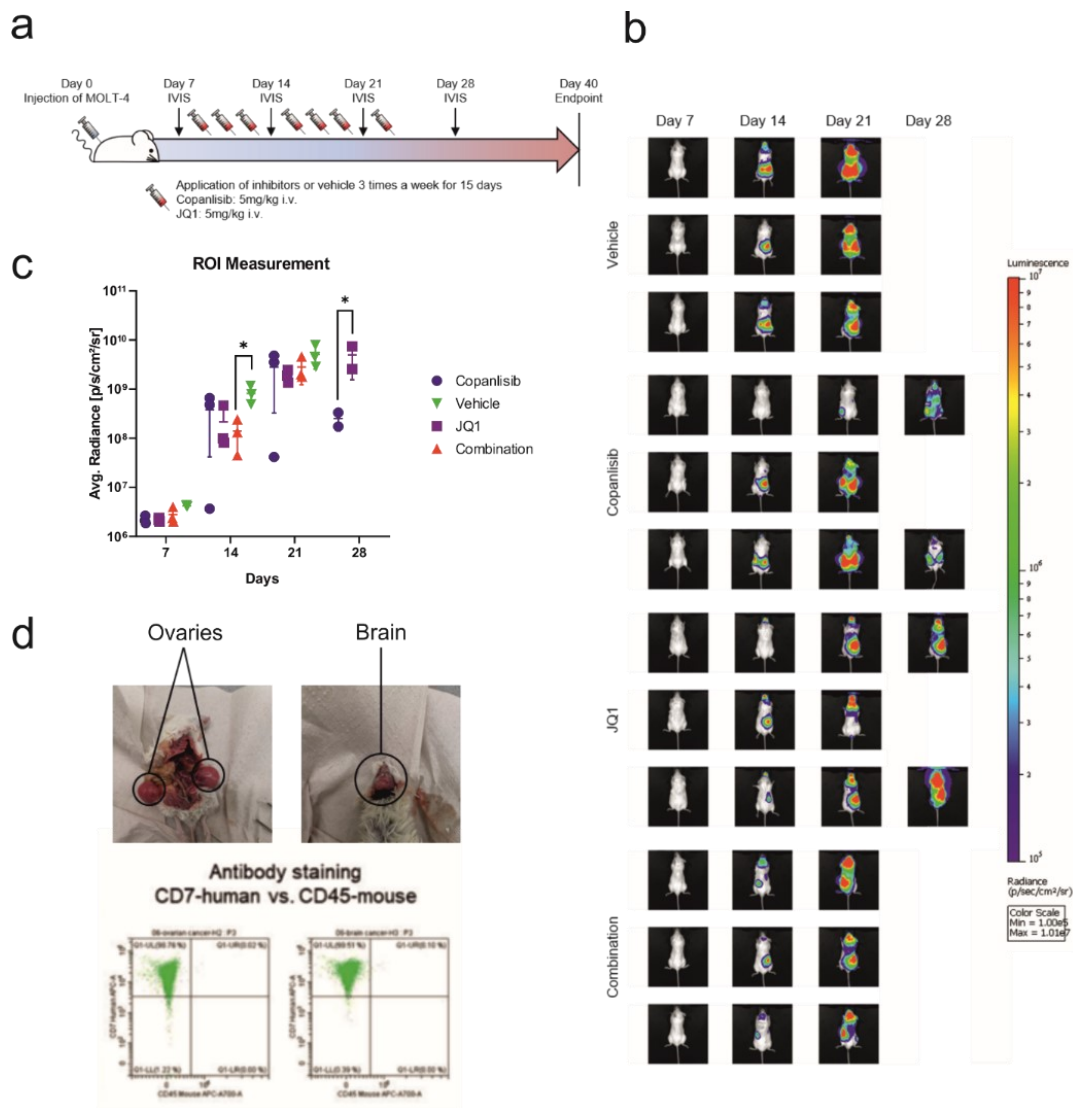
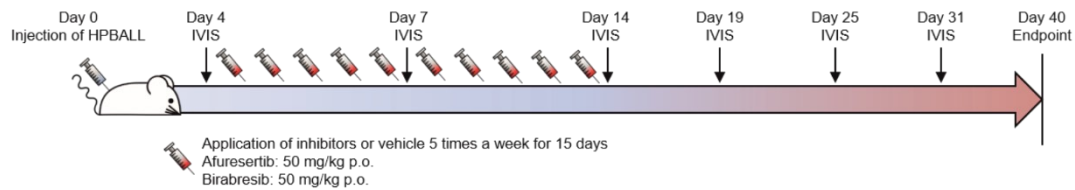


**Figure 35: *In vivo* validation of copanlisib and JQ1 in MOLT4 xenotransplanted mice**  
 a) Presentation of the preclinical *in vivo* study with treatment and IVIS measurement schedule.  
 b) IVIS images of mice from the respective treatment group after 7, 14, 21 and 28 days post xenotransplantation. c) Conclusion of ROI measurement results. d) Representative pictures of investigated ovary cancer and brain infiltration with flow cytometric validation of the ovary and brain biopsy sample, respectively.  $p < 0.05$ ; \*\*,  $p < 0.01$ ; \*\*\*,  $p < 0.001$  (student's t-test).

### 3.4.2. *In vivo* experiments with AKT inhibitor afuresertib and BRD4 inhibitor birabresib

The next *in vivo* experiment was performed with afuresertib and birabresib, as this combination showed promising synergistic effects in PTEN<sup>mut</sup> T-ALL cell lines (Figures 26 through 29). Five mice were selected for this preclinical evaluation for each treatment group consisting of vehicle as control, afuresertib (50 mg/kg), birabresib (50 mg/kg), and the combination of afuresertib with birabresib (both 50 mg/kg). Thus, 20 mice were injected with  $1 \times 10^6$  cells of luciferase transduced (PTEN<sup>mut</sup>) HPBALL-luc i.v. After four days the first measurement of engraftment was made, and engraftment of all 20 mice could be monitored by avg. radiance measurements. The oral administration (p.o.) of afuresertib or birasertib alone or in combination started on the same day for next five days (daily) using an oral gavage. After five days, most of the combination-treated mice lost weight, but without exceeding the highest level of the abort criteria. After two days treatment pause, the mice gained weight again. Hence, the treatment was continued for the following five days. One mouse of the birabresib treatment group had to be sacrificed on day 10 due to severe behavioral disorders (circling behavior) and high weight loss. Avg. radiance of each mouse for each group and timepoint was determined and presented in a grouped plot (Figure 36b). The single treatment with afuresertib showed a non-significant lower signal intensity after seven days ( $6.2 \times 10^8$  p/s/cm<sup>2</sup>/sr for afuresertib and  $7.9 \times 10^8$  p/s/cm<sup>2</sup>/sr for vehicle,  $p=0.2155$ ). However, all combination treated mice had to be sacrificed on day 14 after radiance measurement due to extreme weight loss. The examination of the intestines had shown that there had been an accumulation of the active ingredient. On day 14 and 15, afuresertib treated mouse was found dead in the cage. The examination of the abdomen also revealed an accumulation of fluid in the intestine. Since the birabresib and vehicle treated mice had still no problems in this regard, an incompatibility of the compound afuresertib may cause respiratory difficulties in the intestine. One week later, on day 19, the average radiance was more of the same in all groups ranging from  $1$  to  $8 \times 10^9$  p/s/cm<sup>2</sup>/sr. In the following weeks, two more afuresertib-treated mice died. Investigation of the disease progression of the remaining mice on day 31 showed no improvement with afuresertib or birabresib.

a



b

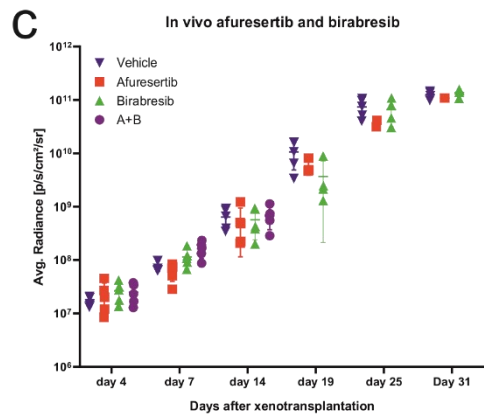
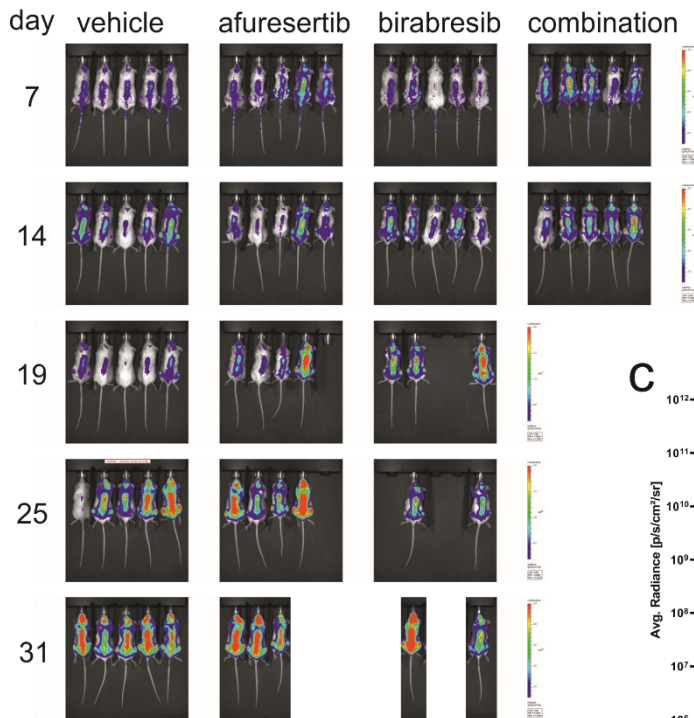


### Figure 36: *In vivo* validation of afuresertib and birabresib

a) Presentation of the preclinical *in vivo* study with treatment and IVIS measurement schedule. b) IVIS pictures of the respective treatment groups and the day post transfection. The scaling was adjusted for each measurement time point and is used to compare the intensities between the individual treatment groups of the specific day. c) ROIs of each mice from each treatment group were measured for each indicated timepoint.

## 3.5. Identification of novel MYC targeting drugs

As strategies to inhibit MYC have changed from searching for potent direct inhibitors to searching for indirect targets, a large number of proteins and pathways have been described that are less difficult to target and achieve effective reduction of MYC indirectly. In this section, the targets BRD4 were tested in combination with HDAC as dual inhibitors and HSP90 inhibitors.



### 3.5.1. Investigation of novel dual HDAC/BRD4 inhibitors

Dual HDAC/BRD4 targeting inhibitors were synthesized by the group of Prof. Dr. Finn Hansen at the Institute of Clinical Pharmacy, University of Leipzig, based on the pharmacophore of the BRD4 inhibitor XD14, which allows interaction with the acetyllysine recognition site of BRD4 and the adjacent phenyl group for hydrophobic interactions, also known as "WL-trap" [171], and the zinc-binding group based on panobinostat, which is a hydrophobic linker acting like a "cap" (Figure 37).

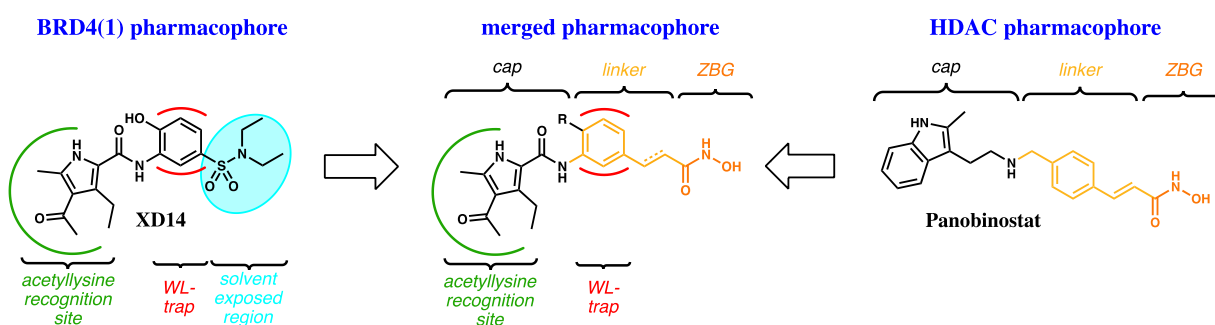


**Figure 37: Strategy for the production of new dual inhibitors based on the combination of pharmacophore regions of the respective reference inhibitors**

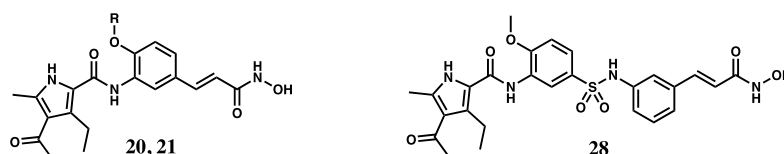
Left: Pharmacophore for BRD4(1) aligned with XD14, containing 4-acyl pyrrole moiety as acetyllysine recognition site, an adjacent phenyl group interacting with the WL trap and the solvent exposed sulfonamide moiety. Right: Pharmacophore for HDACs aligned to panobinostat. Middle: merged pharmacophore and 4-acyl pyrrole based dual HDAC/BRD4 targeting inhibitors.

The first generation of dual inhibitors, including compounds 20, 21 and 28 showed already promising binding affinities to HDAC proteins HDAC1 and HDAC6 comparable to the HDAC reference inhibitor vorinostat (Table 27). Compound 20 showed even higher affinity to HDAC6 compared to vorinostat with  $IC_{50}$  values of 0.042  $\mu$ M for 20 and 0.051  $\mu$ M for vorinostat and Compound 28 demonstrated higher affinity to HDAC1 compared to vorinostat  $IC_{50}$  values of 0.097  $\mu$ M for 28 and 0.120  $\mu$ M for vorinostat. However, the binding affinity of the dual inhibitors against BRD4 were relatively weak compared to the BRD4 reference inhibitor XD14. Whereas XD14 showed an BRD4 affinity at a concentration of 0.016  $\mu$ M, the binding affinity of the dual inhibitors was much higher with  $K_D$  values ranging from 2.66 to 3.67  $\mu$ M. When the killing efficacy was examined, only compound 20 showed a notable killing effect in the tested T-ALL cell lines MOLT4 and TALL1 as well as in the AML cell line HL60. Using a concentration of 5  $\mu$ M, cell viability was reduced to 3.5% for MOLT4, 15.1% for TALL1, and 22.1% for HL60. Based on this, the aim of the second-generation inhibitors was to create more



balanced dual inhibitors that keep the affinity to HDACs like it was the case for compound 20 but with improved BRD4 binding efficacy.

**Table 27: Target activity of the first generation dual HDAC/BRD4 targeting inhibitors**  
K<sub>D</sub> values describe the measured antibody affinity. IC<sub>50</sub> values demonstrate the required concentration to bind 50% of the respective HDAC proteins.



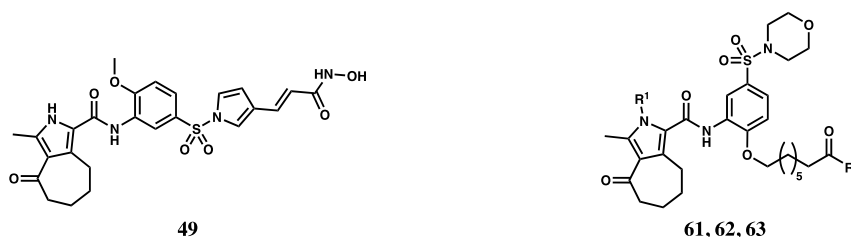
	R	IC <sub>50</sub> [μM]		BRD4(1)	Cell Viability <sup>a</sup> [%]		
		HDAC1	HDAC6	K <sub>D</sub> [μM]	MOLT4 <sup>b</sup>	TALL1 <sup>b</sup>	HL60 <sup>c</sup>
<b>20</b>	-CH <sub>3</sub>	0.179 ± 0.008	0.042 ± 0.005	2.98 (2.09 – 4.72) <sup>d</sup>	3.50 ± 3.7	15.1 ± 2.6	22.1 ± 2.8
<b>21</b>	-H	0.142 ± 0.019	0.080 ± 0.010	2.66 (2.04 – 3.38) <sup>d</sup>	105.1 ± 0.7	87.6 ± 6.7	88.2 ± 9.9
<b>28</b>	-CH <sub>3</sub>	0.097 ± 0.001	0.073 ± 0.008	3.67 (2.49 – 5.55) <sup>d</sup>	106.4 ± 2.4	85.6 ± 5.8	98.7 ± 4.4
<b>vorinostat</b>		0.120 ± 0.012	0.051 ± 0.007	n.d.	n.d.	n.d.	n.d.
<b>XD14<sup>37</sup></b>		n.d.	n.d.	0.16 ± 0.01	n.d.	n.d.	n.d.

<sup>a</sup>cell viability compared to control determined at 5 μM each; <sup>b</sup>adult T-cell acute lymphoblastic leukemia (T-ALL); <sup>c</sup>adult acute myeloid leukemia (AML); n.d.: not determined. <sup>d</sup>99% confidence intervals for K<sub>D</sub> [μM].

The following, generation of created dual-HDAC/BRD4 inhibitors were modified on their BRD4 binding scaffold by changing the acetyllysine-mimicking part to a bicyclic 4-acyl pyrrole. Thus, the active ingredients with the IDs 49 and 61 were created. Moreover, to investigate the dual mode of action two more compounds were designed as negative controls that either have substitutions to diminish the HDAC binding affinity or BRD4 binding affinity (Table 28). Compound 49 showed higher affinity against BRD4, but still about eight times weaker than the reference inhibitor XD14 (K<sub>D</sub> values 0.79 μM vs. 0.16 μM). The compound 61 showed binding affinities against BRD4 and HDACs that were at the same level or even better than for the reference inhibitors XD14 and vorinostat. Compound 49 showed even higher killing effectivity against T-ALL cell lines according to the cell viability after 5 μM treatment for MOLT4 (4.0%) and TALL1 (10.6%), compared to the first-generation compound 20. However, HL60 was

found to be less affected as the cell viability was still 42.3% after 5  $\mu\text{M}$  treatment. The biological function of 61 and its negative controls 62 and 63 was investigated further by biological *in vitro* assays (Figure 40).

**Table 28: Target activity of the second generation dual HDAC/BRD4 targeting inhibitors**  $K_D$  values describe the measured antibody affinity.  $\text{IC}_{50}$  values demonstrate the required concentration to bind 50% of the respective HDAC proteins.



	R <sup>1</sup>	R <sup>2</sup>	IC <sub>50</sub> [ $\mu\text{M}$ ]		BRD4(1)	Cell Viability <sup>a</sup> [%]		
			HDAC1	HDAC6	K <sub>D</sub> [ $\mu\text{M}$ ]	MOLT-4	TALL-1	HL-60
<b>49</b>			0.09 $\pm$ 0.01	0.05 $\pm$ 0.01	0.79 (0.46 - 1.37) <sup>b</sup>	4.0 $\pm$ 0.4	10.6 $\pm$ 0.5	42.3 $\pm$ 4.1
<b>61</b>	H	-NH-OH	0.16 $\pm$ 0.01	0.07 $\pm$ 0.01	0.08 (0.030 - 0.171) <sup>b</sup>	1.7 $\pm$ 0.2	50.0 $\pm$ 3.5	35.9 $\pm$ 3.0
<b>62</b>	Me	-NH-OH	0.33 $\pm$ 0.05	0.32 $\pm$ 0.04	n.d.	114.9 $\pm$ 4.3	82.3 $\pm$ 3.5	80.8 $\pm$ 5.5
<b>63</b>	H	-O-Me	> 10 <sup>c</sup>	> 10 <sup>d</sup>	n.d.	68.6 $\pm$ 2.2	70.3 $\pm$ 3.9	104.3 $\pm$ 3.1
<b>vorinostat</b>			0.10 $\pm$ 0.01	0.04 $\pm$ 0.01	n.d.	n.d.	n.d.	n.d.
<b>XD14</b> <sup>37</sup>			n.d.	n.d.	0.16 $\pm$ 0.01	n.d.	n.d.	n.d.

<sup>a</sup> cell viability compared to control determined at 5  $\mu\text{M}$  each; <sup>b</sup> 99% confidence intervals for K<sub>D</sub> [ $\mu\text{M}$ ]; <sup>c</sup> < 10% inhibition at stated concentration; n.d.: not determined; <sup>d</sup> < 20% inhibition at stated concentration.

To study the biological function of the most balanced dual inhibitor 61, we performed a 24h treatment of the aggressive, high MYC expressing T-ALL cell line HPBALL with the compounds 61 (dual HDAC/BET inhibitor), 62 (BRD4(1) negative control) and 63 (HDAC negative control) in comparison to the 1:1 combination of 62 and 63. Apoptosis induction was measured as before by Annexin V/PI staining on the outside of the cell membrane by flow cytometry and by quantification of intracellular caspase 3/7 by a bioluminescence-based assay (Figures 38a and b). In both cases the dual inhibitor 61 induced significantly more apoptosis than the control compounds 62 and 63 as well as the combination of both ( $p < 0.001$ ). To investigate the molecular mechanism after 24h

of treatment, a WB analysis was performed with a focus on MYC expression (Figure 38c). MYC expression was effectively decreased after 61 exposures compared to treatment with 62 (BRD4(1) negative control) and 63 (HDAC negative control) but was comparable to the 1:1 combination of 62 and 63 (Figure 38c).

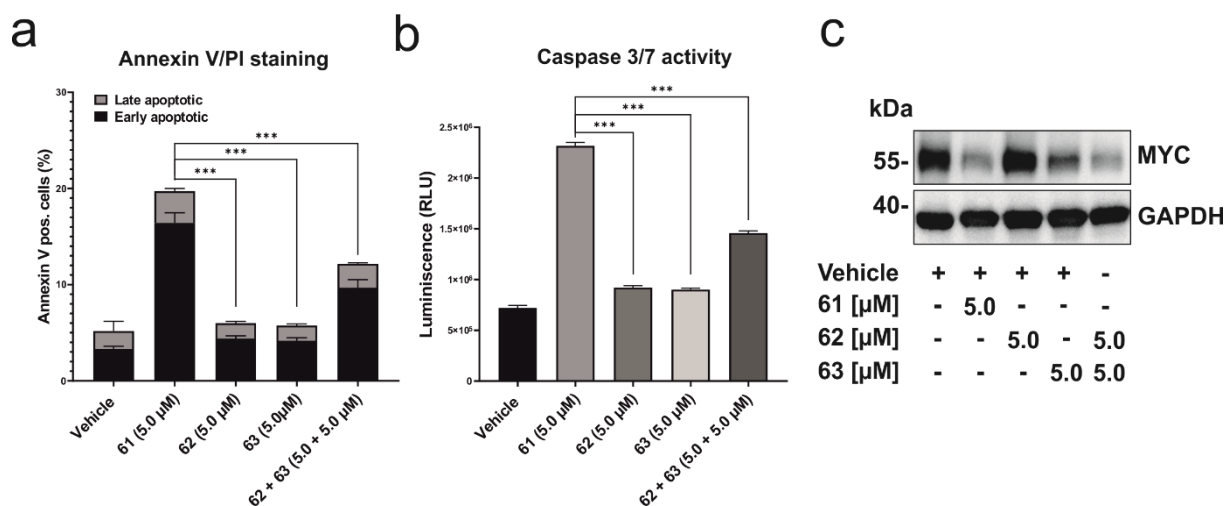


**Figure 38: Biological validation of 61 in comparison to 62 or 63 and their combination**

a) Apoptosis detection after 24h treatment by Annexin V/ PI staining measured by flow cytometry. Significant differences were assessed by the sum of early and late apoptotic cells. Comparisons were made between compound 61 with 62 or 63, as well as their combination c) Quantitative measurement of caspase 3/7 activity by bioluminescence measurement after 48h treatment. The amount of the indicated caspase 3/7 signal results in the level of apoptosis. Comparisons were made again between compound 61 with 62 or 63, as well as their combination c) WB analysis of MYC expression after 24h compound treatment with the indicated concentrations. \*,  $p < 0.05$ ; \*\*,  $p < 0.01$ ; \*\*\*,  $p < 0.001$  (student's t-test).

Based on previously performed target-based data and *in vitro* activity against selected leukemia cell lines, compounds 5b, 20, 49 and 61 were selected as the most promising compounds from the three generations and their anti-cancer properties were investigated by further *in vitro* analyses. In order to evaluate the efficacy of dual HDAC/BRD4 targeting inhibitors, the compounds were first analyzed together with reference controls on a semi-automated drug screening platform using six cell lines from different leukemia entities, including T-ALL, B-ALL, AML and CML. The results are summarized in Table 29. Second-generation inhibitors 49 and 61, and first-generation inhibitor 20 showed improved  $IC_{50}$  values in most cases compared to the reference HDAC inhibitor ricolinostat. It is remarkable that in both B-ALL cell lines (HAL01 and REH) only the second generation of compounds (49 and 61) with sub micromolar  $K_D$  values at BRD4(1) (49:  $K_D = 0.79 \mu$ M; 61:  $K_D = 0.076 \mu$ M) had a cytotoxic effect (Table 28).

**Table 29: IC<sub>50</sub> values of dual HDAC/BET compounds for different leukemia entities**

The table shows the indicated IC<sub>50</sub> [μM] values of the tested compounds with regard to their cell entity including standard deviation. All experiments were performed in triplicates.

IC <sub>50</sub> [μM]						
Compound	T-ALL		AML / CML		B-ALL	
	HPBALL	TALL-1	HL-60	K562	HAL01	REH
<b>5b</b>	> 25	5.16 ± 0.78	> 25	7.38 ± 0.13	> 25	> 25
<b>20</b>	6.79 ± 0.33	2.88 ± 0.02	7.82 ± 0.25	3.40 ± 0.10	> 25	> 25
<b>49</b>	6.31 ± 0.35	2.33 ± 0.17	4.63 ± 0.15	2.90 ± 0.02	6.41 ± 0.60	9.76 ± 0.53
<b>61</b>	7.13 ± 0.52	2.93 ± 0.13	2.75 ± 0.01	5.99 ± 0.28	5.93 ± 0.32	7.79 ± 0.78
<b>birabresib</b>	7.01 ± 0.40	1.35 ± 0.04	0.82 ± 0.03	2.84 ± 0.18	2.53 ± 0.15	15.32 ± 1.30
<b>ricolinostat</b>	6.70 ± 0.19	3.88 ± 0.03	10.37 ± 1.06	6.02 ± 0.10	> 25	> 25

Encouraged by the low IC<sub>50</sub> values determined (Table 29), further functional *in vitro* assays were performed, apoptosis measurement and target evaluation of downstream signaling pathways by WB using a Philadelphia chromosome (Ph+), BCR-ABL1+ positive CML cell line K562. Apoptosis induction by the experimental compounds was evaluated after their 24h, 48h, and 72h exposure along with ricolinostat and birabresib as reference inhibitors for the HDAC and BET bromine domains, respectively, using Annexin V/PI staining followed by flow cytometric analysis (Figure 39a). Interestingly, the dual HDAC/BRD4 targeting inhibitors induced higher apoptosis levels after 24h, 48h and 72h exposure compared to the reference inhibitor birabresib. It is also worth mentioning that exposure of compounds 49 and 20 at almost half of the concentrations (49: 2.9 μM and 20: 3.4 μM vs. ricolinostat: 6.0 μM) were able to induce apoptosis similar to ricolinostat. The protein assessment by WB after treatment with 5b, 20, 49 and 61 showed a strong similarity to ricolinostat exposure, i.e., higher intensities of acetylated α tubulin and acetylated histone H3 protein bands (Figure 39b). In addition, both the dual HDAC/BRD4 targeting inhibitors and ricolinostat significantly increased the expression of cleaved PARP protein, the marker for induced apoptosis, but not with birabresib exposure, which is consistent with previous results. However, all inhibitors used (including ricolinostat) ultimately led to a downregulation of MYC expression.

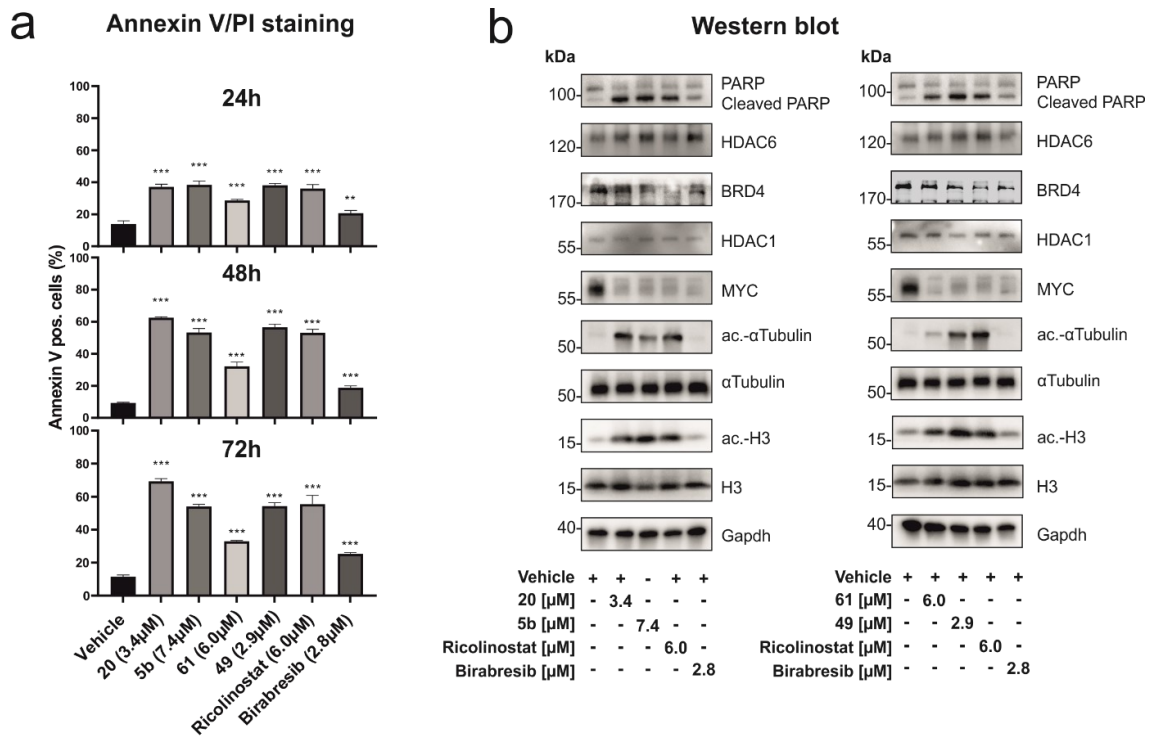


**Figure 39: Biological evaluation of dual HDAC/BRD4 targeting inhibitors**

a) Conclusion of results from apoptosis assay by Annexin V/PI measurement after 24h, 48h and 72h treatment with the indicated concentrations. The percentage of cells that were Annexin V positive, but PI negative were considered as early apoptotic and the percentage of cells that were both Annexin V and PI positive were considered as late apoptotic. Significant differences of the apoptosis between the vehicle and the tested compounds are indicated above the bars. .  $p < 0.05$ ; \*\*,  $p < 0.01$ ; \*\*\*,  $p < 0.001$  (student's t-test). b) Target assessment by WB. Direct target and downstream signaling analysis of cell lysates after 24h treatment with the indicated concentrations of the used compounds.

In order to analyze the efficacy of the dual HDAC/BRD4 targeting inhibitors compared to a 1:1 combination of the reference inhibitors ricolinostat and birabresib, further *in vitro* validations were performed. To achieve a better comparability of the dual inhibitors with reference inhibitors alone or their combination exposure, HPBALL cell line was treated using the same concentration (5.0 µM) for all compounds. The results of the caspase 3/7 measurement after 48h treatment indicated that the dual compounds 20, 49 and 61 are more effective in this assay compared to single treatments with ricolinostat or birabresib (Figure 40a). Furthermore, compared to a 1:1 combination of ricolinostat and birabresib (2.5 µM each, 5.0 µM combined) all three dual inhibitors (20, 49 and 61) achieved significantly higher activity in the caspase 3/7 assay than the combination of the reference inhibitors ( $p < 0.001$ ). Notably, in the case of 49 this remarkable effect could also be observed when compared to a higher concentrated combination of ricolinostat and birabresib (5.0 µM each) (Figure 40a).

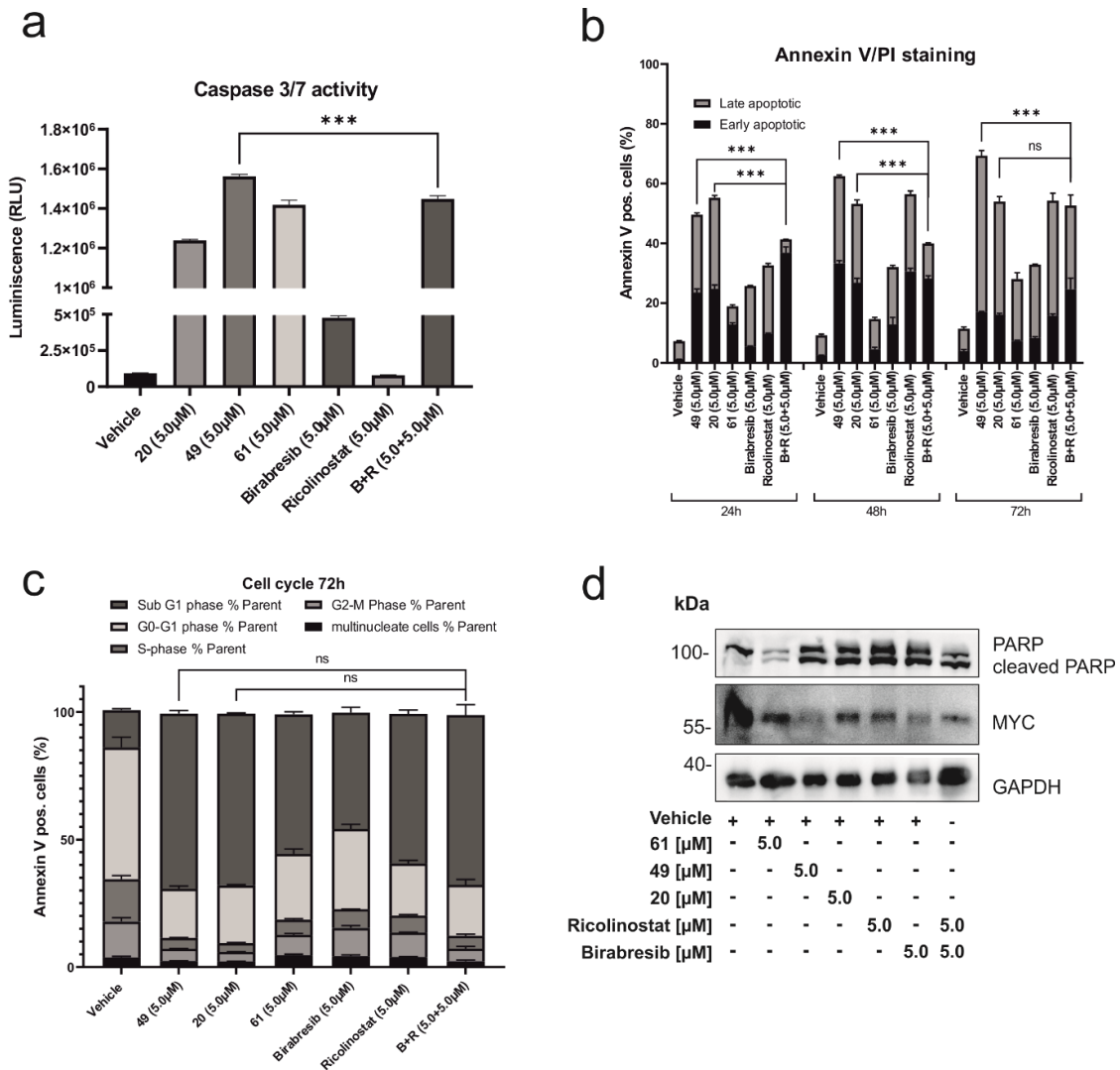


**Figure 40: Cytotoxic activity of dual HDAC/BRD4 targeting inhibitors 20, 49 and 61 in comparison to the reference HDACi ricolinostat and reference BET inhibitor birabresib**  
a) Apoptosis measurement after 48h treatment using caspase 3/7 assay. b) Conclusion of results from apoptosis assay via Annexin V/PI measurement after 24h, 48h and 72h treatment. For all time points, the combination of birabresib and ricolinostat was compared with experimental dual inhibitors. Significance was calculated using the sum of (early and late) apoptotic cells. c) Cell cycle analysis after 72h treatment. Different cell cycle stages were compared between the experimental compounds and the combination of ricolinostat with birabresib. d) Representative WBs of HPBALL lysates taken after 24h treatment with the indicated compounds. p<0.05; \*\*, p<0.01; \*\*\*, p<0.001 (student's t-test).

To investigate whether the apoptosis induction efficacy of dual HDAC/BRD4 targeting inhibitors exceeds the efficacy of the combination of reference inhibitors, apoptosis was determined by Annexin V/PI measurement after 24h, 48h and 72h (Figure 40b). In fact, a significant increase in apoptosis was observed after 24h and 48h treatment with compounds 49 and 20 compared to the combination of reference inhibitors (5.0 µM each, Figure 40b). After 72h, compound 49 still showed a significantly increased

apoptosis induction, while the efficacy of compound 20 was at the same level as that of the combination of reference inhibitors. Next, the previously obtained results were validated in a cell cycle experiment. Treatment of the dual HDAC/BRD4 targeting inhibitors 49, 20 and 61 showed high proportions of sub-G1 phase cells (markers of apoptosis induction) but were comparable to the combination of reference inhibitors without significant differences (Figure 40c). Finally, the expression of MYC at the protein level was investigated by WB after 24h compound treatment (Figure 40d). Low levels of MYC were found in the cells treated with the experimental compounds as well as in the cells treated with the reference inhibitors alone and in combination. The data summarized in Figure 40a to c show that in the case of the cell line with high MYC expression HPBALL 49 is more efficient in inducing apoptosis than 61, although 61 is a more balanced dual inhibitor in terms of target activity.

### 3.5.2. Investigation of novel C-terminal HSP90 inhibitors

Novel inhibitors based on a previously described peptidomimetic called aminoxyrone (AX) [159] that target heterodimerization of HSP90 by destroying the C-terminal domain (CTD) without inducing a heat shock response (HSR) are the subject of the following results section. The newly synthesized experimental compounds tested in this thesis were provided by Prof. Dr. Thomas Kurz from the Institute of Medicinal Chemistry, University of Düsseldorf, Germany. The compounds are based on the structure of AX, with a few modifications reducing its size, which classifies the compounds as small molecule inhibitors. Several biological tests were performed to validate whether the substances are still effective in CTD inhibition of HSP90. The first task was to solve new types of connections in a suitable vehicle. For the compound Exp102 no issues appeared while dissolving, whereas Exp101 was barely dissolvable in DMSO even after warming the compound in a 50°C water bath accompanied with sonification for 30 min. A clear solution was only reached with Exp102, while a rather hazy solution was reached with Exp101.

The biological efficacy of the experimental compounds was determined in a preliminary experiment with two increasing concentrations (6  $\mu$ M and 12  $\mu$ M) and served as an estimate of the pharmacological potential (Figure 41). The compounds were tested on 3 cell lines, including HPBALL and the imatinib-resistant (ImR) CML cell lines K562 and KCL22. Novobiocin (NB), a HSP90 CTD inhibitor was used as the reference

inhibitor in a concentration of 0.1 mM. Cell lines were seeded on a 96-well plate containing the indicated compound concentrations and were incubated for 72h. Upon exposure, a significantly higher reduction in cell viability was measured with Exp 102, followed by Exp101 and reference inhibitor NB, in all three tested leukemic cell lines at the specific concentration.

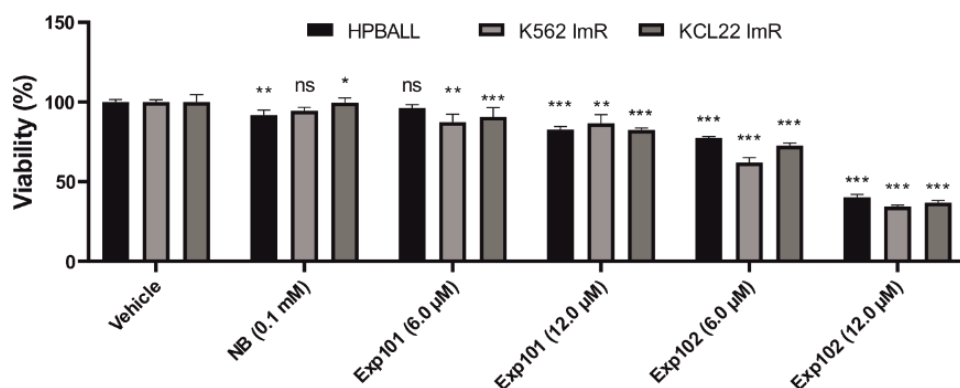


**Figure 41: Preliminary drug screening with two concentrations in three different cell lines**

$0.5 \times 10^6$  cells were seeded in 96 well plate and treated with the compounds  $n=3$ . After 72h cell viability was measured using CTG relative to vehicle control.  $p < 0.05$ ; \*\*,  $p < 0.01$ ; \*\*\*,  $p < 0.001$  (student's t-test).

To determine the  $IC_{50}$  values of the experimental compounds, a drug screen was performed with a concentration range from 5 to 25000 nM in a variety of different leukemia subtypes, including imatinib resistant cell models (K562, KCL22 and SUPB15) and bortezomib resistant cell model (HL60) as well as T-ALL cell lines (MOLT4, DND41, TALL1 and HPBALL) (Figure 42a). Corresponding to the previous results, the  $IC_{50}$  value of Exp101 was in most cases in a concentration between 15 and 20  $\mu\text{M}$ . In case of HPBALL the  $IC_{50}$  value was determined at about 7  $\mu\text{M}$  while the compound showed no effect on the imatinib resistant cell line KCL22 and the bortezomib resistant cell line HL60. In the case of Exp102, the values determined were significantly lower, with most  $IC_{50}$  values being around 4 to 10  $\mu\text{M}$ . Again, the imatinib resistant cell lines KCL22 ImR and SUPB15 ImR showed greater resistance to the experimental compound compared to their wild-type counterparts. T-ALL cell lines were in generally sensitive against Exp102, with the lowest determined  $IC_{50}$  values (3.31  $\mu\text{M}$  +/- 0.23  $\mu\text{M}$  for DND41, 4.03  $\mu\text{M}$  +/- 0.40  $\mu\text{M}$  for HPBALL, 5.46  $\mu\text{M}$  +/- 0.73  $\mu\text{M}$  for MOLT4 and 6.34  $\mu\text{M}$  +/- 0.04  $\mu\text{M}$  for TALL1). Next, the biological activity of the compounds was investigated by Annexin V/PI staining in three different cell lines (K562



ImR, KCL22 ImR and HPBALL) after 24h treatment (Figure 42b). The used concentrations were based on the IC<sub>50</sub> values determined in the previous drug screening. Apoptosis induction was similar in all tested cell lines, showing a trend of Exp102 being more potent with the half of the used concentrations compared to Exp101. In all cases, NB showed no apoptosis induction even with the high concentration that was used (0.1 mM), underlining the high potency of the novel AX derivates Exp101 and Exp102.

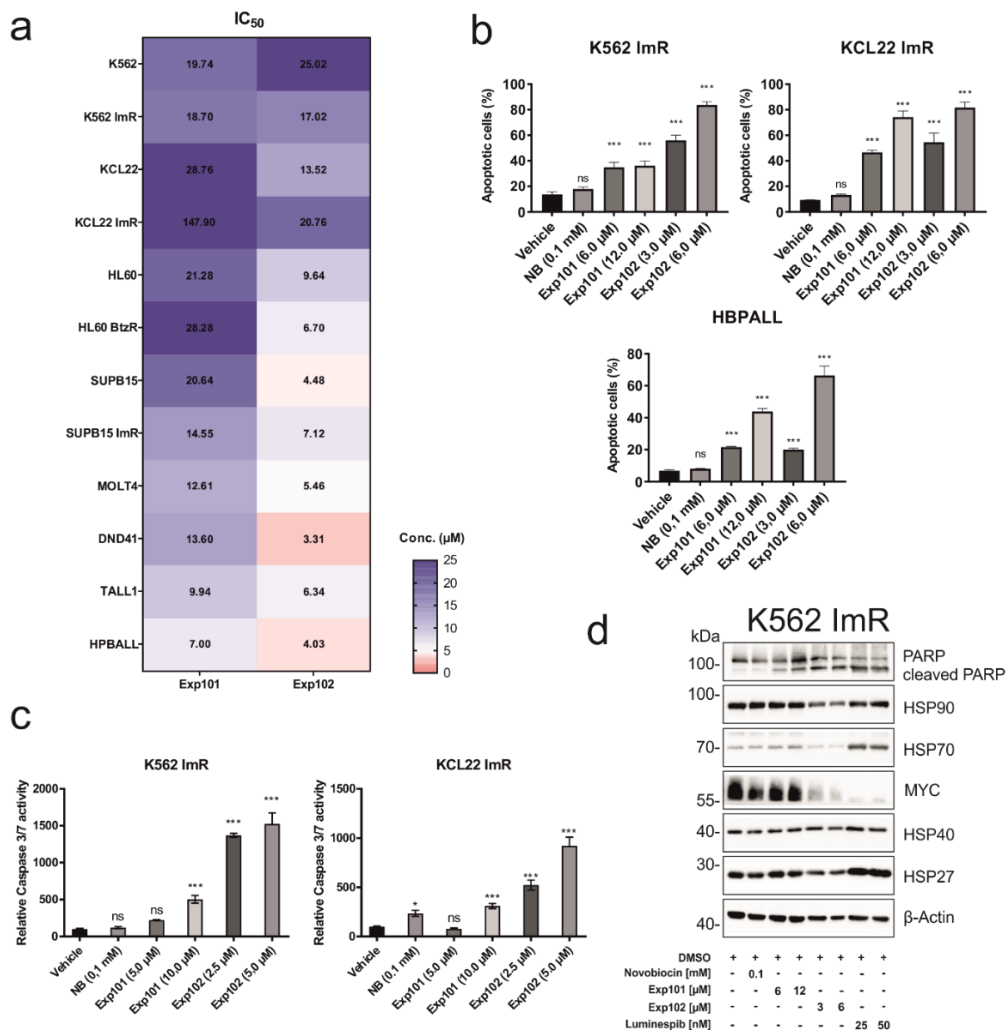


**Figure 42: In vitro validation of first generation of small molecule HSP90-CTD inhibitors**  
a) Heatmap of IC<sub>50</sub> values from drug screening for Exp101 and Exp102 in different leukemia cell lines. b) Annexin V/PI staining results after 24h treatment of three different cell lines. c) Caspase 3/7 measurement after 48h treatment if two imatinib resistant cell models. d) Protein assessment of treated K562 ImR cells. p<0.05; \*\*, p<0.01; \*\*\*, p<0.001 (student's t-test).

Apoptosis induction was further investigated by caspase 3/7 assay (Figure 42c). Therefore, imatinib resistant (ImR) cell lines K562 ImR and KCL22 ImR were treated for 24h with the experimental compounds and NB as a reference inhibitor. In

KCL22 ImR the compounds Exp101 and Exp102 were significantly more potent in inducing apoptosis compared to the reference inhibitor NB ( $p < 0.001$ ). Similar results were observed with the cell line K562 ImR ( $p < 0.001$ ). Thus, protein lysates of the K562 ImR cells were harvested after 24h treatment with the indicated doses and examined by WB (Figure 42d). HSR was detected by increased HSP70 and HSP27 and was only visible in samples treated with N-terminal HSP90 inhibitor AUY922 (luminespib). Interestingly, expression of cleaved PARP (marker of apoptosis) was elevated upon exposure of the inhibitors, with NB as an exception. The total amount of MYC was slightly decreased with the reference inhibitor NB and completely eradicated with the use of AUY922. The experimental agent Exp101 apparently had no minimal effect on MYC and HSP90 expression, whereas Exp102 significantly reduced total MYC protein levels along with lower HSP90 levels, even at half the concentration used compared with Exp101.

The chemical structure of the second-generation small molecule HSP90-CTD inhibitors (Exp201 and Exp202) were based on the potent inhibitor Exp102 of the first-generation inhibitors. The second-generation inhibitors exhibited better solubility in DMSO as compared to the first-generation inhibitors. While compound Exp201 still contained the aromatic benzene ring and an alkyl radical attached to the backbone structure, compound Exp202 instead contained two alkyl radicals without an additional methoxybenzene ring.

The  $IC_{50}$  values of the compounds were determined using drug screening in different cell entities (Figure 43a). Large differences in potencies were found between the compounds Exp201 and Exp202. While Exp201 showed a similar effect to its predecessor Exp102, compound Exp202 appears to be much more potent. This statement can be confirmed by looking at the  $IC_{50}$  values, which are mostly found in the lower  $\mu\text{M}$  range (between 1  $\mu\text{M}$  and 5  $\mu\text{M}$ ). This is a substantial increase over the previous inhibitor Exp102. Further the inhibitory activity of compound Exp202 was investigated by proliferation/viability assay on MOLT4 cell line at 1.8  $\mu\text{M}$  and 3.6  $\mu\text{M}$ , with NB at 0.3 mM (Figure 43b). Whereas the cell count of vehicle treated MOLT4 increased steadily to  $1.5 \times 10^6$  after 72h, the compound Exp202 in a concentration reduced the cell proliferation by half (around  $0.7 \times 10^6$ ). The investigation of apoptosis by Annexin V/PI staining after 24h compound treatment using MOLT4, also showed that the experimental compound Exp202 could compete the effect of the almost 100-

times higher concentrated reference inhibitor NB (58.5% vs. 76.0% apoptotic cells,  $p < 0.001$ ) (Figure 43c). The next apoptosis experiment that was performed was the caspase 3/7 assay after 48h treatment using again MOLT4 (Figure 43d). This time Exp202 induced even higher apoptosis than the 100-times higher concentrated reference compound NB (20% higher caspase 3/7 signal of Exp202 vs. NB  $p < 0.001$ ).

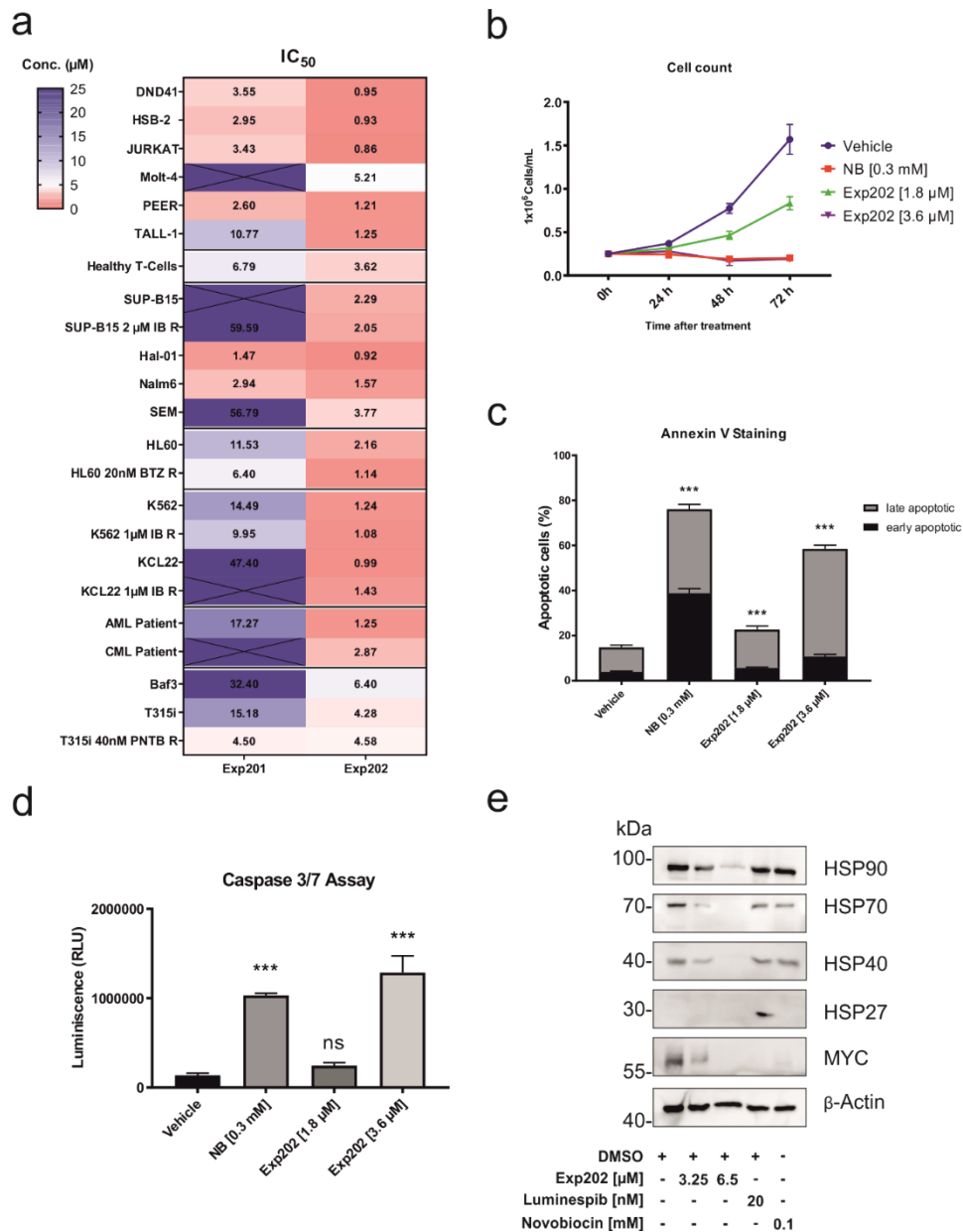


**Figure 43: *In vitro* validation of second-generation small molecule HSP90-CTD inhibitors**  
a) Heatmap of  $\text{IC}_{50}$  values from drug screening for Exp201 and Exp202 in different leukemia cell lines. b) Proliferation tracking of MOLT4 cells after treatment induction. Measurements were performed after 24h, 48h and 72h after compound substitution. c) Annexin V/PI assay after 24h compound substitution using MOLT4 d) Caspase 3/7 assay after 48h compound substitution using MOLT4. e) WB of MOLT4 lysates after 24h treatment.  $p < 0.05$ ; \*\*,  $p < 0.01$ ; \*\*\*,  $p < 0.001$  (student's t-test).

Finally, the effects of the compound Exp202 on the molecular level were investigated by WB using lysates of 24h treated MOLT4 cells (Figure 43e). AUY922 was again used as a HSR inducing reference inhibitor and NB as a CTD-targeting reference inhibitor. No HSR was observed when compounds Exp202 and NB were used, whereas HSR was obvious in AUY922 treated cells, indicated by an increase of HSP27. Interestingly, the increased use of Exp202 decreased the total amount of HSP90 and other HSP-protein family members such as HSP70 and HSP40, which was not observed by NB treated cells. However, MYC was slightly decreased already with a low concentration of Exp202 (3.25  $\mu$ M) and totally diminished with a concentration of 6.5  $\mu$ M.

In order to optimize the efficacy of the compounds, three variants with different chemical modifications in the catalytically active site and at the backbone structure were developed in the third generation of compounds based on the chemical structure of Exp202. Among them, Exp301 and Exp303 differ only in minor nuances in the alkyl residues. The backbone structure of Exp302 also resembles that of Exp202, but this compound is modified in the catalytic region by an additional methoxybenzene ring, as was the case with the first-generation inhibitor Exp102.

The effectiveness of the new generation of CTD inhibitors Exp301, Exp302 and Exp303 with Exp202 as a control has been broadly tested by an extended drug screening on numerous cell lines and patient cells of different tumor entities in triplicates, including T-ALL, T-LBL, B-ALL, AML, CML, and neuroblastoma cell lines (Table 30).

The determined drug screening values showed a high efficacy of the new generation of CTD HSP90 inhibitors, based on the predecessor Exp202. Comparing the killing efficacy of the Exp202 compound with the third-generation compounds, no major differences were observed. The biggest difference observed between the two generations is that the T-LBL cell line SUPT1 was significantly more sensitive to the third generation of HSP90 CTD compounds ( $IC_{50}$  10.5  $\mu$ M for Exp202 vs 2.9  $\mu$ M for Exp301). Conclusively, the values determined through the cell lines were in the lower micromolar range, which indicates a particularly effective activity of the compounds. Of particular note is the fact that the inhibitors tested are highly effective in TKI resistant CML and AML cell lines (highlighted with an R after the cell line designation) with  $IC_{50}$  values ranging from 1 to 5  $\mu$ M in most of the inhibitors tested. The highest sensitivity could be observed in the group of B-ALL cell lines and patient cells. Here, the lowest

## Results

IC<sub>50</sub> values varied from 1.0 to 2.0  $\mu$ M. In the case of the tested medulloblastoma cell lines however, the second generation HSP90 inhibitor Exp202 showed higher effectivity compared to the third generation (IC<sub>50</sub> values ranging 2.2 to 3.8  $\mu$ M for Exp202 and between 3.8 to 8.3  $\mu$ M for third generation compounds). In most of the cases Exp202 revealed two to three times lower IC<sub>50</sub> values in medulloblastoma cell lines.

**Table 30 Results of extended drug screening of 2<sup>nd</sup> and 3<sup>rd</sup> generation HSP90 inhibitors**

Tumor Entity	Cell line	Exp202		Exp301		Exp302		Exp303	
		MW	SD	MW	SD	MW	SD	MW	SD
T-ALL	TALL1	1.95	0.1	1.4	0.02	1.69	0.14	1.89	0.37
	TALL1 MYC OE	2.54	0.04	1.51	0.12	2.75	0.38	2.12	0.29
	MOLT4	1.83	0.14	2.01	0.18	4.03	0.4	2.08	0.09
	DND41	2.71	0.04	1.88	0.06	4.28	0.23	4.03	0.28
	PEER	1.33	0.09	1.28	0.06	1.97	0.22	1.57	0.09
	HBPALL	5.7	0.46	2.07	0.08	4.19	0.19	6.53	0.46
	JURKAT	1.28	0.07	1.24	0.1	2.75	0.18	1.16	0.02
	HSB2	1.35	0.06	1.16	0.13	2.26	0.41	2.07	0.44
T-LBL	SUPT1	10.47	1.61	2.94	0.43	4.92	1.07	4.55	1.33
AML/CML Resistant to TKI	THP1R	4.22	0.49	5.44	1.69	8.26	1.26	6.66	1.76
	K562R	5.56	0.3	2.67	0.15	4.67	0.44	4.49	0.28
	KCL22R	3.94	0.49	4.49	0.12	9.29	0.65	4.31	0.31
	HL60R	1.91	0.13	4.19	0.09	6.93	0.97	2.33	0.17
AML/CML	HL60	2.41	0.09	4.42	0.17	10.32	1.32	2.96	0.95
	K562	3.7	0.2	2.35	0.03	3.91	0.33	5.33	0.21
	KCL22	3.49	0.13	2.38	0.18	5.49	0.19	4.38	0.32
	THP1	3.34	0.43	5.4	0.09	10.75	0.45	9.86	2.27
B-ALL	HAL01	1.39	0.08	1.65	0.06	2.53	0.28	2.87	0.28
	SEM	1.38	0.06	1.02	0.03	1.73	0.14	1.98	0.07
	Patient 1272	1	0.15	1.09	0.06	1.7	0.32	1.36	0.11
	Patient 3791	1.2	0.07	1.09	0.12	1.45	0.16	1.66	0.14
	MUTZ5	2.03	0.26	2.15	0.38	2.32	0.35	3.02	0.62
	SUPB15	1.62	0.1	2.11	0.12	3.98	0.17	3.5	0.08
	A697	1.56	0.13	1.21	0.02	1.57	0.09	3.6	0.41
	MHH-CALL4	1.4	0.05	1.35	0.1	1.72	0.17	2.65	0.49
Burkitt Lymphoma	RAJI	2.5	0.23	1.27	0.07	1.83	0.09	3.53	0.51
Medulloblastoma	CHLA-266	2.19	0.22	3.75	0.07	4.73	0.41	6.27	0.28
	DAOY	3.72	0.25	8.02	0.88	8.25	0.54	6.92	0.31

To examine the capability of apoptosis, induction the compound Exp301 was biologically validated in the T-ALL cell line HPBALL (Figure 44a). Therefore, an Annexin V/PI assay was performed after 24h treatment with the indicated doses of the used compounds. Coumermycin A1 (C-A) was used as a reference inhibitor instead of novobiocin because C-A showed higher potency in a recently published study [172]. The apoptosis inducing effect of Exp301 was significantly higher compared to first generation compound Exp102 (37.8% vs. 46.1% apoptotic cells, respectively,

$p < 0.001$ ). Only a slight induction of apoptosis was examined with the reference inhibitor C-A when compared to the vehicle ( $p = 0.0220$ ). However, the experimental compounds Exp102 and Exp301 induced significantly higher apoptosis compared to the reference inhibitor C-A,  $p < 0.001$ .

Finally, investigation of HPBALL cell lysates after 24h treatment with Exp102, Exp301 and the reference inhibitors was performed using WB (Figure 44b). A strong reduction of MYC was only observed with Exp301, without reducing the total protein amount of HSP90 like it was the case with the second-generation compound Exp202 (Figure 43e). Moreover, HSR was again, only induced by AUY922, as it can be observed with an increased HSP70 lane.

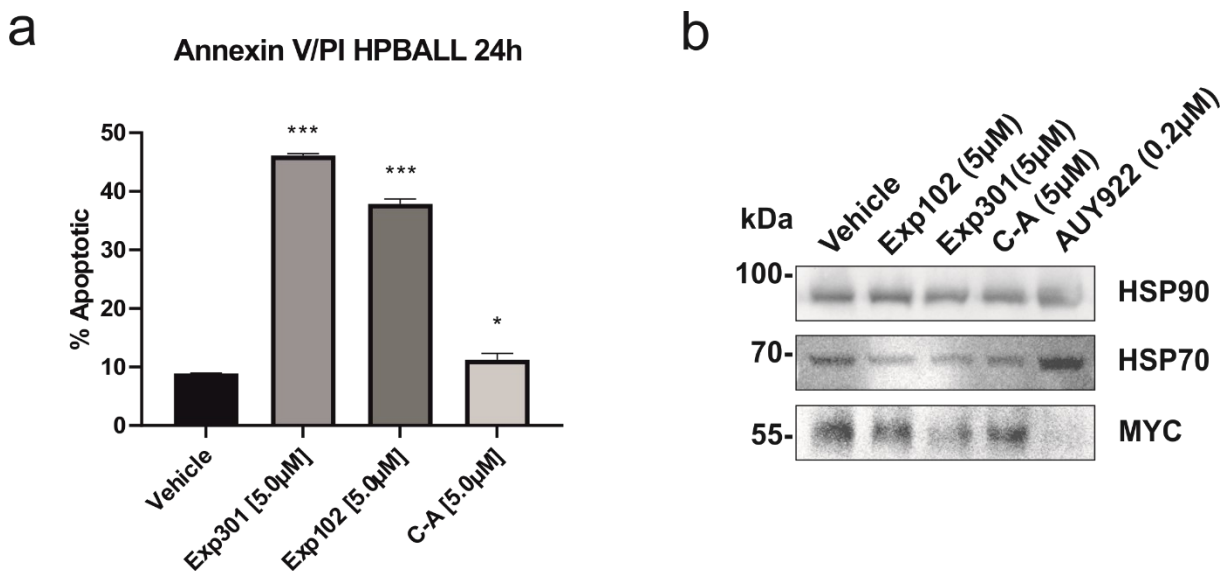


**Figure 44: *In vitro* validation of third-generation small molecule HSP90-CTD inhibitors**  
a) Apoptosis measurement with Annexin V/PI staining after 24h treatment.  $p < 0.05$ ; \*\*,  $p < 0.01$ ; \*\*\*,  $p < 0.001$  (student's t-test). b) Target assessment by WB of HPBALL lysates after 24h treatment.

## 4. Discussion

Modern treatment approaches have increased the survival rates over the past 30 years with an average 5-year event-free survival up to 90%. This is mainly due to the development of new therapeutic methods and the combination of existing therapeutics. Today, T-ALL patients with treatment protocols like the AIEOP-BFM defines leukemia subtypes, which is used for risk stratification [10]. Unlike B-ALL, genetic stratification markers have not yet been considered in patient risk assessment for T-ALL. Several genetic markers have now been described that have a significant impact on disease progression and prognosis but have not yet been used in treatment selection. Molecular stratification could pave the way for targeted therapeutic approaches that show a high potential for the treatment of various tumor entities, including therapy resistant and relapsed T-ALL.

### 4.1. PTEN Mutations are associated with increased MYC stability

In this work, the first goal was to characterize a set of T-ALL cell line models with respect to the most prominent T-ALL dysregulations, including PI3K/AKT- and Raf/MEK/ERK signaling pathways, Notch1 activating mutations and the expression of MYC on mRNA and protein level (Figure 8a). An obvious correlation between the absence of PTEN accompanied with increased AKT phosphorylation and increased MYC was observed (Figure 8a). PTEN mutations have an unfavorable effect, according to the most T-ALL study groups [93, 110, 111, 113], with few exceptions postulating no significant differences [173, 174]. The possible association with MYC via the PI3K/AKT signaling pathway could play a role in worsening prognosis, as MYC overexpression is the driving factor in many cancers like breast cancer, pancreatic cancers, osteosarcomas, and hepatocellular carcinomas [175-178]. However, no correlation to MYC mRNA expression levels an PTEN absence was made (Figure 7). Previous studies showed similar observations and explained the poor correlation with many posttranscriptional modulations that may contribute to MYC stability [93]. Normally, the transcription and expression of MYC is highly regulated. This serves to counteract the oncogenic potency of the transcription factor MYC, as Important cellular processes such as cell growth, proliferation and apoptosis are under its control [78, 179, 180]. The strong regulation of MYC becomes obvious when considering the half-

lives of the mRNA and protein, which are 30 min for the mRNA and 20 min for the protein [181, 182]. The molecular mechanism behind the proteasome-mediated degradation depends on MYC phosphorylation at position T58, which is initiated by the ubiquitin proteasome system [183]. In the case of PTEN<sup>mut</sup> T-ALL cells, the PI3K/AKT pathway is uninhibited and thus reduces the phosphorylation of MYC at site T58 by inhibition of GSK3 $\beta$  function [117]. In fact, a reduction of MYC phosphorylation on site T58 was noticed in PTEN<sup>mut</sup> cell lines (Figure 11a), underlining this hypothesis. However, the absence of PTEN does not impact the MYC E-Box binding activity since no significant differences were observed (Figure 10). Additionally, attempts have been made to confirm these observations in T-ALL PDX cells, but the WBs were unsuccessful even after several repetitions. It was only possible to confirm the presence or absence of PTEN (Figure 12). The PTEN signal of Patient 4 was very low compared to the control cell line and Patient 1, but it could be explained by a low total protein amount indicated by the low housekeeper signal. Therefore, patient samples 1 and 4 were categorized following as PTEN<sup>wt</sup> and patient samples 2 and 3 as PTEN<sup>mut</sup>.

#### **4.2. PTEN mutations increase susceptibility for GC resistance**

Using a drug screen with dexamethasone has shown that the group of PTEN<sup>mut</sup> cell lines were significantly resistant (Figure 14a and b). This finding is in line with the previously described correlation between the PI3K/AKT axis with GC resistance [165, 184, 185]. Finding the genetic mechanism behind this appears to be interesting. Therefore, gene expression sets of different T-ALL cell lines were examined and tested whether there is an association with MYC (Figure 16). Upon correlation with the database, MYC target genes were found significantly enriched in PTEN<sup>mut</sup> T-ALL cell lines when compared to PTEN<sup>wt</sup> group. The highest significant value was reached with ARNTL2, which is a transcription factor closely linked to the process of circadian rhythm [168]. Glucocorticoids are known to be an adrenal circadian output downstream of the central and peripheral clocks, possibly affecting the circadian clock itself and interacting with other clock outputs in the circadian regulation of physiology [167, 186]. Whether the circadian rhythm plays a role in glucocorticoid resistance remains to be determined. It may be possible that ARNTL2 influences the expression of various factors that could suppress glucocorticoid accessibility. Interestingly, overexpression of ARNTL2 has been described in some solid tumor entities, which may have a major impact on tumor cell proliferation and invasion [187, 188]. However, the decision was



made to proceed analysis with the second most significantly upregulated gene ABCA5, which belongs to the family of ABC transporter that are associated with resistance mechanisms [189, 190]. More precisely, ABCA5 is known as an efflux transporter for steroids [191, 192], that is probably the reason for more frequent emergence of glucocorticoid resistance in PTEN mutated T-ALL. ABCA5 was also higher expressed in the available PTEN<sup>mut</sup> T-ALL cell lines compared to the wild types (Figure 17). Interestingly, using a PI3K/mTOR inhibitor BEZ235 was able to modulate the glucocorticoid resistance in pediatric T-ALL [193]. The sensitivity to dexamethasone resulting from inhibition could presumably have arisen from the reduction of MYC and thus decreased expression of the transporter molecule ABCA5. However, these factors have not yet been linked to the PI3K/AKT pathway and thus require further investigation.

### **4.3. PI3K and AKT inhibitors are well suited for PTEN<sup>mut</sup> cells**

In the next step, the cell lines were examined in high-throughput drug screening for a response to certain inhibitors (Figure 18). PTEN<sup>mut</sup> cells demonstrated increased sensitivity to PI3K and AKT inhibition (Figure 18b and 19). Two inhibitors stood out in particular, copanlisib the PI3K inhibitor and afuresertib the AKT inhibitor. Copanlisib (BAY 80–6946) is an i.v. available, highly selective, and reversible pan-class I PI3K inhibitor with predominant activity against the p110 $\alpha$  and p110 $\delta$  isoforms, currently in clinical development and recently FDA approved for follicular lymphoma [194]. Copanlisib has already shown high potency against lymphomas and other cancer types, including complete remission in rat xenograft models for breast cancer [195]. The second compound, afuresertib (GSK2110183), is a highly effective inhibitor of AKT. Interestingly, high sensitivity against afuresertib was found in hematological cell lines comprising ALL, non-Hodgkin's lymphoma and chronic lymphoblastic leukemia [196]. In a clinical study, afuresertib was shown to be safe and well tolerated (PKB112835). Moreover, afuresertib has demonstrated clinical efficacy in a number of hematological malignancies, which makes this inhibitor interesting [197].

Inhibition of the PI3K/AKT pathway was particularly effective in the PTEN<sup>mut</sup> group compared with the PTEN<sup>wt</sup> group. This was demonstrated by focused drug screening in T-ALL cell lines with different PTEN status (Figure 21) and a PTEN knockdown model (Figure 23). However, patient cells (Patients 2 and 3) that did not show PTEN

expression at the protein level (Figure 12) also demonstrated clear sensitivity to the inhibitors copanlisib and afuresertib (Figure 22). The fact that the PI3K/AKT inhibitors indicated increased efficacy in response to the absence of PTEN supports the notion that these cell lines are particularly dependent on this pathway. The PI3K/AKT pathway is found to be degenerated in many different tumor entities like ovarian-, cervix-, breast- or pancreas cancers, independent of germline mutations [198-201]. Therefore, inhibition of this pathway appears to be a promising approach for future targeted therapies. The search for respective small molecules was initiated early, resulting in a variety of highly potent PI3K/AKT-targeting small molecules, which are available today [202, 203]. The decision was made to proceed for *in vitro* biological validation of the preselected inhibitors copanlisib and afuresertib.

#### **4.3.1. PI3K and AKT inhibitors in combination with other, MYC related inhibitors demonstrated promising effectivity *in vitro***

The first step of the *in vitro* validation was to find a synergistic inhibitor to increase the killing efficacy. Treatment with only one specific agent carries the risk that the malignant cells develop resistance mechanisms due to their unstable genome, such as the upregulation of an alternative signaling pathway that can counteract the effect of the inhibitor [204]. With combinatorial drug screening experiments, the synergistic effect of PI3K and AKT inhibitors together with BRD4 inhibitors was found in most of the PTEN<sup>mut</sup> cell lines and thus formed the basis for subsequent analyses (Figure 24 and 26). The combination of PI3K and BRD4 inhibitors has already been described as particularly effective in reduction of cancer cell growth and metastasis [205]. It is therefore not surprising that this combination also shows a synergistic effect in PTEN<sup>mut</sup> T-ALL cell lines. BRD4 inhibitors are meanwhile described as bona fide MYC inhibitors, because of the reduced MYC transcription, which comes along with BRD4 inhibition [97] and are therefore well suited as supportive inhibitors. The first *in vitro* validated combination was copanlisib with JQ1 (Figure 25). The effect of apoptosis induction when the compounds were used in combination was a long-lasting effect with steadily increasing numbers even after 72h of treatment, while the individually treated samples remained at the same level (Figure 25a). Additionally, at the protein level, it was shown that even small amounts of both inhibitors in combination have a large effect on MYC expression (Figure 25b). These results highlight the MYC decreasing effectivity of targeting both cellular pathways simultaneously. Considering a planned *in vivo*

application and clinical relevance, the combination of afuresertib and birabresib was next investigated, demonstrating synergy in apoptosis induction in all three PTEN<sup>mut</sup> cell lines tested (Figure 27). In the next step, HPBALL was investigated further on dual AKT/BRD4 inhibition. The assumption that the inhibition of the PI3K/AKT signaling pathway would improve MYC stability by increasing phosphorylation at the T58 site, which ultimately accelerates degradation [206], was confirmed using WB analysis of cell lysates after treatment with afuresertib and birabresib (Figure 29a). It was noticed that phosphorylation of MYC on its stabilizing site S62 was increased in the birabresib alone treated sample, suggesting that some cell mechanisms were ongoing to rescue MYC stability by increased phosphorylation of S62 site, maybe due to increased Raf/MEK/ERK pathway as hypothesized in schematic Figure 29b. The combination of afuresertib with birabresib showed complete reduction of MYC protein, even at the lowest drug concentrations used, without increased phosphorylation of MYC site S62 (Figure 29a), indicating an effective mechanism of action.

Next to BRD4 inhibitors, Aurora Kinase inhibitors (including AURKA-, AURKB- and pan-Aurora inhibitors) were found to be interesting in high MYC expressing cell lines because the protein was already described to be a direct target of MYC and it mediates MYC protein stability due to inhibition of GSK3 $\beta$  like it is the case in AKT [102, 129]. Based on the screening of Aurora Kinase inhibitors in the MYC overexpression model TALL1, it was found that the additional amount of MYC contributes to an increased sensitivity towards AURKA inhibitor like alisertib (Figure 30b). Alisertib is an orally available and selective AURKA inhibitor, which impairs the function of AURKA during the mitosis spindle and thus causes a mitotic accumulation. Additionally, alisertib is described to induce apoptosis and autophagy through targeting the AKT/mTOR/AMPK/p38 pathway in leukemic cells [207-209]. Thus, it is well suited for inhibition of resistant and highly proliferating cancers.

Another correlation between the increased MYC protein and an increased sensitivity to AURKA inhibitors was discovered in the imatinib resistant BCR-ABL1+ cell model SUPB15, which proved to be interesting (Figure 31). This is likely due to long-term treatment with imatinib, whereby PTEN is most likely mutated by the upregulation of DNA methyltransferases and proteins of the Polycomb group [170]. Loss of PTEN may have contributed in part to the upregulation of MYC in the imatinib-resistant cell model SUPB15. The biological effects of AURKA inhibition together with PI3K inhibition was

further investigated in a T-ALL cell line model HPBALL. The synergistic activity of alisertib and copanlisib combination was calculated using BLISS model (Figure 30c). Further, investigation of the cell cycle in treated HPBALL demonstrated the mode of action of AURKA inhibitors, as AURKA inhibited cells were blocked in the G2 phase (Figure 30d). Using target validation at the protein level, the inhibition of AURKA led to an increased phosphate transfer from GSK3 $\beta$  to MYC T58 (Figure 30f). However, no reduction of GSK3 $\beta$  phosphorylation was discovered in the case of alisertib alone treated cells, as it was the case for copanlisib. This potentially implies that the effect of AURKA on GSK3 $\beta$  is minimal. Further, the WB results of the AURKA proteins and their phosphorylation status raised some questions. As what caused the increase of total AURKA levels upon Alisertib treatment, which was decreased significantly with copanlisib, and higher AURKA phosphorylation with their combination (Figure 30f). This remains to be investigated further.

Finally, one additional indirect MYC inhibitor class was recognized when investigating the PTEN knock down cell model in DND41 (PTEN<sup>wt</sup> T-ALL cell line) on the high throughput drug screening (Figure 32a). Somehow, knocking down the PTEN led to an increase in MEK inhibitor sensitivity. This was later validated in a focused screening with a MEK inhibitor cobimetinib (Figure 32b). Cobimetinib is a potent and highly sensitive MEK1 inhibitor and has demonstrated to induce growth inhibition in a broad range of cancer types, especially in BRAF or KRAS mutants. In combination with PI3K inhibition cobimetinib triggers robust apoptosis and tumor growth inhibition [210, 211]. It was further analyzed, if a combination of the PI3K inhibitor copanlisib with the MEK inhibitor cobimetinib are synergistic. Hypothetically, this combination should have a forcing effect on the degradation of MYC, since both axes of stabilization are manipulated (MEK/ERK for phosphorylation of MYC site S62 and PI3K/AKT for inhibition of GSK3 $\beta$ ). Interestingly, this combination was only indicating synergy in PTEN<sup>wt</sup> cells, with high phosphorylation of MEK (Figure 8a and 33), which may be likely due to mutations in the Raf/MEK/ERK pathway [212]. However, the simultaneous inhibition of the MEK/ERK pathway and PI3K/AKT in DND41 wildtype cells reduced the protein amount of MYC, as it can be seen in the WB analysis (Figure 34c). The amount of phosphorylated MYC at site S62 was reduced and at the same time the phosphorylation of T58 increased. Interestingly, although the combination of both compounds showed no increase in apoptosis (Figure 34d) the cells were significantly

reduced in its proliferation activity (Figure 34c). It is likely that MYC is mainly responsible for proliferation activity in the case of the DND41 cell line, and another cellular mechanism may prevent the triggering of apoptosis by other means.

#### **4.4. *In vivo* validation of Copanlisib and JQ1 demonstrated a partially successful therapeutic approach in PTEN<sup>mut</sup> T-ALL**

The compounds copanlisib and JQ1 showed high efficacy in apoptosis induction and MYC lowering in the PTEN<sup>mut</sup> cell line MOLT4, particularly in combination (Figure 25). Therefore, an *in vivo* experiment was performed using MOLT4 (MOLT4-Luc). One mouse treated with copanlisib alone showed a very low mean radiant power at 14 days after xenografting compared with the other mice (Figure 35c). It is questionable whether copanlisib treatment reduced cell proliferation in this case or whether proliferation was simply lower because of a rather unsuccessful i.v. injection followed by delayed engraftment. On the same day 14 of measurement, the group of mice treated with the combination showed a significantly lower radiation signal compared with the mice treated with vehicle. However, monitoring after 21 days showed that the radiance values of the combination-treated mice were almost at the same level as those of the vehicle-treated mice. It remains unclear whether continuous treatment would have resulted in better therapeutic success. However, in the combination treatment and vehicle groups, mice did not survive to the next day of measurement on day 28. In each of the remaining treatment groups (copanlisib and JQ1 alone treatment), one mouse survived to the next monitoring on day 28 after xenografting. Strikingly, one mouse in the copanlisib-treated group showed significantly less radiation than that treated with JQ1 alone. However, because the number of animals at day 28 was too small, statistics could not be obtained. All remaining mice had to be sacrificed in the following days due to reaching the termination criteria. Examination of the IVIS images (Figure 35b) revealed that most mice had one or two bioluminescence "hot spots" in the abdominal region. This was found to be cell invasion in the ovaries causing aggressive ovarian cancer. Nevertheless, this appeared irregularly, and in some cases, involvement of the ovaries was not observed. The infiltration of the ovaries is rarely associated with leukemias [213] and therefore uncommon for T-ALL, which presented a problem for using the MOLT4 cell line for further *in vivo* experiments, since the process of leukemia is significantly affected by the infiltration of the ovaries. To validate the therapeutic success of copanlisib and JQ1 further experiments with

higher animal number and longer treatment schedule with an alternative T-ALL cell model must be considered.

#### **4.5. *In vivo* validation of afuresertib and birabresib**

The combination of AKT inhibitor afuresertib and the BRD4 inhibitor birabresib was tested *in vivo*, due to their promising *in vitro* results. Both compounds are of clinical relevance since both entered at least the clinical phase 1. To counteract the low number of mice in the previous *in vivo* experiment, it was decided to use five mice per treatment group. In addition, a treatment interval of 5 times per week was chosen and the induction time was set at four days after xenotransplantation. To avoid the involvement of the ovaries as happened in MOLT4, a different PTEN<sup>mut</sup> cell line was selected that does not affect the ovaries (HPBALL). However, none of the treatment group achieved therapeutic success in controlling T-ALL (Figure 36). On the contrary, gastrointestinal toxicities were mentioned when afuresertib was applied orally. Gastrointestinal toxicities are not uncommon and an emerging problem in targeted therapies that can cause mild to severe side effects observed patients [214]. Especially in the case of PI3K/AKT inhibitors gastrointestinal toxicities are often reported leading to stomatitis or diarrhea [215, 216]. To circumvent such problems in future, the method of application must be considered very well. The relatively simple delivery of drugs via oral gavage or i.p. injections is offset by an increased likelihood of gastrointestinal toxicity [217, 218]. The method of i.v. injection provides nearly 100% bioactivity [219], which is particularly beneficial in blood disorders such as leukemia and is preferred over other treatment methods for further *in vivo* treatments.

#### **4.6. Biological validation of novel dual HDAC/BRD4 inhibitors demonstrated high activity in MYC dependent cell lines**

The first set of novel inhibitors validated in this work were dual HDAC/BRD4 targeting inhibitors, which seems a promising strategy since both targets, HDAC and BRD4, are correlated [220]. Thus, HDACs control the degree of acetylation of lysine residues on histone tails, thereby shaping the acetylation profile of the genome, while BET proteins read the histone acetylation code, facilitating the activation of specific target genes [221, 222].

Using XD14 as the basis for the BRD4 pharmacophore and the pharmacophores of several established HDAC inhibitors such as vorinostat, panobinostat and resminostat as a starting point. With regard to MYC, BRD4 is an important target because it plays a crucial role in mediating MYC transcription [96]. XD14 is a similar compound to birabresib and JQ1, discussed above with a slight difference in their chemical structure. Unlike birabresib and JQ1 that share the same triazobenzodiazepine scaffold, XD14 contains a 4-acylpyrrole scaffold. However, both compound groups share similar binding effectivities to BRD4 and are therefore ideally suited as BRD4 inhibitors. Inhibition of HDAC molecules became interesting, because HDACs are epigenetic regulators and were found to be overexpressed in different cancer types [223, 224]. Accordingly, inhibition of HDACs can result in anti-cancer effect [224-227]. In the context of MYC, it was found that HDACs have a large influence on the function of MYC and an inhibition of HDACs by vorinostat result in a reduced acetylation of MYC at site K323 and subsequently to a reduction of MYC protein in AML patients [140]. The combination of both inhibitors is therefore a good strategy to effectively downregulate MYC along two different axes [150].

The first discussed compound 61, which is basically a hybrid of XD14 and vorinostat exposed the most balanced inhibition of BET and HDAC inhibition (Figure 38). Interestingly, when combining both closely related compounds 62 and 63 that either are inactivated on the BRD4 specific pharmacophore or HDAC, respectively, the effectivity of the single dual inhibitor 61 could not be reached (Figure 38). These results demonstrate the beneficial effects of using a dual inhibitor instead of two single compounds simultaneously in the case when targets are molecularly close to each other, as it is true with BET and HDAC proteins. However, the greatest cytotoxic effect was achieved by inhibitor 49 based on XD14 and resminostat. In different leukemia entities  $IC_{50}$  values in a low micromolar range was reached (Table 29). More important, 49 showed in apoptosis assays better effectivity than the reference inhibitors birabresib and ricolinostat and the 1:1 combination of both in AML and T-ALL cell lines (Figure 39a and 40b). Although compound 61 was the most balanced dual inhibitor, the results of inhibitor 49 showed a significantly higher potency in killing the tested leukemia cell lines. This is probably since compound 49 has a higher target activity towards HDACs compared to inhibitor 61 ( $IC_{50}$  [ $\mu$ M] 0.09 vs. 0.16 for HDAC1 and 0.05 vs. 0.07 for HDAC6) and thus has an optimal activity distribution to effectively kill tumor cells, even

though the potency against BRD4 was measured to be ten times lower in 49 compared to 61 ( $IC_{50}$  [ $\mu$ M] 0.79 vs. 0.08) (Table 29). In addition, the high potency of decreasing MYC was demonstrated by WB with these dual inhibitors, highlighting the successful approach of tackling two different MYC axes by one single compound (Figure 39b).

#### **4.7. Development of novel CTD-HSP90 inhibitors**

The secondly experimental compounds presented were novel small molecules that target the CTD of HSP90 based on the previously published peptidomimetic AX that successfully targeted the CDT of HSP90 [159]. HSP90 inhibition has received much attention in the field of cancer treatment in recent years, as MYC is known to be a bona fide client of, and thus highly dependent on, the chaperone activity of HSP90, making it a rational target for MYC-dependent leukemias in particular [228]. Recently, there have been some reports that HSP90 inhibitors can cause serious side effects. For example, AUY922 caused night blindness in 20% of patients and about 7% developed third-degree eye damage [155, 229]. AUY922 is like many other first developed HSP90 inhibitors tackling the N-Terminal domain (NTD), which is known to drive the heat shock response (HSR), which can ultimately be the reason for the currently reported fails in clinical trials [230, 231]. Interestingly, silencing HSR proteins like HSF-1, HSP70 and HSP27 resulted in increased cytotoxicity in malignant cancers, suggesting that the increase of the HSR mediated thorough NTD HSP90 inhibitors may induce a contrary effect leading to an escape mechanism of the cells [232-234]. The inhibition of the CTD of HSP90 though, has been reported to be cytotoxic against malignant cells without inducing HSR [158, 235, 236].

The HSP90 inhibitors addressed in this work target a specific region of the HSP90 protein, specifically the one responsible for heterodimerization. The disruption of both HSP90 monomers causes a loss of function of the protein without initiating an HSR, which was already demonstrated with a peptidomimetic inhibitor in a recent publication [159]. Although the peptidomimetic  $\alpha$ -aminoxy hexapeptide AX showed high potency in *in vitro* cell experiments and in a preclinical mouse model the molecule is too big to find its way in clinical use [159]. Therefore, smaller molecules based on the chemical structure of AX were synthesized and tested in preliminary *in vitro* experiments. The first generation of small inhibitors Exp101 and Exp102 were tested in a drug screen for its killing effectivity in different leukemia models (Figure 42a). Although the compound



Exp102 inhibited the cell growth in most of the cases with an IC<sub>50</sub> value between 4 and 12 µM, the small molecule still cannot compete the precursor AX. However, the investigation of the function confirmed an apoptosis inducing effect, which was by far more effective than the reference inhibitor for CTD-HSP90 targeting novobiocin (Figure 42b). Using target assessment by WB of cells treated with the compounds and reference inhibitors, HSR was not reported in the experimental compounds but with the reference NTD-HSP90 inhibitor AUY922 (Figure 42d). To reach a higher effectivity of the new small molecules the second generation was synthesized based on Exp102, with different modifications. Both compounds showed improved effectivity, with Exp202 as the most effective one in different leukemia types with even improved growth reduction compared to AX (Figure 43). Exp202 even competed the following generation of inhibitors, which were slightly weaker in cytotoxicity (Exp301, Exp302) or on the same level (Exp303) through different cancer entities (Figure 44a). This successful biological validation enables further investigation of the small molecules in preclinical animal models. However, this would require pharmacokinetic analyses to find a suitable method of administration (oral, intraperitoneal, or intravenous). It would also be necessary to investigate how the half-life of the active ingredients behaves in the body of the animals and whether damage to the organs occurs. These active ingredients could be a particularly effective treatment against highly resistant leukemias.

## 5. Outlook

This thesis focused on the oncoprotein MYC as a potential target for a novel therapeutic approach to treat refractory and relapsed T-ALL. As a result of the characterization of the cell lines, a correlation of the absence of the tumor suppressor PTEN with an increase in MYC protein was found. To validate the association between PTEN mutation and increased MYC in patients, a larger patient cohort needs to be analyzed. Furthermore, the loss of PTEN was associated with increased resistance to the frontline chemotherapeutic agent dexamethasone. Genetic analyses of different cell lines showed increased expression of the efflux-transport molecule ABCA5 in the absence of the tumor suppressor PTEN. The role of ABCA5 in resistance mechanisms is poorly understood to date. Further analyses, such as the use of shRNA or CRISP/Cas9 to silence the expression of ABCA5, could provide important insights in possible resistance mechanism. Specifically, one approach could be to downregulate the expression of ABCA5 in a dexamethasone-resistant cell line (e.g., HPBALL) and then use drug screening to determine whether altered sensitivity is now present.

The following results of the high throughput drug screening showed that PTEN mutated cell lines and patient leukemia cells were correlated with an increased response against PI3K/AKT targeting substances. These results underline the potential of PTEN mutations that can be used as stratification markers for future targeted therapy approaches. Therefore, novel PI3K/AKT targeting substances can be frequently examined to screen consistently for more effective compounds. The genetic correlation between PTEN mutations and the susceptibility against PI3K/AKT pathway inhibition could be finally validated with shRNA for AKT or PI3K for example to circumvent possible off-target effects emerging from the inhibitors that have been used. In addition, synergism between PI3K/AKT inhibitors and other signaling pathways related to MYC should continue to be investigated, as it has been done in this work with BRD4, the Raf/MEK/ERK pathway, and Aurora kinases. Possible examples would be the subsequent inhibition of the HDAC proteins or the HSP90 protein, as in both cases it was indicated that the respective inhibition has a reducing effect on MYC.

Although the *in vivo* efficacy of the PI3K/AKT inhibitors copanlisib and afuresertib could not be confirmed in this work, further experimental approaches especially with the compound copanlisib should be considered. Because copanlisib is available

intravenously, it is an excellent antileukemic agent since biological activity is immediately ensured in the bloodstream. More frequent and earlier intravenous applications are recommended for subsequent *in vivo* studies. If the efficacy of a PI3K/AKT pathway inhibitor is successful in a xenograft mouse model using a cell line model, the next step would be to validate it in a xenograft mouse model using primary patient (PDX) cells. In case the results of the PDX mouse model with a PI3K/AKT inhibitor are also promising, stratification of PTEN mutations should be considered for future therapeutic approaches of refractory and relapsed T-ALL in the clinic.

A second possible stratification marker in T-ALL could be the hyperphosphorylation of MEK, which probably results from mutations in the Raf/MEK/ERK pathway, as it was the case in the cell lines DND41 and HSB2. The presence of mutations in the Raf/MEK/ERK signaling pathway thus resulting in a MEK hyperphosphorylation should be validated further in T-ALL patient samples. The relationship between MEK hyperphosphorylation and increased sensitivity to MEK inhibitors must be validated. Subsequently, the *in vitro* validated combination of MEK and PI3K inhibitors must be evaluated in an *in vivo* model.

With regard to highly expressing MYC cell lines and patient cells, the use of Aurora kinase inhibitors should also be considered for testing in preclinical T-ALL mouse models. Since the combination of PI3K inhibition with AURKA inhibition showed promising effectivity in PTEN<sup>mut</sup> and high MYC expressing cell lines *in vitro*, this combination should be tested *in vivo* as well.

The experimental MYC inhibitors addressed in this work, the dual BRD4/HDAC and HSP90-CTD inhibitors would need to be prepared for *in vivo* experiments as a next step. Pharmacodynamic experiments in mice could provide information on how the compounds are absorbed in the body and which application method is best suited for each compound. In addition, the toxicity of the compounds and the duration of action must be determined. If these questions are answered, there will be no further obstacles to the *in vivo* validation of the experimental compounds.

## 6. Literature

1. *Childhood Acute Lymphoblastic Leukemia Treatment (PDQ(R)): Health Professional Version*, in *PDQ Cancer Information Summaries*. 2002: Bethesda (MD).
2. Birbrair, A. and P.S. Frenette, *Niche heterogeneity in the bone marrow*. *Ann N Y Acad Sci*, 2016. **1370**(1): p. 82-96.
3. Sawyers, C.L., C.T. Denny, and O.N. Witte, *Leukemia and the disruption of normal hematopoiesis*. *Cell*, 1991. **64**(2): p. 337-50.
4. Laval, G. and A.J. Tuyns, *Environmental factors in childhood leukaemia*. *Br J Ind Med*, 1988. **45**(12): p. 843-4.
5. Ramos, O.F., E.C. Moron, and R. De Castro Arenas, *Platelet function abnormalities in acute leukaemia*. *Haematologia (Budap)*, 1981. **14**(4): p. 383-91.
6. Khan, M., R. Siddiqi, and K. Naqvi, *An update on classification, genetics, and clinical approach to mixed phenotype acute leukemia (MPAL)*. *Ann Hematol*, 2018. **97**(6): p. 945-953.
7. Coebergh, J.W., et al., *Leukaemia incidence and survival in children and adolescents in Europe during 1978-1997. Report from the Automated Childhood Cancer Information System project*. *Eur J Cancer*, 2006. **42**(13): p. 2019-36.
8. Parkin, D.M., *The global burden of cancer*. *Semin Cancer Biol*, 1998. **8**(4): p. 219-35.
9. Dores, G.M., et al., *Acute leukemia incidence and patient survival among children and adults in the United States, 2001-2007*. *Blood*, 2012. **119**(1): p. 34-43.
10. Conter, V., et al., *Early T-cell precursor acute lymphoblastic leukaemia in children treated in AIEOP centres with AIEOP-BFM protocols: a retrospective analysis*. *Lancet Haematol*, 2016. **3**(2): p. e80-6.
11. Goldberg, J.M., et al., *Childhood T-cell acute lymphoblastic leukemia: the Dana-Farber Cancer Institute acute lymphoblastic leukemia consortium experience*. *J Clin Oncol*, 2003. **21**(19): p. 3616-22.
12. Einsiedel, H.G., et al., *Long-term outcome in children with relapsed ALL by risk-stratified salvage therapy: results of trial acute lymphoblastic leukemia-relapse study of the Berlin-Frankfurt-Munster Group 87*. *J Clin Oncol*, 2005. **23**(31): p. 7942-50.
13. Reismuller, B., et al., *Long-term outcome of initially homogeneously treated and relapsed childhood acute lymphoblastic leukaemia in Austria--a population-based report of the Austrian Berlin-Frankfurt-Munster (BFM) Study Group*. *Br J Haematol*, 2009. **144**(4): p. 559-70.
14. Bernbeck, B., et al., *Symptoms of childhood acute lymphoblastic leukemia: red flags to recognize leukemia in daily practice*. *Klin Padiatr*, 2009. **221**(6): p. 369-73.
15. Grover, S.A., A.N. Barkun, and D.L. Sackett, *The rational clinical examination. Does this patient have splenomegaly?* *JAMA*, 1993. **270**(18): p. 2218-21.
16. Antony, R., D. Roebuck, and I.M. Hann, *Unusual presentations of acute lymphoid malignancy in children*. *J R Soc Med*, 2004. **97**(3): p. 125-7.
17. Jones, O.Y., et al., *A multicenter case-control study on predictive factors distinguishing childhood leukemia from juvenile rheumatoid arthritis*. *Pediatrics*, 2006. **117**(5): p. e840-4.
18. Pui, C.H. and S.C. Howard, *Current management and challenges of malignant disease in the CNS in paediatric leukaemia*. *Lancet Oncol*, 2008. **9**(3): p. 257-68.
19. Cannon, J.L., S.R. Oruganti, and D.W. Vidrine, *Molecular regulation of T-ALL cell infiltration into the CNS*. *Oncotarget*, 2017. **8**(49): p. 84626-84627.
20. Pui, C.H. and E. Thiel, *Central nervous system disease in hematologic malignancies: historical perspective and practical applications*. *Semin Oncol*, 2009. **36**(4 Suppl 2): p. S2-S16.
21. Pui, C.H. and W.E. Evans, *Treatment of acute lymphoblastic leukemia*. *N Engl J Med*, 2006. **354**(2): p. 166-78.
22. Buonamici, S., et al., *CCR7 signalling as an essential regulator of CNS infiltration in T-cell leukaemia*. *Nature*, 2009. **459**(7249): p. 1000-4.

23. Borowitz, M.J., *Mixed phenotype acute leukemia*. Cytometry B Clin Cytom, 2014. **86**(3): p. 152-3.
24. Koch, U. and F. Radtke, *Mechanisms of T cell development and transformation*. Annu Rev Cell Dev Biol, 2011. **27**: p. 539-62.
25. Han, H., et al., *Inducible gene knockout of transcription factor recombination signal binding protein-J reveals its essential role in T versus B lineage decision*. Int Immunol, 2002. **14**(6): p. 637-45.
26. Ciofani, M. and J.C. Zuniga-Pflucker, *Notch promotes survival of pre-T cells at the beta-selection checkpoint by regulating cellular metabolism*. Nat Immunol, 2005. **6**(9): p. 881-8.
27. Larmonie, N.S., et al., *Breakpoint sites disclose the role of the V(D)J recombination machinery in the formation of T-cell receptor (TCR) and non-TCR associated aberrations in T-cell acute lymphoblastic leukemia*. Haematologica, 2013. **98**(8): p. 1173-84.
28. Klein, L., et al., *Antigen presentation in the thymus for positive selection and central tolerance induction*. Nat Rev Immunol, 2009. **9**(12): p. 833-44.
29. Farber, D.L., N.A. Yudanin, and N.P. Restifo, *Human memory T cells: generation, compartmentalization and homeostasis*. Nat Rev Immunol, 2014. **14**(1): p. 24-35.
30. Michael Litt, B.P., Ying Li, Yi Qiu and Suming Huang, *Molecular Morphogenesis of T-Cell Acute Leukemia*. IntechOpen, 2012.
31. Bene, M.C., et al., *Proposals for the immunological classification of acute leukemias. European Group for the Immunological Characterization of Leukemias (EGIL)*. Leukemia, 1995. **9**(10): p. 1783-6.
32. Gokbuget, N., et al., *Adult patients with acute lymphoblastic leukemia and molecular failure display a poor prognosis and are candidates for stem cell transplantation and targeted therapies*. Blood, 2012. **120**(9): p. 1868-76.
33. Burger, R., et al., *Heterogeneity of T-acute lymphoblastic leukemia (T-ALL) cell lines: suggestion for classification by immunophenotype and T-cell receptor studies*. Leuk Res, 1999. **23**(1): p. 19-27.
34. van Grotel, M., et al., *Prognostic significance of molecular-cytogenetic abnormalities in pediatric T-ALL is not explained by immunophenotypic differences*. Leukemia, 2008. **22**(1): p. 124-31.
35. Niehues, T., et al., *A classification based on T cell selection-related phenotypes identifies a subgroup of childhood T-ALL with favorable outcome in the COALL studies*. Leukemia, 1999. **13**(4): p. 614-7.
36. Follini, E., M. Marchesini, and G. Roti, *Strategies to Overcome Resistance Mechanisms in T-Cell Acute Lymphoblastic Leukemia*. Int J Mol Sci, 2019. **20**(12).
37. Brammer, J.E., et al., *Multi-center analysis of the effect of T-cell acute lymphoblastic leukemia subtype and minimal residual disease on allogeneic stem cell transplantation outcomes*. Bone Marrow Transplant, 2017. **52**(1): p. 20-27.
38. Borowitz, M.J., et al., *Clinical significance of minimal residual disease in childhood acute lymphoblastic leukemia and its relationship to other prognostic factors: a Children's Oncology Group study*. Blood, 2008. **111**(12): p. 5477-85.
39. Ma, M., et al., *Early T-cell precursor leukemia: a subtype of high risk childhood acute lymphoblastic leukemia*. Front Med, 2012. **6**(4): p. 416-20.
40. Jain, N., et al., *Early T-cell precursor acute lymphoblastic leukemia/lymphoma (ETP-ALL/LBL) in adolescents and adults: a high-risk subtype*. Blood, 2016. **127**(15): p. 1863-9.
41. Zhang, J., et al., *The genetic basis of early T-cell precursor acute lymphoblastic leukaemia*. Nature, 2012. **481**(7380): p. 157-63.
42. Coustan-Smith, E., et al., *Minimal disseminated disease in childhood T-cell lymphoblastic lymphoma: a report from the children's oncology group*. J Clin Oncol, 2009. **27**(21): p. 3533-9.

43. Inukai, T., et al., *Clinical significance of early T-cell precursor acute lymphoblastic leukaemia: results of the Tokyo Children's Cancer Study Group Study L99-15*. Br J Haematol, 2012. **156**(3): p. 358-65.
44. Moricke, A., et al., *Dexamethasone vs prednisone in induction treatment of pediatric ALL: results of the randomized trial AIEOP-BFM ALL 2000*. Blood, 2016. **127**(17): p. 2101-12.
45. Teuffel, O., et al., *Dexamethasone versus prednisone for induction therapy in childhood acute lymphoblastic leukemia: a systematic review and meta-analysis*. Leukemia, 2011. **25**(8): p. 1232-8.
46. Simone, J.V., *History of the treatment of childhood ALL: a paradigm for cancer cure*. Best Pract Res Clin Haematol, 2006. **19**(2): p. 353-9.
47. Waber, D.P., et al., *Neuropsychological outcomes of a randomized trial of prednisone versus dexamethasone in acute lymphoblastic leukemia: findings from Dana-Farber Cancer Institute All Consortium Protocol 00-01*. Pediatr Blood Cancer, 2013. **60**(11): p. 1785-91.
48. Pui, C.H., et al., *Pediatric acute lymphoblastic leukemia: where are we going and how do we get there?* Blood, 2012. **120**(6): p. 1165-74.
49. Asselin, B.L., et al., *Effectiveness of high-dose methotrexate in T-cell lymphoblastic leukemia and advanced-stage lymphoblastic lymphoma: a randomized study by the Children's Oncology Group (POG 9404)*. Blood, 2011. **118**(4): p. 874-83.
50. Gokbuget, N., et al., *High single-drug activity of nelarabine in relapsed T-lymphoblastic leukemia/lymphoma offers curative option with subsequent stem cell transplantation*. Blood, 2011. **118**(13): p. 3504-11.
51. Berg, S.L., et al., *Phase II study of nelarabine (compound 506U78) in children and young adults with refractory T-cell malignancies: a report from the Children's Oncology Group*. J Clin Oncol, 2005. **23**(15): p. 3376-82.
52. Gollard, R.P. and S. Selco, *Irreversible myelopathy associated with nelarabine in T-cell acute lymphoblastic leukemia*. J Clin Oncol, 2013. **31**(19): p. e327-31.
53. Kawakami, M., et al., *Irreversible neurological defects in the lower extremities after haploidentical stem cell transplantation: possible association with nelarabine*. Am J Hematol, 2013. **88**(10): p. 853-7.
54. Drynan, L.F., T.L. Hamilton, and T.H. Rabbitts, *T cell tumorigenesis in Lmo2 transgenic mice is independent of V-D-J recombinase activity*. Oncogene, 2001. **20**(32): p. 4412-5.
55. Begley, C.G., et al., *Chromosomal translocation in a human leukemic stem-cell line disrupts the T-cell antigen receptor delta-chain diversity region and results in a previously unreported fusion transcript*. Proc Natl Acad Sci U S A, 1989. **86**(6): p. 2031-5.
56. Xia, Y., et al., *TAL2, a helix-loop-helix gene activated by the (7;9)(q34;q32) translocation in human T-cell leukemia*. Proc Natl Acad Sci U S A, 1991. **88**(24): p. 11416-20.
57. Mellentin, J.D., S.D. Smith, and M.L. Cleary, *lyl-1, a novel gene altered by chromosomal translocation in T cell leukemia, codes for a protein with a helix-loop-helix DNA binding motif*. Cell, 1989. **58**(1): p. 77-83.
58. Bernard, O.A., et al., *A new recurrent and specific cryptic translocation, t(5;14)(q35;q32), is associated with expression of the Hox11L2 gene in T acute lymphoblastic leukemia*. Leukemia, 2001. **15**(10): p. 1495-504.
59. Royer-Pokora, B., U. Loos, and W.D. Ludwig, *TTG-2, a new gene encoding a cysteine-rich protein with the LIM motif, is overexpressed in acute T-cell leukaemia with the t(11;14)(p13;q11)*. Oncogene, 1991. **6**(10): p. 1887-93.
60. McGuire, E.A., et al., *The t(11;14)(p15;q11) in a T-cell acute lymphoblastic leukemia cell line activates multiple transcripts, including Ttg-1, a gene encoding a potential zinc finger protein*. Mol Cell Biol, 1989. **9**(5): p. 2124-32.
61. Draheim, K.M., et al., *A DNA-binding mutant of TAL1 cooperates with LMO2 to cause T cell leukemia in mice*. Oncogene, 2011. **30**(10): p. 1252-60.

62. Palomero, T. and A. Ferrando, *Therapeutic targeting of NOTCH1 signaling in T-cell acute lymphoblastic leukemia*. Clin Lymphoma Myeloma, 2009. **9 Suppl 3**: p. S205-10.
63. Jundt, F., R. Schwarzer, and B. Dorken, *Notch signaling in leukemias and lymphomas*. Curr Mol Med, 2008. **8**(1): p. 51-9.
64. Demarest, R.M., F. Ratti, and A.J. Capobianco, *It's T-ALL about Notch*. Oncogene, 2008. **27**(38): p. 5082-91.
65. Lin, C., et al., *Mutations increased overexpression of Notch1 in T-cell acute lymphoblastic leukemia*. Cancer Cell Int, 2012. **12**: p. 13.
66. Ferrando, A., *NOTCH mutations as prognostic markers in T-ALL*. Leukemia, 2010. **24**(12): p. 2003-4.
67. Weng, A.P., et al., *Activating mutations of NOTCH1 in human T cell acute lymphoblastic leukemia*. Science, 2004. **306**(5694): p. 269-71.
68. Sandy, A.R. and I. Maillard, *Notch signaling in the hematopoietic system*. Expert Opin Biol Ther, 2009. **9**(11): p. 1383-98.
69. Zou, J., et al., *Notch1 is required for hypoxia-induced proliferation, invasion and chemoresistance of T-cell acute lymphoblastic leukemia cells*. J Hematol Oncol, 2013. **6**: p. 3.
70. Jenkinson, S., et al., *Impact of NOTCH1/FBXW7 mutations on outcome in pediatric T-cell acute lymphoblastic leukemia patients treated on the MRC UKALL 2003 trial*. Leukemia, 2013. **27**(1): p. 41-7.
71. Breit, S., et al., *Activating NOTCH1 mutations predict favorable early treatment response and long-term outcome in childhood precursor T-cell lymphoblastic leukemia*. Blood, 2006. **108**(4): p. 1151-7.
72. Sanchez-Martin, M. and A. Ferrando, *The NOTCH1-MYC highway toward T-cell acute lymphoblastic leukemia*. Blood, 2017. **129**(9): p. 1124-1133.
73. Weng, A.P., et al., *c-Myc is an important direct target of Notch1 in T-cell acute lymphoblastic leukemia/lymphoma*. Genes Dev, 2006. **20**(15): p. 2096-109.
74. Hecht, J.L. and J.C. Aster, *Molecular biology of Burkitt's lymphoma*. J Clin Oncol, 2000. **18**(21): p. 3707-21.
75. Adhikary, S. and M. Eilers, *Transcriptional regulation and transformation by Myc proteins*. Nat Rev Mol Cell Biol, 2005. **6**(8): p. 635-45.
76. Pelengaris, S., M. Khan, and G. Evan, *c-MYC: more than just a matter of life and death*. Nat Rev Cancer, 2002. **2**(10): p. 764-76.
77. Meyer, N. and L.Z. Penn, *Reflecting on 25 years with MYC*. Nat Rev Cancer, 2008. **8**(12): p. 976-90.
78. Dang, C.V., *MYC on the path to cancer*. Cell, 2012. **149**(1): p. 22-35.
79. Fernandez, P.C., et al., *Genomic targets of the human c-Myc protein*. Genes Dev, 2003. **17**(9): p. 1115-29.
80. Kim, J., J.H. Lee, and V.R. Iyer, *Global identification of Myc target genes reveals its direct role in mitochondrial biogenesis and its E-box usage in vivo*. PLoS One, 2008. **3**(3): p. e1798.
81. Hurlin, P.J. and S. Dezfouli, *Functions of myc:max in the control of cell proliferation and tumorigenesis*. Int Rev Cytol, 2004. **238**: p. 183-226.
82. Bretones, G., M.D. Delgado, and J. Leon, *Myc and cell cycle control*. Biochim Biophys Acta, 2015. **1849**(5): p. 506-16.
83. Mannava, S., et al., *Direct role of nucleotide metabolism in C-MYC-dependent proliferation of melanoma cells*. Cell Cycle, 2008. **7**(15): p. 2392-400.
84. McMahon, S.B., *MYC and the control of apoptosis*. Cold Spring Harb Perspect Med, 2014. **4**(7): p. a014407.
85. Roderick, J.E., et al., *c-Myc inhibition prevents leukemia initiation in mice and impairs the growth of relapsed and induction failure pediatric T-ALL cells*. Blood, 2014. **123**(7): p. 1040-50.
86. Chen, H., H. Liu, and G. Qing, *Targeting oncogenic Myc as a strategy for cancer treatment*. Signal Transduct Target Ther, 2018. **3**: p. 5.

87. La Starza, R., et al., *Genetic profile of T-cell acute lymphoblastic leukemias with MYC translocations*. *Blood*, 2014. **124**(24): p. 3577-82.
88. Dose, M., et al., *c-Myc mediates pre-TCR-induced proliferation but not developmental progression*. *Blood*, 2006. **108**(8): p. 2669-77.
89. Zhang, Y., et al., [*Significance of C-myc expression in T-lymphoblastic lymphoma/leukemia and its relation with prognosis*]. *Zhonghua Bing Li Xue Za Zhi*, 2015. **44**(8): p. 571-7.
90. Erikson, J., et al., *Deregulation of c-myc by translocation of the alpha-locus of the T-cell receptor in T-cell leukemias*. *Science*, 1986. **232**(4752): p. 884-6.
91. Carabet, L.A., P.S. Rennie, and A. Cherkasov, *Therapeutic Inhibition of Myc in Cancer. Structural Bases and Computer-Aided Drug Discovery Approaches*. *Int J Mol Sci*, 2018. **20**(1).
92. Palomero, T., et al., *NOTCH1 directly regulates c-MYC and activates a feed-forward-loop transcriptional network promoting leukemic cell growth*. *Proc Natl Acad Sci U S A*, 2006. **103**(48): p. 18261-6.
93. Bonnet, M., et al., *Posttranscriptional deregulation of MYC via PTEN constitutes a major alternative pathway of MYC activation in T-cell acute lymphoblastic leukemia*. *Blood*, 2011. **117**(24): p. 6650-9.
94. King, B., et al., *The ubiquitin ligase FBXW7 modulates leukemia-initiating cell activity by regulating MYC stability*. *Cell*, 2013. **153**(7): p. 1552-66.
95. DeAngelo, D.J., et al., *Phase 1 clinical results with tandutinib (MLN518), a novel FLT3 antagonist, in patients with acute myelogenous leukemia or high-risk myelodysplastic syndrome: safety, pharmacokinetics, and pharmacodynamics*. *Blood*, 2006. **108**(12): p. 3674-81.
96. Delmore, J.E., et al., *BET bromodomain inhibition as a therapeutic strategy to target c-Myc*. *Cell*, 2011. **146**(6): p. 904-17.
97. Filippakopoulos, P., et al., *Selective inhibition of BET bromodomains*. *Nature*, 2010. **468**(7327): p. 1067-73.
98. Doroshow, D.B., J.P. Eder, and P.M. LoRusso, *BET inhibitors: a novel epigenetic approach*. *Ann Oncol*, 2017. **28**(8): p. 1776-1787.
99. Kharenko, O.A. and H.C. Hansen, *Novel approaches to targeting BRD4*. *Drug Discov Today Technol*, 2017. **24**: p. 19-24.
100. He, T.C., et al., *Identification of c-MYC as a target of the APC pathway*. *Science*, 1998. **281**(5382): p. 1509-12.
101. Sharma, V.M., et al., *Notch1 contributes to mouse T-cell leukemia by directly inducing the expression of c-myc*. *Mol Cell Biol*, 2006. **26**(21): p. 8022-31.
102. Dar, A.A., A. Belkhiri, and W. El-Rifai, *The aurora kinase A regulates GSK-3beta in gastric cancer cells*. *Oncogene*, 2009. **28**(6): p. 866-75.
103. Cross, D.A., et al., *Inhibition of glycogen synthase kinase-3 by insulin mediated by protein kinase B*. *Nature*, 1995. **378**(6559): p. 785-9.
104. Bachireddy, P., P.K. Bendapudi, and D.W. Felsher, *Getting at MYC through RAS*. *Clin Cancer Res*, 2005. **11**(12): p. 4278-81.
105. Davis, R.J., M. Welcker, and B.E. Clurman, *Tumor suppression by the Fbw7 ubiquitin ligase: mechanisms and opportunities*. *Cancer Cell*, 2014. **26**(4): p. 455-64.
106. Remke, M., et al., *High-resolution genomic profiling of childhood T-ALL reveals frequent copy-number alterations affecting the TGF-beta and PI3K-AKT pathways and deletions at 6q15-16.1 as a genomic marker for unfavorable early treatment response*. *Blood*, 2009. **114**(5): p. 1053-62.
107. Liu, Y., et al., *The genomic landscape of pediatric and young adult T-lineage acute lymphoblastic leukemia*. *Nat Genet*, 2017. **49**(8): p. 1211-1218.
108. Palomero, T., et al., *Mutational loss of PTEN induces resistance to NOTCH1 inhibition in T-cell leukemia*. *Nat Med*, 2007. **13**(10): p. 1203-10.
109. Mullighan, C.G., et al., *Genome-wide analysis of genetic alterations in acute lymphoblastic leukaemia*. *Nature*, 2007. **446**(7137): p. 758-64.



110. Szarzynska-Zawadzka, B., et al., *PTEN abnormalities predict poor outcome in children with T-cell acute lymphoblastic leukemia treated according to ALL IC-BFM protocols*. Am J Hematol, 2019. **94**(4): p. E93-E96.
111. Paganin, M., et al., *The presence of mutated and deleted PTEN is associated with an increased risk of relapse in childhood T cell acute lymphoblastic leukaemia treated with AIEOP-BFM ALL protocols*. Br J Haematol, 2018. **182**(5): p. 705-711.
112. Jotta, P.Y., et al., *Negative prognostic impact of PTEN mutation in pediatric T-cell acute lymphoblastic leukemia*. Leukemia, 2010. **24**(1): p. 239-42.
113. Zuurbier, L., et al., *The significance of PTEN and AKT aberrations in pediatric T-cell acute lymphoblastic leukemia*. Haematologica, 2012. **97**(9): p. 1405-13.
114. Mendes, R.D., et al., *The relevance of PTEN-AKT in relation to NOTCH1-directed treatment strategies in T-cell acute lymphoblastic leukemia*. Haematologica, 2016. **101**(9): p. 1010-7.
115. Paganin, M. and A. Ferrando, *Molecular pathogenesis and targeted therapies for NOTCH1-induced T-cell acute lymphoblastic leukemia*. Blood Rev, 2011. **25**(2): p. 83-90.
116. Fruman, D.A., et al., *The PI3K Pathway in Human Disease*. Cell, 2017. **170**(4): p. 605-635.
117. Gregory, M.A., Y. Qi, and S.R. Hann, *Phosphorylation by glycogen synthase kinase-3 controls c-myc proteolysis and subnuclear localization*. J Biol Chem, 2003. **278**(51): p. 51606-12.
118. Martelli, A.M., et al., *The Key Roles of PTEN in T-Cell Acute Lymphoblastic Leukemia Development, Progression, and Therapeutic Response*. Cancers (Basel), 2019. **11**(5).
119. Wang, X., et al., *Phosphorylation regulates c-Myc's oncogenic activity in the mammary gland*. Cancer Res, 2011. **71**(3): p. 925-36.
120. Arnold, H.K. and R.C. Sears, *Protein phosphatase 2A regulatory subunit B56alpha associates with c-myc and negatively regulates c-myc accumulation*. Mol Cell Biol, 2006. **26**(7): p. 2832-44.
121. Welcker, M., et al., *The Fbw7 tumor suppressor regulates glycogen synthase kinase 3 phosphorylation-dependent c-Myc protein degradation*. Proc Natl Acad Sci U S A, 2004. **101**(24): p. 9085-90.
122. Yada, M., et al., *Phosphorylation-dependent degradation of c-Myc is mediated by the F-box protein Fbw7*. EMBO J, 2004. **23**(10): p. 2116-25.
123. Sears, R., et al., *Ras enhances Myc protein stability*. Molecular Cell, 1999. **3**(2): p. 169-179.
124. Sears, R., et al., *Multiple Ras-dependent phosphorylation pathways regulate Myc protein stability*. Genes & Development, 2000. **14**(19): p. 2501-2514.
125. Sears, R.C., *The life cycle of C-myc: from synthesis to degradation*. Cell Cycle, 2004. **3**(9): p. 1133-7.
126. den Hollander, J., et al., *Aurora kinases A and B are up-regulated by Myc and are essential for maintenance of the malignant state*. Blood, 2010. **116**(9): p. 1498.
127. Fathi, A.T., et al., *Phase I study of the aurora A kinase inhibitor alisertib with induction chemotherapy in patients with acute myeloid leukemia*. Haematologica, 2017. **102**(4): p. 719-727.
128. Mahadevan, D., et al., *Alisertib added to rituximab and vincristine is synthetic lethal and potentially curative in mice with aggressive DLBCL co-overexpressing MYC and BCL2*. PLoS One, 2014. **9**(6): p. e95184.
129. Jiang, J., et al., *Direct Phosphorylation and Stabilization of MYC by Aurora B Kinase Promote T-cell Leukemogenesis*. Cancer Cell, 2020. **37**(2): p. 200-215 e5.
130. Seto, E. and M. Yoshida, *Erasers of histone acetylation: the histone deacetylase enzymes*. Cold Spring Harb Perspect Biol, 2014. **6**(4): p. a018713.
131. Sarkar, R., et al., *Histone deacetylase 3 (HDAC3) inhibitors as anticancer agents: A review*. Eur J Med Chem, 2020. **192**: p. 112171.

132. Fullgrabe, J., E. Kavanagh, and B. Joseph, *Histone onco-modifications*. *Oncogene*, 2011. **30**(31): p. 3391-403.
133. Ropero, S. and M. Esteller, *The role of histone deacetylases (HDACs) in human cancer*. *Mol Oncol*, 2007. **1**(1): p. 19-25.
134. Altucci, L., et al., *Acute myeloid leukemia: therapeutic impact of epigenetic drugs*. *Int J Biochem Cell Biol*, 2005. **37**(9): p. 1752-62.
135. Insinga, A., et al., *Inhibitors of histone deacetylases induce tumor-selective apoptosis through activation of the death receptor pathway*. *Nat Med*, 2005. **11**(1): p. 71-6.
136. Nebbioso, A., et al., *Tumor-selective action of HDAC inhibitors involves TRAIL induction in acute myeloid leukemia cells*. *Nat Med*, 2005. **11**(1): p. 77-84.
137. Jelinkova, I., et al., *Platinum(IV) complex LA-12 exerts higher ability than cisplatin to enhance TRAIL-induced cancer cell apoptosis via stimulation of mitochondrial pathway*. *Biochem Pharmacol*, 2014. **92**(3): p. 415-24.
138. Vjetrovic, J., et al., *Senescence-secreted factors activate Myc and sensitize pretransformed cells to TRAIL-induced apoptosis*. *Aging Cell*, 2014. **13**(3): p. 487-96.
139. Zhu, X., et al., *Cisplatin-mediated c-myc overexpression and cytochrome c (cyt c) release result in the up-regulation of the death receptors DR4 and DR5 and the activation of caspase 3 and caspase 9, likely responsible for the TRAIL-sensitizing effect of cisplatin*. *Med Oncol*, 2015. **32**(4): p. 133.
140. Nebbioso, A., et al., *c-Myc Modulation and Acetylation Is a Key HDAC Inhibitor Target in Cancer*. *Clin Cancer Res*, 2017. **23**(10): p. 2542-2555.
141. Juan, L.J., et al., *Histone deacetylases specifically down-regulate p53-dependent gene activation*. *J Biol Chem*, 2000. **275**(27): p. 20436-43.
142. Zhang, H., et al., *Histone deacetylases function as novel potential therapeutic targets for cancer*. *Hepatol Res*, 2017. **47**(2): p. 149-159.
143. Ho, J.S., et al., *p53-Dependent transcriptional repression of c-myc is required for G1 cell cycle arrest*. *Mol Cell Biol*, 2005. **25**(17): p. 7423-31.
144. Ferrante, F., et al., *HDAC3 functions as a positive regulator in Notch signal transduction*. *Nucleic Acids Res*, 2020. **48**(7): p. 3496-3512.
145. Koch, U. and F. Radtke, *Notch in T-ALL: new players in a complex disease*. *Trends Immunol*, 2011. **32**(9): p. 434-42.
146. Chen, J., et al., *Discovery of selective HDAC/BRD4 dual inhibitors as epigenetic probes*. *Eur J Med Chem*, 2020: p. 112868.
147. Cheng, G., et al., *Design, synthesis and biological evaluation of novel indole derivatives as potential HDAC/BRD4 dual inhibitors and anti-leukemia agents*. *Bioorg Chem*, 2019. **84**: p. 410-417.
148. Amemiya, S., et al., *Synthesis and evaluation of novel dual BRD4/HDAC inhibitors*. *Bioorg Med Chem*, 2017. **25**(14): p. 3677-3684.
149. Shao, M., et al., *Structure-based design, synthesis and in vitro antiproliferative effects studies of novel dual BRD4/HDAC inhibitors*. *Bioorg Med Chem Lett*, 2017. **27**(17): p. 4051-4055.
150. Bhadury, J., et al., *BET and HDAC inhibitors induce similar genes and biological effects and synergize to kill in Myc-induced murine lymphoma*. *Proc Natl Acad Sci U S A*, 2014. **111**(26): p. E2721-30.
151. Mishra, V.K., et al., *Histone deacetylase class-I inhibition promotes epithelial gene expression in pancreatic cancer cells in a BRD4- and MYC-dependent manner*. *Nucleic Acids Res*, 2017.
152. Picard, D., *Heat-shock protein 90, a chaperone for folding and regulation*. *Cell Mol Life Sci*, 2002. **59**(10): p. 1640-8.
153. Zhang, H. and F. Burrows, *Targeting multiple signal transduction pathways through inhibition of Hsp90*. *J Mol Med (Berl)*, 2004. **82**(8): p. 488-99.
154. Carystinos, G.D., et al., *Unexpected induction of the human connexin 43 promoter by the ras signaling pathway is mediated by a novel putative promoter sequence*. *Mol Pharmacol*, 2003. **63**(4): p. 821-31.

155. Jhaveri, K., et al., *Heat shock protein 90 inhibitors in the treatment of cancer: current status and future directions*. Expert Opin Investig Drugs, 2014. **23**(5): p. 611-28.
156. Duerfeldt, A.S. and B.S. Blagg, *Hsp90 inhibition: elimination of shock and stress*. Bioorg Med Chem Lett, 2010. **20**(17): p. 4983-7.
157. Eskew, J.D., et al., *Development and characterization of a novel C-terminal inhibitor of Hsp90 in androgen dependent and independent prostate cancer cells*. BMC Cancer, 2011. **11**: p. 468.
158. Koay, Y.C., et al., *Chemically accessible hsp90 inhibitor that does not induce a heat shock response*. ACS Med Chem Lett, 2014. **5**(7): p. 771-6.
159. Bhatia, S., et al., *Targeting HSP90 dimerization via the C terminus is effective in imatinib-resistant CML and lacks the heat shock response*. Blood, 2018. **132**(3): p. 307-320.
160. Abel, T., et al., *Specific gene delivery to liver sinusoidal and artery endothelial cells*. Blood, 2013. **122**(12): p. 2030-8.
161. Di Veroli, G.Y., et al., *Combenefit: an interactive platform for the analysis and visualization of drug combinations*. Bioinformatics, 2016. **32**(18): p. 2866-8.
162. Kurokawa, M. and S. Kornbluth, *Caspases and kinases in a death grip*. Cell, 2009. **138**(5): p. 838-54.
163. Nicoletti, I., et al., *A rapid and simple method for measuring thymocyte apoptosis by propidium iodide staining and flow cytometry*. J Immunol Methods, 1991. **139**(2): p. 271-9.
164. Piovan, E., et al., *Direct reversal of glucocorticoid resistance by AKT inhibition in acute lymphoblastic leukemia*. Cancer Cell, 2013. **24**(6): p. 766-76.
165. Blackburn, J.S., et al., *Clonal evolution enhances leukemia-propagating cell frequency in T cell acute lymphoblastic leukemia through Akt/mTORC1 pathway activation*. Cancer Cell, 2014. **25**(3): p. 366-78.
166. Ferrando, A.A., et al., *Gene expression signatures define novel oncogenic pathways in T cell acute lymphoblastic leukemia*. Cancer Cell, 2002. **1**(1): p. 75-87.
167. So, A.Y., et al., *Glucocorticoid regulation of the circadian clock modulates glucose homeostasis*. Proc Natl Acad Sci U S A, 2009. **106**(41): p. 17582-7.
168. Hogenesch, J.B., et al., *The basic helix-loop-helix-PAS protein MOP9 is a brain-specific heterodimeric partner of circadian and hypoxia factors*. J Neurosci, 2000. **20**(13): p. RC83.
169. Leonard, G.D., T. Fojo, and S.E. Bates, *The role of ABC transporters in clinical practice*. Oncologist, 2003. **8**(5): p. 411-24.
170. Nishioka, C., et al., *Imatinib causes epigenetic alterations of PTEN gene via upregulation of DNA methyltransferases and polycomb group proteins*. Blood Cancer J, 2011. **1**(12): p. e48.
171. Lucas, X., et al., *4-Acyl pyrroles: mimicking acetylated lysines in histone code reading*. Angew Chem Int Ed Engl, 2013. **52**(52): p. 14055-9.
172. Cele, F.N., H. Kumalo, and M.E. Soliman, *Mechanism of Inhibition of Hsp90 Dimerization by Gyrase B Inhibitor Coumermycin A1 (C-A1) Revealed by Molecular Dynamics Simulations and Thermodynamic Calculations*. Cell Biochem Biophys, 2016. **74**(3): p. 353-63.
173. Jenkinson, S., et al., *Impact of PTEN abnormalities on outcome in pediatric patients with T-cell acute lymphoblastic leukemia treated on the MRC UKALL2003 trial*. Leukemia, 2016. **30**(1): p. 39-47.
174. Petit, A., et al., *Oncogenetic mutations combined with MRD improve outcome prediction in pediatric T-cell acute lymphoblastic leukemia*. Blood, 2018. **131**(3): p. 289-300.
175. Escot, C., et al., *Genetic alteration of the c-myc protooncogene (MYC) in human primary breast carcinomas*. Proc Natl Acad Sci U S A, 1986. **83**(13): p. 4834-8.
176. Motoshima, K., et al., *[Immunohistological study on ras and myc oncogene products in pancreatic cancer]*. Nihon Geka Gakkai Zasshi, 1990. **91**(1): p. 123-9.

177. Ladanyi, M., et al., *Sporadic amplification of the MYC gene in human osteosarcomas*. *Diagn Mol Pathol*, 1993. **2**(3): p. 163-7.
178. Kawate, S., et al., *Amplification of c-myc in hepatocellular carcinoma: correlation with clinicopathologic features, proliferative activity and p53 overexpression*. *Oncology*, 1999. **57**(2): p. 157-63.
179. Cole, M.D., *The myc oncogene: its role in transformation and differentiation*. *Annu Rev Genet*, 1986. **20**: p. 361-84.
180. Prendergast, G.C., *Mechanisms of apoptosis by c-Myc*. *Oncogene*, 1999. **18**(19): p. 2967-87.
181. Dani, C., et al., *Extreme instability of myc mRNA in normal and transformed human cells*. *Proc Natl Acad Sci U S A*, 1984. **81**(22): p. 7046-50.
182. Hann, S.R. and R.N. Eisenman, *Proteins encoded by the human c-myc oncogene: differential expression in neoplastic cells*. *Mol Cell Biol*, 1984. **4**(11): p. 2486-97.
183. Thomas, L.R. and W.P. Tansey, *Proteolytic control of the oncoprotein transcription factor Myc*. *Adv Cancer Res*, 2011. **110**: p. 77-106.
184. Wei, G., et al., *Gene expression-based chemical genomics identifies rapamycin as a modulator of MCL1 and glucocorticoid resistance*. *Cancer Cell*, 2006. **10**(4): p. 331-42.
185. Beesley, A.H., et al., *Glucocorticoid resistance in T-lineage acute lymphoblastic leukaemia is associated with a proliferative metabolism*. *Br J Cancer*, 2009. **100**(12): p. 1926-36.
186. Dickmeis, T., *Glucocorticoids and the circadian clock*. *J Endocrinol*, 2009. **200**(1): p. 3-22.
187. Lu, M., et al., *ARNTL2 knockdown suppressed the invasion and migration of colon carcinoma: decreased SMOG2-EMT expression through inactivation of PI3K/AKT pathway*. *Am J Transl Res*, 2020. **12**(4): p. 1293-1308.
188. Wang, Z., et al., *ARNTL2 promotes pancreatic ductal adenocarcinoma progression through TGF/BETA pathway and is regulated by miR-26a-5p*. *Cell Death Dis*, 2020. **11**(8): p. 692.
189. Fletcher, J.I., et al., *ABC transporters as mediators of drug resistance and contributors to cancer cell biology*. *Drug Resist Updat*, 2016. **26**: p. 1-9.
190. Theodoulou, F.L. and I.D. Kerr, *ABC transporter research: going strong 40 years on*. *Biochem Soc Trans*, 2015. **43**(5): p. 1033-40.
191. Fu, Y., et al., *ABCA5 regulates amyloid-beta peptide production and is associated with Alzheimer's disease neuropathology*. *J Alzheimers Dis*, 2015. **43**(3): p. 857-69.
192. Petry, F., et al., *Subcellular localization of rat Abca5, a rat ATP-binding-cassette transporter expressed in Leydig cells, and characterization of its splice variant apparently encoding a half-transporter*. *Biochem J*, 2006. **393**(Pt 1): p. 79-87.
193. Hall, C.P., C.P. Reynolds, and M.H. Kang, *Modulation of Glucocorticoid Resistance in Pediatric T-cell Acute Lymphoblastic Leukemia by Increasing BIM Expression with the PI3K/mTOR Inhibitor BEZ235*. *Clin Cancer Res*, 2016. **22**(3): p. 621-32.
194. Mensah, F.A., J.P. Blaize, and L.J. Bryan, *Spotlight on copanlisib and its potential in the treatment of relapsed/refractory follicular lymphoma: evidence to date*. *Onco Targets Ther*, 2018. **11**: p. 4817-4827.
195. Liu, N., et al., *BAY 80-6946 is a highly selective intravenous PI3K inhibitor with potent p110alpha and p110delta activities in tumor cell lines and xenograft models*. *Mol Cancer Ther*, 2013. **12**(11): p. 2319-30.
196. Dumble, M., et al., *Discovery of novel AKT inhibitors with enhanced anti-tumor effects in combination with the MEK inhibitor*. *PLoS One*, 2014. **9**(6): p. e100880.
197. Spencer, A., et al., *The novel AKT inhibitor afuresertib shows favorable safety, pharmacokinetics, and clinical activity in multiple myeloma*. *Blood*, 2014. **124**(14): p. 2190-5.
198. Shayesteh, L., et al., *PIK3CA is implicated as an oncogene in ovarian cancer*. *Nat Genet*, 1999. **21**(1): p. 99-102.

199. Ma, Y.Y., et al., *PIK3CA as an oncogene in cervical cancer*. *Oncogene*, 2000. **19**(23): p. 2739-44.
200. Bellacosa, A., et al., *Molecular alterations of the AKT2 oncogene in ovarian and breast carcinomas*. *Int J Cancer*, 1995. **64**(4): p. 280-5.
201. Cheng, J.Q., et al., *Amplification of AKT2 in human pancreatic cells and inhibition of AKT2 expression and tumorigenicity by antisense RNA*. *Proc Natl Acad Sci U S A*, 1996. **93**(8): p. 3636-41.
202. Fresno Vara, J.A., et al., *PI3K/Akt signalling pathway and cancer*. *Cancer Treat Rev*, 2004. **30**(2): p. 193-204.
203. Alzahrani, A.S., *PI3K/Akt/mTOR inhibitors in cancer: At the bench and bedside*. *Semin Cancer Biol*, 2019. **59**: p. 125-132.
204. Knight, Z.A., H. Lin, and K.M. Shokat, *Targeting the cancer kinome through polypharmacology*. *Nat Rev Cancer*, 2010. **10**(2): p. 130-7.
205. Andrews, F.H., et al., *Dual-activity PI3K-BRD4 inhibitor for the orthogonal inhibition of MYC to block tumor growth and metastasis*. *Proc Natl Acad Sci U S A*, 2017. **114**(7): p. E1072-E1080.
206. Farrell, A.S. and R.C. Sears, *MYC degradation*. *Cold Spring Harb Perspect Med*, 2014. **4**(3).
207. Gorgun, G., et al., *A novel Aurora-A kinase inhibitor MLN8237 induces cytotoxicity and cell-cycle arrest in multiple myeloma*. *Blood*, 2010. **115**(25): p. 5202-13.
208. Sloane, D.A., et al., *Drug-resistant aurora A mutants for cellular target validation of the small molecule kinase inhibitors MLN8054 and MLN8237*. *ACS Chem Biol*, 2010. **5**(6): p. 563-76.
209. Bavetsias, V. and S. Linardopoulos, *Aurora Kinase Inhibitors: Current Status and Outlook*. *Front Oncol*, 2015. **5**: p. 278.
210. Hoeflich, K.P., et al., *Intermittent administration of MEK inhibitor GDC-0973 plus PI3K inhibitor GDC-0941 triggers robust apoptosis and tumor growth inhibition*. *Cancer Res*, 2012. **72**(1): p. 210-9.
211. Will, M., et al., *Rapid induction of apoptosis by PI3K inhibitors is dependent upon their transient inhibition of RAS-ERK signaling*. *Cancer Discov*, 2014. **4**(3): p. 334-47.
212. Squiban, B., S.T. Ahmed, and J.K. Frazer, *Creation of a human T-ALL cell line online database*. *Leuk Lymphoma*, 2017. **58**(11): p. 2728-2730.
213. Christoulas, D., et al., *Relapse of ovarian cancer with bone marrow infiltration and concurrent emergence of therapy-related acute myeloid leukemia: a case report*. *J Clin Oncol*, 2011. **29**(11): p. e295-6.
214. Bossi, P., M. Lucchesi, and A. Antonuzzo, *Gastrointestinal toxicities from targeted therapies: measurement, duration and impact*. *Curr Opin Support Palliat Care*, 2015. **9**(2): p. 163-7.
215. Boers-Doets, C.B., et al., *Mammalian target of rapamycin inhibitor-associated stomatitis*. *Future Oncol*, 2013. **9**(12): p. 1883-92.
216. Pessi, M.A., et al., *Targeted therapy-induced diarrhea: A review of the literature*. *Crit Rev Oncol Hematol*, 2014. **90**(2): p. 165-79.
217. Stuurman, F.E., et al., *Oral anticancer drugs: mechanisms of low bioavailability and strategies for improvement*. *Clin Pharmacokinet*, 2013. **52**(6): p. 399-414.
218. Al Shoyaib, A., S.R. Archie, and V.T. Karamyan, *Intraperitoneal Route of Drug Administration: Should it Be Used in Experimental Animal Studies?* *Pharm Res*, 2019. **37**(1): p. 12.
219. Uttam Garg, C.F., *Chapter 7 - Therapeutic Drug Monitoring in Infants and Children*, Elsevier, 2016, (Clinical Challenges in Therapeutic Drug Monitoring.): p. Pages 165-184.
220. Manzotti, G., A. Ciarrocchi, and V. Sancisi, *Inhibition of BET Proteins and Histone Deacetylase (HDACs): Crossing Roads in Cancer Therapy*. *Cancers (Basel)*, 2019. **11**(3).
221. Choudhary, C., et al., *Lysine acetylation targets protein complexes and co-regulates major cellular functions*. *Science*, 2009. **325**(5942): p. 834-40.

222. Shi, J. and C.R. Vakoc, *The mechanisms behind the therapeutic activity of BET bromodomain inhibition*. Mol Cell, 2014. **54**(5): p. 728-36.
223. Conte, M., et al., *HDAC2 deregulation in tumorigenesis is causally connected to repression of immune modulation and defense escape*. Oncotarget, 2015. **6**(2): p. 886-901.
224. Roche, J. and P. Bertrand, *Inside HDACs with more selective HDAC inhibitors*. Eur J Med Chem, 2016. **121**: p. 451-483.
225. Di Liddo, R., et al., *Histone deacetylase inhibitors restore IL-10 expression in lipopolysaccharide-induced cell inflammation and reduce IL-1beta and IL-6 production in breast silicone implant in C57BL/6J wild-type murine model*. Autoimmunity, 2016: p. 1-11.
226. Krieger, V., et al., *Synthesis of Peptoid-Based Class I-Selective Histone Deacetylase Inhibitors with Chemosensitizing Properties*. J Med Chem, 2019. **62**(24): p. 11260-11279.
227. Krieger, V., et al., *Design, Multicomponent Synthesis, and Anticancer Activity of a Focused Histone Deacetylase (HDAC) Inhibitor Library with Peptoid-Based Cap Groups*. J Med Chem, 2017. **60**(13): p. 5493-5506.
228. Lee, J., et al., *Activation of MYC, a bona fide client of HSP90, contributes to intrinsic ibrutinib resistance in mantle cell lymphoma*. Blood Adv, 2018. **2**(16): p. 2039-2051.
229. Zhou, D., et al., *A rat retinal damage model predicts for potential clinical visual disturbances induced by Hsp90 inhibitors*. Toxicol Appl Pharmacol, 2013. **273**(2): p. 401-9.
230. Wang, M., et al., *Development of Heat Shock Protein (Hsp90) Inhibitors To Combat Resistance to Tyrosine Kinase Inhibitors through Hsp90-Kinase Interactions*. J Med Chem, 2016. **59**(12): p. 5563-86.
231. Butler, L.M., et al., *Maximizing the Therapeutic Potential of HSP90 Inhibitors*. Mol Cancer Res, 2015. **13**(11): p. 1445-51.
232. Maloney, A., et al., *Gene and protein expression profiling of human ovarian cancer cells treated with the heat shock protein 90 inhibitor 17-allylamino-17-demethoxygeldanamycin*. Cancer Res, 2007. **67**(7): p. 3239-53.
233. McCollum, A.K., et al., *Up-regulation of heat shock protein 27 induces resistance to 17-allylamino-demethoxygeldanamycin through a glutathione-mediated mechanism*. Cancer Res, 2006. **66**(22): p. 10967-75.
234. Guo, F., et al., *Abrogation of heat shock protein 70 induction as a strategy to increase antileukemia activity of heat shock protein 90 inhibitor 17-allylamino-demethoxy geldanamycin*. Cancer Res, 2005. **65**(22): p. 10536-44.
235. Wang, Y. and S.R. McAlpine, *Heat-shock protein 90 inhibitors: will they ever succeed as chemotherapeutics?* Future Med Chem, 2015. **7**(2): p. 87-90.
236. Wang, Y. and S.R. McAlpine, *N-terminal and C-terminal modulation of Hsp90 produce dissimilar phenotypes*. Chem Commun (Camb), 2015. **51**(8): p. 1410-3.